Title

ORIENTATION AND ENERGY TRANSFER STUDIES ON CHLOROPHYLL IN THE PHOTOSYNTHETIC MEMBRANE

Author

Nairn, J.A.

Publication Date

1981-12-01

LBL-13827

Lawrence Berkeley Laboratory
UNIVERSITY OF CALIFORNIA

CHEMICAL BIODYNAMICS DIVISION

ORIENTATION AND ENERGY TRANSFER STUDIES ON CHLOROPHYLL IN THE PHOTOSYNTHETIC MEMBRANE

John Arthur Nairn
(Ph.D. thesis)

December 1981

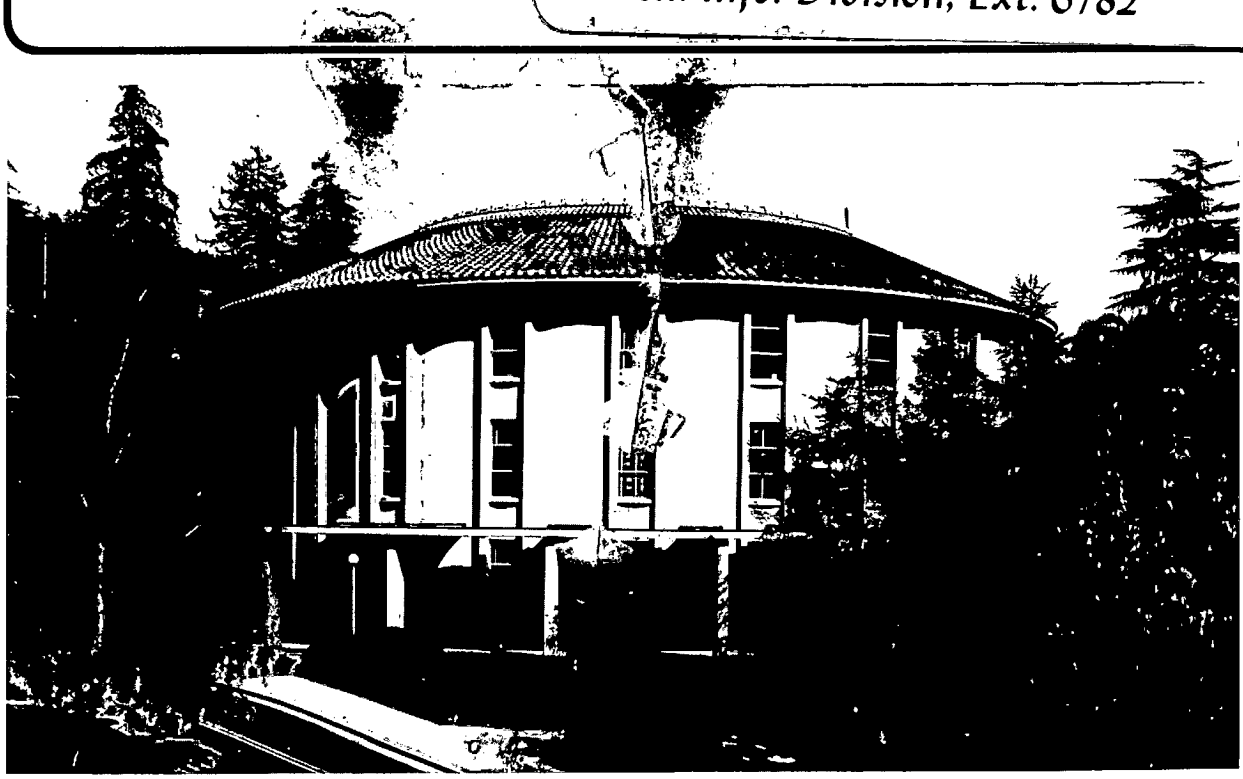

Prepared for the U.S. Department of Energy under Contract W-7405-ENG-48

DISCLAIMER

ORIENTATION AND ENERGY TRANSFER STUDIES ON CHLOROPHYLL IN THE PHOTOSYNTHETIC MEMBRANE

By

John A. Nairn

ABSTRACT

The aim of this thesis is to study the light reactions of photosynthesis. The two methods of study used are orientation dependent spectroscopy and picosecond resolution of the fluorescence decay kinetics.

Analysis of spectroscopic measurements on complex partially ordered ensembles, such as photosynthetic systems, is usually limited by knowledge of the orientational distribution function. A new method of parametrically representing the distribution function using a physical model of the partially ordered ensemble is described in Chapter II. The parametric representation of the distribution function is the density of states function. Many formulas are included which can be used to calculate density of states functions for a large range of problems.

Fluorescence decay kinetics in chloroplasts from green plants and algae are investigated using a synchronously pumped, mode-locked dye laser as an excitation source. This setup can resolve fluorescence lifetimes as short as 25 ps.

The fluorescence decay kinetics are found to be characterized by three exponential components. The slow phase is 1 to 2 ns, and the two

faster phases are 350 to 750 ps and 50 to 100 ps. The exact lifetime and yield of each component depends on the experimental conditions. The results are shown to be consistent with a model of the photosynthetic unit described in Chapter V. Briefly, the fast phases are "prompt" fluorescence which results from excitation lost in transit to the reaction center of photosystem II. The slow phase is "delayed" fluorescence which results from excitation that returns to the chlorophyll antenna after a charge separation and recombination reaction in the photosystem II reaction center.

The addition of Mg^{+2} to broken chloroplasts induces changes in the primary processes of photosynthesis. The effects of these changes on the fluorescence decay kinetics are reported in Chapter VI. The results are interpreted by postulating two effects of Mg^{+2} that occur at different levels of added Mg^{+2}. As the concentration of Mg^{+2} is increased from 0.0 to 0.75 mM the lifetimes of the slow and middle phases increase. These increases indicate that connections between photosystem II and photosystem I are altered resulting in a decreased rate of energy spillover from photosystem II to photosystem I. As the concentration of Mg^{+2} is increased up to 2 mM, the yield of the slow phase increases at F_{max}, but at F_0 it decreases from a peak at low concentrations of Mg^{+2}. In conjunction with the intensity dependence of the fluorescence decay in the presence and absence of Mg^{+2}, these changes indicate that effects on the chlorophyll a/b light-harvesting antenna cause both an increase in the absorption cross section of photosystem II and an initiation of communication between photosystem II units. Investigation of the fluorescence lifetimes and yields during the P to S fluorescence decline in chloroplasts, described in Chapter VII, suggests that the transition

to the S state is analogous to removal of the Mg^{+2} effect.

In Chapter VIII, five kinetic components are found in the low-temperature fluorescence decay kinetics from spinach chloroplasts. Three of these components are present at short wavelengths (670 and 680 nm); they appear to be analogous to the room-temperature fluorescence decay components, and their behavior adds support to the model in Chapter V. Two new components are observable at long wavelengths (>710 nm). One long-wavelength component is a resolvable risetime of 50 to 150 ps, and the other is a slow decay of 2 to 3 ns. The resolvable risetime is a direct observation of energy transfer from the bulk chlorophyll antenna to the small pigment bed of chlorophyll responsible for the long-wavelength emission.

These fluorescence decay studies greatly increase the effectiveness of fluorescence as a non-destructive probe into the photosynthetic unit. The complex nature of the fluorescence decay in chloroplasts has now been characterized. Knowledge of the three fluorescence decay components and the ability to measure these components under various sample conditions can provide much information.

TABLE OF CONTENTS

ACKNOWLEDGEMENTS

I have learned much in the time I have spent in Berkeley. I would like to thank some of the people who made it possible:

Ken Sauer, my research director, for never being too busy to further my scientific training.

Rich Friesner, for his theoretical insights that contributed to the development of the orientational averaging theory.

Wolfgang Haehnel, for his considerable scientific talents that were indespensible in the fluorescence decay experiments.

Paul Reisberg, for help with fluorescence decay experiments and for many computer simulations that contributed to interpretation of our data.

The people and staff of the Melvin Calvin Laboratory, for their willingness and ability to help - both in scientific and personal matters. Special thanks go to Dick O'Brien, Gary Smith, Mike Press, Beth Klingel, and the members of the computer staff.

My parents, for their continued financial and emotional support throughout my college education.

This work was supported by the Division of Biological Energy Conversion, Office of Basic Energy Sciences of the U.S. Department of Energy under Contract Number W-7405-ENG-48.

ABBREVIATIONS

Chl a_1	chlorophyll a antenna of photosystem I
Chl a_2	chlorophyll a antenna of photosystem II
Chl a/b LH	chlorophyll a/b light-harvesting antenna
DCMU	3-(3',4'-dichlorophenyl)-1,1-dimethyl urea
EPR	electron paramagnetic resonance
F_{max}	maximum fluorescence level in chloroplasts
F_0	minimum fluorescence level in chloroplasts
FWHM	full-width-half-maximum
HEPES	N-2-hydroxyethylpiperazine-N'-2-ethanesulfonic acid
LAS	laboratory axis system
MAS	molecular axis system
MOM	method of moments
NADP	nicotinamide adenine dinucleotide phosphate
NLLS	non-linear least squares
Ph	pheophytin
P_{680}	primary electron donor in photosystem II
P_{700}	primary electron donor in photosystem I
Q	electron acceptor in photosystem II
RS	rotation scheme
TAC	time-to-amplitude converter
$\underline{v}$	vector $\underline{v}$, vectors denoted by underlining

CHAPTER I

INTRODUCTION

I-1. THE LIGHT REACTIONS

The photosynthetic light reactions in green plants and in photosynthetic bacteria convert absorbed light energy into chemical potential energy. They begin with the absorption of an incident photon by a light-harvesting array of pigment molecules - mostly chlorophyll molecules. Electronic excitation is then transferred through the pigment array until it is trapped by a reaction center which contains a primary donor and intial acceptors for a series of electron transfer reactions. The electron transfer reactions, which are driven by the trapped electronic excitation energy, provide the mechanism for the storage of chemical potential energy.

The complete set of light reactions in green plants is divided into two systems - photosystem I and photosystem II. Photosystem I is involved in the storage of chemical potential energy by reducing $NADP^+$ to NADPH. Photosystem II is involved in splitting water into molecular oxygen and reducing equivalents. The oxygen is evolved and the reducing equivalents provide a source of electrons for the photosystem I light reaction. Photosystem I and photosystem II are localized in the thylakoid membrane which is an internal membrane component of the green plant photosythetic organelle called a chloroplast. An electron micrograph of a chloroplast is shown in Fig. I-1 [1]. The thylakoid membrane is partitioned into stacked regions (grana) and unstacked

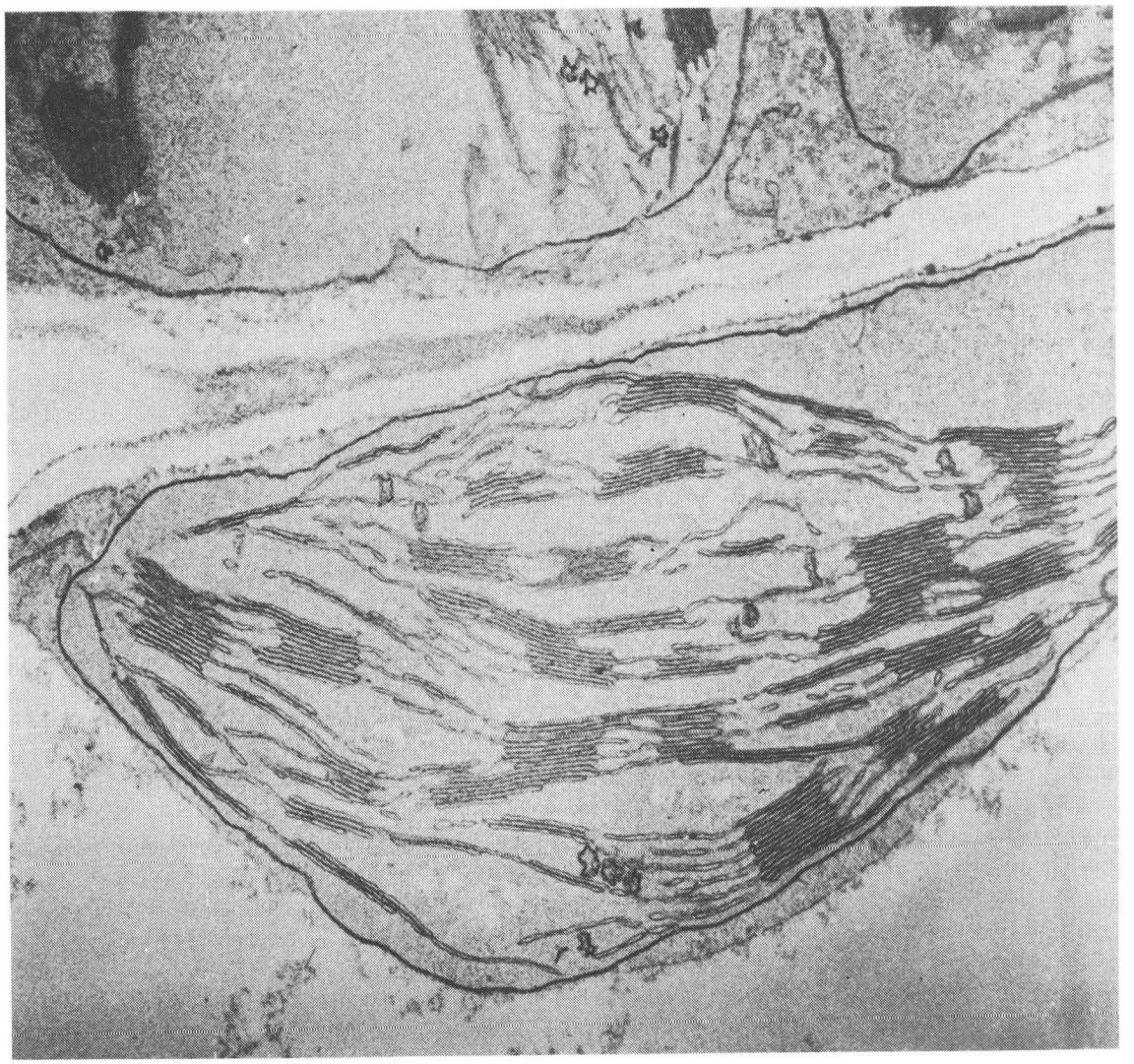

XBB 821-170

Figure I-1: Electron micrograph of a chloroplast displaying the arrangement of the thylakoid membranes (from Ref. [1]).

regions (stroma). The outer membrane defines the envelope of the chloroplast.

Detergent treatments of thylakoid membranes has resulted in the isolation of three major protein complexes - the chlorophyll a/b protein, the photosystem I complex, and the photosystem II complex [2]. About 50% of the green plant chlorophyll is found in chlorophyll a/b proteins [3]. The chlorophyll a/b protein subunit has a molecular weight of 35,000 daltons and contains three molecules each of chlorophyll a and chlorophyll b [4]. The two photosystem complexes contain both light-harvesting chlorophyll a molecules and the reaction center of that photosystem. A reaction center from each photosystem together with a set of light-harvesting chlorophyll and associated electron transport components is known as a photosynthetic unit.

The detailed organization of the chlorophyll-protein complexes within the thylakoid membrane is not known. Some of the basic features are shown in Fig. I-2 which illustrates a hypothetical section of a thylakoid membrane. The photosystem I and photosystem II complexes together with the chlorophyll a/b proteins are spread throughout the membrane. P_{700} and P_{680} shown in Fig. I-2 are the primary electron donors in photosystem I and photosystem II respectively. These electron donors are specialized chlorophyll a molecules, or chlorophyll a dimers, which are distinquished from the light-harvesting chlorophyll by the ability to initiate electron transfer reactions and their red-shifted absorption spectrum. P_{700} and P_{680} refer to pigments absorbing at 700 nm and 680 nm respectively [5,6].

The study of the photsynthetic light reactions in this thesis follows two directions. The first direction is an attempt to elucidate

Figure I-2: Hypothetical section of a thylakoid membrane. Chl a/b, P680, and P700 are defined in the text. RC1 and RC2 are the photosystem I and photosystem II complexes (K. Sauer, private communication).

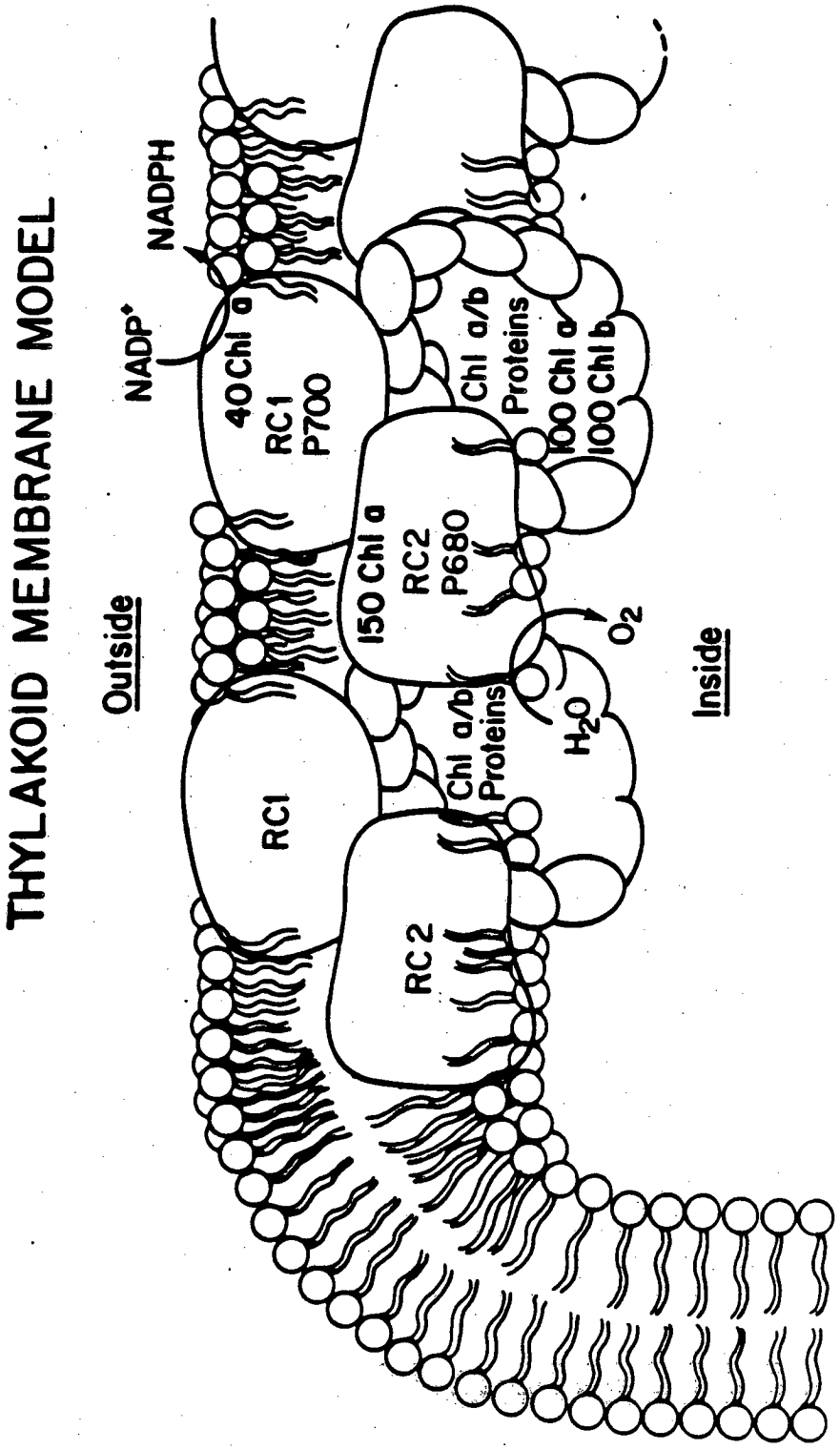
THYLAKOID MEMBRANE MODEL
Outside
Inside
NADP+
NADPH
40 Chl a
RC1
P700
150 Chl a
RC2
P680
Chl a/b
Proteins
100 Chl a
100 Chl b
RC1
RC2
Chl a/b
Proteins
H2O
O2

specific orientation details for the model in Fig. I-2. To this end, we have developed new methods for extracting structural information from spectroscopy of complex partially ordered systems. The second direction examines the transit of electronic excitation energy through the photosynthetic unit. This question is studied by picosecond resolution of the fluorescence decay kinetics.

I-2. ORIENTATIONAL AVERAGING

The orientation of photosynthetic pigments with respect to the thylakoid membrane, or the orientation of these pigments with respect to each other, can be characterized through studies involving linear dichroism, fluorescence polarization, magnetic resonance, or X-ray crsytallography on ordered samples. A highly ordered sample is best obtained through crystallization, but unfortunately only one chlorophyll-protein complex has been crystallized to date [7]. Partial order in photosynthetic samples can be induced in a magnetic field [8,9], in an electric field [10], in a stretched film [11-13], or in a flow system [14,15]. Partial order in biological systems is generally complex and the problem with analyzing spectroscopic studies on these types of samples is incomplete knowledge of the distribution function.

In Chapter II is presented a new approach to orientational averaging which is particularly useful for analyzing spectroscopic data from complex partially ordered systems. The techniques described in Chapter II were introduced in Refs. [16-19] and first applied to calculate the orientation of the reaction center in the photosynthetic

bacterium Rhodopseudomonas viridis with respect to the membrane [20]. In this thesis emphasis is placed on actual use of our orientational averaging theory through provision of detailed examples. Our techniques are generally applicable to complex orientational averaging problems; we hope that their use will encourage new quantitative studies on partially ordered systems.

I-3. FLUORESCENCE DECAY KINETICS

The room-temperature fluorescence emission spectrum from chloroplasts has a maximum at 680 to 685 nm and a tail that extends beyond 730 nm [21]. The fluorescence yield at 680 nm is a function of the state of an electron acceptor Q in photosystem II [22]. When Q is reduced, it is not capable of accepting an electron from P_{680}, the primary electron donor in photosystem II. If all photosystem II's have Q reduced, the chloroplasts are said to be in the all-closed state. In the all-closed state, the fluorescence yield is at a maximum level, F_{max}. When Q is oxidized and capable of accepting an electron from P_{680}, the reaction center in photosystem II is open. In the all-open state, the fluorescence yield is at a minimum level, F_0. The ability of Q to quench fluorescence when it is oxidized is the origin of the nomenclature Q for quencher. Action spectra and the fluorescence emission spectra of subchloroplast particles enriched in either photosystem I or photosystem II indicate that at room temperature, all of the variable fluorescence ($F_{max} - F_0$) and most of the background fluorescence (F_0) emanates from photosystem II [21,23,24].

Brody and Rabinowitch were the first to investigate the fluorescence decay kinetics of chloroplasts [25]. Since their work, direct observation of the fluorescence decay on an oscilloscope [25-29] and by phase fluorimetry [30-37] have been used to investigate the time resolved fluorescence decay kinetics as a function of the state of Q. There is general agreement that in the all-open state the average lifetime is about 0.5 ns, and in the all-closed state the average lifetime increases to about 2 ns. Unfortunately, these conventional methods of time resolving fluorescence decays do not have sufficient resolution to investigate the details of picosecond fluorescence decays. This problem is especially apparent in the all-open state, where the decay is very fast.

The application of solid state picosecond lasers to photosynthetic research in the early 1970's promised much better time resolution. The early reports using these lasers were that the average fluorescence lifetime is much shorter then previously reported - 100 to 200 ps as compared to 500 ps [38-45]. The measured fluorescence lifetimes turned out to be artificially shortened by exciton-exciton annihilation processes [46-49]. These excited state interactions are possible because of the large number of excited states created in the chlorophyll light-harvesting antenna by the high-intensity, solid-state laser pulses. More careful studies using these same lasers at reduced intensity are in general agreement with conventional methods [50-54]. The necessity of lowering the laser pulse energy reduces the signal-to-noise ratio of data detected with a streak camera. As a result, these picosecond lasers still do not allow a detailed investigation of the fluorescence decay in chloroplasts.

Single-photon timing [55] has often been used to time resolve fluorescence decays and subnanosecond resolution is possible even with traditional spark gap excitation sources [56,57]. The technique of single-photon timing has been applied to fluorescence decays in chloroplasts [58,59]. The most recent applications have replaced the spark gap excitation source with a synchronously pumped, mode-locked dye laser which has a pulse width of less than 10 ps [60,61]. This type of single-photon timing is capable of picosecond resolution, and the intensity of the laser pulses is low enough that excition-excition annihilation processes are never a problem. The fluorescence decay kinetic studies in this thesis are done using such a single-photon timing system. The details of our picosecond fluorimeter which is estimated to have a 25 ps resolution are described in Chapter III.

In Chapter IV is presented fluorescence decay measurements as a function of the state of Q. In both the all-open state and the all-closed state, we find the fluorescence decay in spinach chloroplasts, in pea chloroplasts, and in green algae to be characterized by three exponential components. A slow component has a lifetime of 1 to 2 ns and two fast components have lifetimes of 350 to 750 ps and 50 to 100 ps. The exact lifetimes and yields of each component depend on the experimental conditions. All of our data are consistent with a modified tripartite model [62-64]. The tripartite model, schematically illustrated in Fig. I-3, was developed by Butler and coworkers [62-64]. It divides the chlorophyll light-harvesting antenna into three parts. The Chl a/b LH antenna is composed of chlorophyll a/b proteins, and the Chl a_1 and Chl a_2 antennae are composed of chlorophyll a light-harvesting proteins closely associated with the reaction centers of

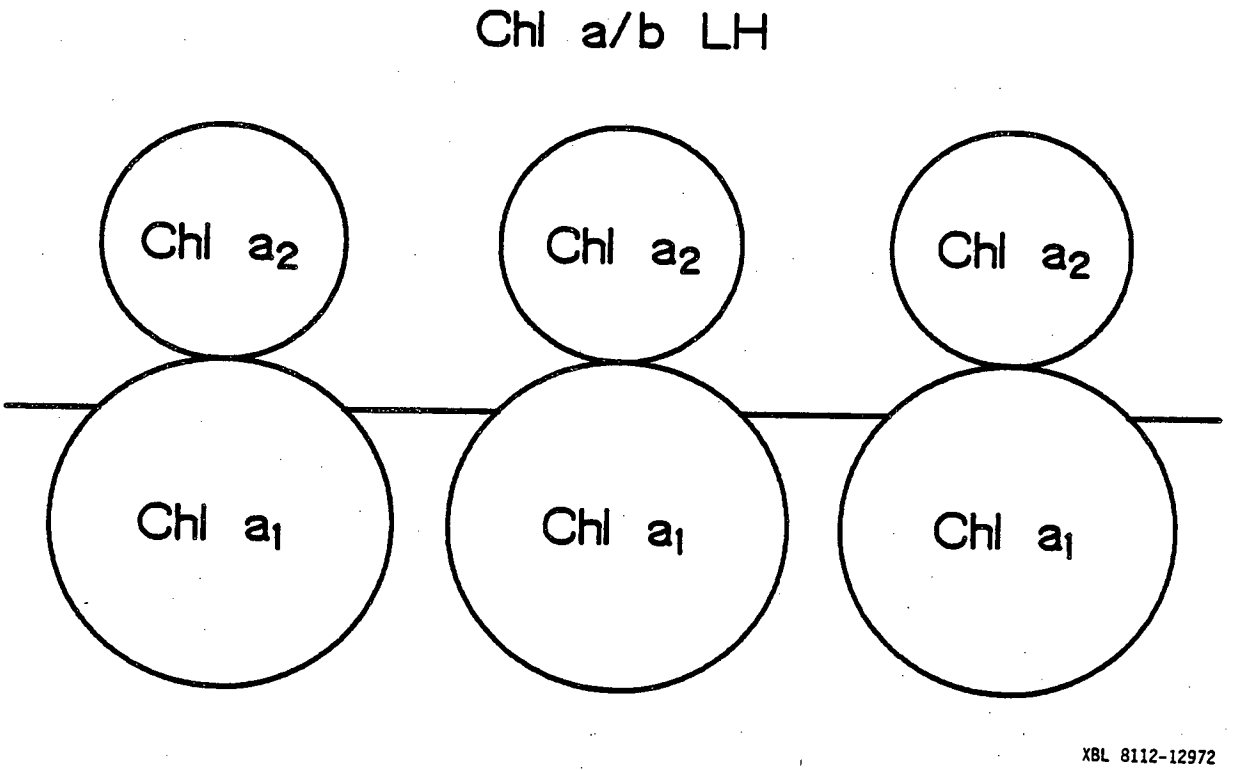

Figure I-3: Schematic representation of the tripartite model (from Ref. [63])

photosystem I and photosystem II, respectively. The relative connections between the components of the tripartite model displayed in Fig. I-3 are intended to illustrate the possible routes of energy transfer between these components.

Complete interpretation of our data requires extension of the tripartite model to explicitly include the electron transfer processes in photosystem II. Recent work by Klimov and coworkers [65-71] has led to the photosystem II reaction center model depicted in Fig. I-4. Under conditions where Q is reduced, they measured a reversible photobleaching of a pheophytin molecule (Ph) in photosystem II subchloroplast particles [65-70] and in chloroplasts [69,70]. Their proposal is that Ph acts as an intermediary electron acceptor between P_{680} and Q. Charge separation between P_{680} and Ph is possible in both the all-open and the all-closed states. In the all-closed state, electron transfer past Ph is not possible, but a charge recombination between P_{680}^{+} and Ph^{-} leading to excited-state chlorophyll molecules may result in "delayed" fluorescence. This mechanism is the origin of the 1 to 2 ns slow component we observe. A detailed kinetic analysis of a tripartite model which includes the photosystem II reaction center processes is presented in Chapter V.

Besides the state of Q, other factors influence the fluorescence properties of chloroplasts. Many of these factors are related to regulation mechanisms by which energy is partitioned between photosystem I and photosystem II. These regulation mechanisms probably are controlled by ionic levels and fluxes in the chloroplasts [72]. The fluorescence decay kinetics in different states of energy distribution are presented in Chapters VI amd VII. In Chapter VI we examine the

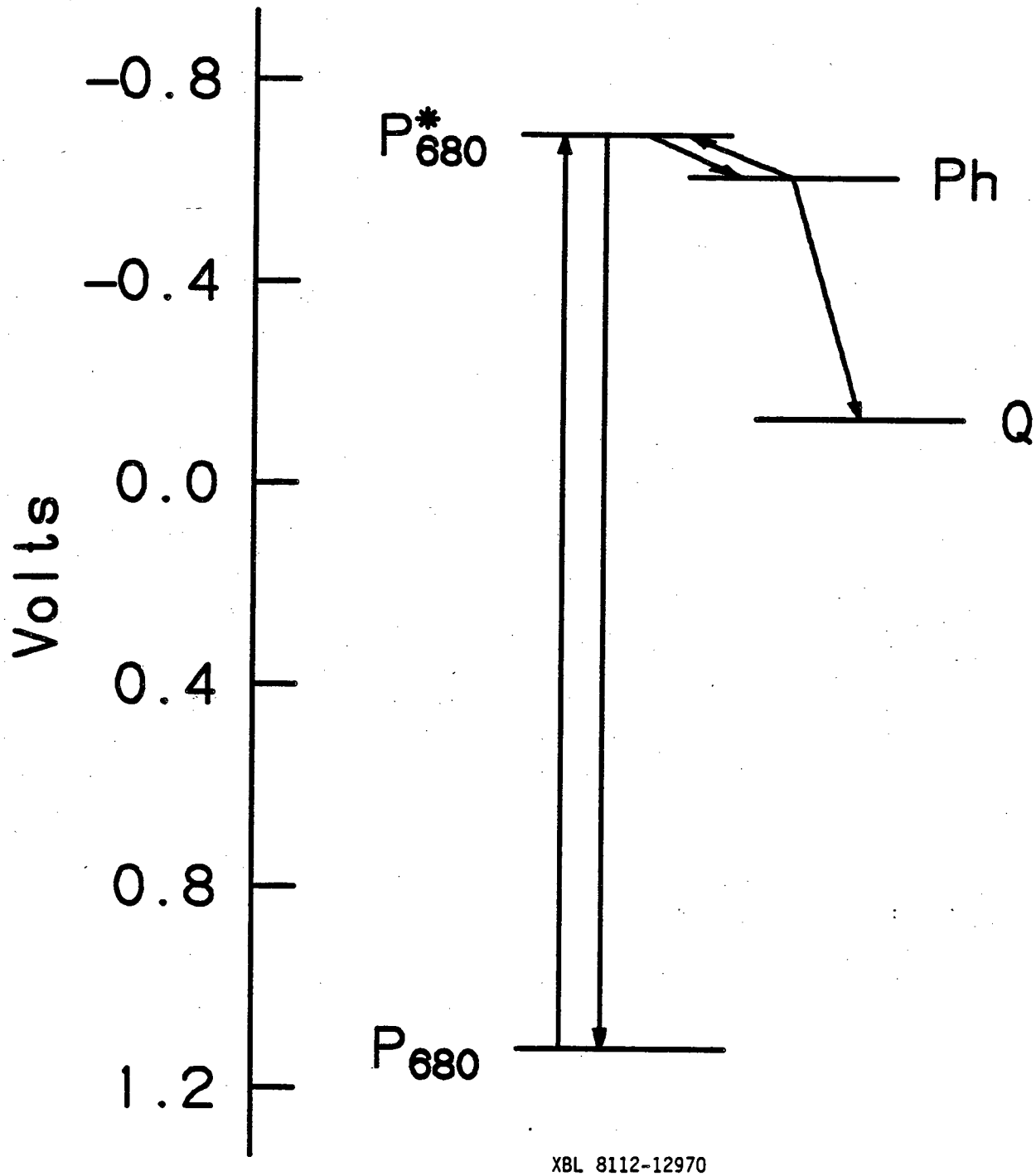

Figure I-4: Midpoint level diagram for the electron donors and acceptors in photosystem II (from Ref. [69]). Abbreviations: P_{680}, primary electron donor; Ph, pheophytin; and Q, secondary electron acceptor.

effect of Mg^{+2} on the room-temperature fluorescence decay kinetics in spinach chloroplasts. In Chapter VII is presented measurement of the fluorescence decay at various stages of the slow transition from the initial high fluorescence yield state (P state) to the steady state low fluorescence yield state (S state) [73] in spinach chloroplasts.

While the room-temperature emission spectrum of chloroplasts is broad and featureless, at 77K the fluorescence emission spectrum is resolved into three peaks at 685 nm, 695 nm, and 735 nm [21]. These peaks have been assigned to the Chl a/b LH antenna, photosystem II, and photosystem I, respectively [74]. In Chapter VIII is presented a wavelength-resolved measurement of the fluorescence decay kinetics in spinach chloroplasts at 77K. The results indicate that it is possible to study fluorescence from different parts of the photosynthetic unit independently of the other parts.

I-4. REFERENCES

1. R. B. Park, in Plant Biochemistry (eds. J. Bonner and J. E. Varner), Academic Press, New York, NY, 124 (1965).
2. J. P. Thornber, Ann. Rev. Plant Physiol. 26, 127 (1975).
3. J. J. Burke, C. L. Ditto, and C. J. Arntzen, Arch. Biochem. Biophys. 187, 252 (1978).
4. K. Kan and J. P. Thornber, Plant Physiol. 57, 47 (1976).
5. G. Doring, H. H. Stiehl, H. T. Witt, Z. Naturforsh. Teil B 22, 639 (1967).
6. B. Kok and G. Hoch, in Light and Life (eds. W. D. McElroy and B. Glass), Johns Hopkins Press, Baltimore, Maryland, 397 (1961).
7. R. E. Fenna and B. W. Matthews, Nature, 258, 573 (1969).
8. J. Breton, Biochem. Biophys. Res. Commun. 59, 1011 (1974).
9. G. Paillotin, A. Vermeglio, and J. Breton, Biochim. Biophys. Acta 545, 249 (1979).
10. W. B. Whitten, R. M. Pearlstein, E. F. Phares, and N. E. Geacintov, Biochim. Biophys. Acta 503, 251 (1978).
11. C. N. Rafferty and R. K. Clayton, Biochim. Biophys. Acta 502, 51 (1978).
12. C. N. Rafferty and R. K. Clayton, Biochim. Biophys. Acta 545, 106 (1979).
13. J. Bolt and K. Sauer, Biochim. Biophys. Acta 546, 54 (1979).
14. S. Morita and T. Miyazaki, Biochim. Biophys. Acta 245, 151 (1971).
15. G. B. Jeffery, Proc. R. Soc. Lond. Ser. A: Math. Phys. Sci. 102, 161 (1923).
16. R. Friesner, J. A. Nairn, and K. Sauer, J. Chem. Phys. 71, 358,

5388 (1979).

17. R. Friesner, J. A. Nairn, and K. Sauer, J. Chem. Phys. 72, 221, (1980).

18. J. A. Nairn, R. Friesner, and K. Sauer, J. Chem. Phys. 74, 5398 (1981).

19. J. A. Nairn, R. Friesner, H. A. Frank, and K. Sauer, Biophys. J. 32, 733 (1980).

20. H. A. Frank, R. Friesner, J. A. Nairn, G. C. Dismukes, and K. Sauer, Biochim. Biophys. Acta 547, 484 (1979).

21. N. K. Boardman, S. W. Thorne, and J. M. Anderson, Proc. Natl. Acad. Sci. USA 56, 586 (1966).

22. L. N. M. Duysens and H. E. Sweers, in Microalgae and Photosynthetic Bacteria (eds. Japanese Society of Plant Physiologists), Univ. of Tokyo Press, Tokyo, 535 (1963).

23. Govindjee and L. Yang, J. Gen. Physiol. 49, 763 (1966).

24. R. B. Park, K. E. Steinbeck, and P. V. Sane, Biochim. Biophys. Acta 253, 204 (1971).

25. S. S. Brody and E. Rabinowitch, Science 125, 555 (1957).

26. G. Tomita and E. Rabinowitch, Biophys. J. 2, 484 (1962).

27. N. R. Murty and E. Rabinowitch, Biophys. J. 5, 655 (1965).

28. W. J. Nicholson and J. I. Furtol, Biochim. Biophys. Acta 143, 577 (1967).

29. G. S. Singhal and E. Rabinowitch, Biophys. J. 9, 586 (1969).

30. L. A. Tumerman, O. F. Borisova, and A. B. Rubin, Biofizika 6, 645 (1961).

31. A. Müller and R. Lumry, Proc. Natl. Acad. Sci. USA 54, 1479 (1965).

32. A. Müller, R. Lumry, and M. S. Walker, Photochem Photobiol. 9, 113

(1969).

33. J.-M. Briantais, H. Merkelo, and Govindjee, Photosynthetica 6, 133 (1972).

34. A. Y. Borisov and M. D. Il'ina, Biochim. Biophys. Acta 305, 364 (1973).

35. I. Moya, Biochim. Biophys. Acta 368, 214 (1974).

36. I. Moya, Govindjee, C. Vernotte, and J.-M. Briantais, FEBS Lett. 75, 13 (1977).

37. S. Malkin, D. Wong, Govindjee, and H. Merkelo, Photobiochem. Photobiol. 1, 83 (1980).

38. M. Seibert, R. R. Alfano, and S. L. Shapiro, Biochim. Biophys. Acta 292, 493 (1973).

39. M. Seibert and R. R. Alfano, Biophys. J. 14, 269 (1974).

40. V. H. Kollman, S. L. Shapiro, and A. J. Campillo, Biochem. Biophys. Res. Commun. 63, 917 (1975).

41. W. Yu, P. P. Ho, R. R. Alfano, and M. Seibert, Biochim. Biophys. Acta 387, 159 (1975).

42. V. Z. Paschenko, S. P. Protosov, A. B. Rubin, K. N. Timofeev, L. M. Zamazova, and L. B. Rubin, Biochim. Biophys. Acta 408, 143 (1975).

43. S. L. Shapiro, V. H. Kollman, and A. J. Campillo, FEBS Lett. 54, 358 (1975).

44. V. Z. Paschenko, A. B. Rubin, and L. B. Rubin, Kvantovaya Elektron. (Moscow) 2, 1336 (1975).

45. G. S. Beddard, G. Porter, C. J. Tredwell, and J. Barber, Nature 258, 166 (1975).

46. D. Mauzerall, J. Chem. Phys. 80, 2306 (1976).

47. D. Mauzerall, Biophys. J. 16, 87 (1976).

48. A. J. Campillo, S. L. Shapiro, V. H. Kollman, K. R. Winn, and R. C. Hyer, Biophys. J. 16, 93 (1976).

49. A. J. Campillo, V. H. Kollman, and S. L. Shapiro, Science 193, 227 (1976).

50. L. Harris, G. Porter, J. A. Synowiec, C. J. Tredwell, and J. Barber, Biochim. Biophys. Acta 449, 329 (1976).

51. G. F. W. Searle, J. Barber, G. Porter, and C. J. Tredwell, Biochim. Biophys. Acta 459, 390 (1977).

52. G. Porter, J. A. Synowiec, and C. J. Tredwell, Biochim. Biophys. Acta 459, 329 (1977).

53. J. Barber, G. F. W. Searle, and C. J. Tredwell, Biochim. Biophys. Acta 501, 174 (1978).

54. G. F. W. Searle, C. J. Tredwell, J. Barber, and G. Porter, Biochim. Biophys. Acta 545, 496 (1979).

55. W. R. Ware, in The Creation and Detection of the Excited State (ed. A. A. Lamola), Vol 1A, 213 (1971).

56. B. Leskovar, C. C. Lo, P. R. Hartig, and K. Sauer, Rev. Sci. Instr. 47, 1113 (1976).

57. P. R. Hartig, K. Sauer, C. C. Lo, and B. Leskovar, Rev. Sci. Instr. 47, 1122 (1976).

58. K. Sauer and G. T. Brewington, in Proc. 4th Int. Congr. Photosynthesis (eds. D. O. Hall, J. Coombs, and T. W. Goodwin), The Biochemical Society, London, 409 (1977).

59. G. Hervo, G. Paillotin, and J. Thiery, J. Chim. Phys. 72, 761 (1975).

60. G. S. Beddard, G. R. Fleming, G. Porter, G. F. W. Searle, and J. A. Synowiec, Biochim. Biophys. Acta 545, 496 (1979).

61. V. A. Shuvalov, V. V. Klimov, E. Dolan, W. W. Parson, and B. Ke, FEBS Lett. 118, 279 (1980).

62. W. L. Butler and M. Kitajima, Biochim. Biophys. Acta 376, 116 (1975).

63. W. L. Butler and R. J. Strasser, Proc. Natl. Acad. Sci. USA 74, 3382 (1977).

64. W. L. Butler, Ann. Rev. Plant Physiol. 29, 345 (1978).

65. V. V. Klimov, A. V. Klevanik, V. A. Shuvalov, and A. A. Krasnovsky, FEBS Lett. 82, 183 (1977).

66. A. V. Klevanik, V. V. Klimov, V. A. Shuvalov, and A. A. Krasnovsky, Dokl. Akad. Nauk SSSR 236, 241 (1977).

67. V. V. Klimov, S. I. Allakhverdiev, and V. Z. Paschenko, Dokl. Akad. Nauk SSSR 236, 1204 (1978).

68. V. V. Klimov, S. I. Allakhverdiev, and A. A. Krasnovsky, Dokl. Akad. Nauk SSSR 249, 485 (1980).

69. V. V. Klimov, S. I. Allakhverdiev, S. Demeter, and A. A. Krasnovsky, Dokl. Akad. Nauk SSSR 249, 227 (1980).

70. V. V. Klimov, S. I. Allakhverdiev, S. I. Shutilova, and A. A. Krasnovsky, Sov. Plant Physiol. 27, 315 (1980).

71. V. V. Klimov, E. Dolan, and B. Ke, FEBS Lett. 112, 97 (1980).

72. J. Barber, in The Intact Chloroplast (ed. J. Barber), Elsevier/North-Holland Press, Amsterdam, 89 (1976).

73. J.-M. Briantais, C. Vernotte, M. Picaud, and G. H. Krause, Biochim. Biophys. Acta 548, 128 (1979).

74. K. Satoh and W. L. Butler, Plant Physiol. 61, 373 (1978).

CHAPTER II

ORIENTATIONAL AVERAGING

II-1. INTRODUCTION

Spectroscopic studies on oriented systems provide important sources of structural information in chemical and biochemical systems. These studies involve preparing a sample in a partially ordered ensemble and measuring a spectroscopic response such as linear dichroism, EPR, or fluorescence polarization. The problem we undertake is how to extract the structural information from an observed response in such a partially ordered ensemble. In biological systems, such as photosynthetic membranes, the analysis problem is often very complicated, because it is difficult to quantitatively describe the partial ordering. To illustrate, some photosynthetic systems (e.g. chloroplasts [1] and bacterial cells [2]) will orient in a magnetic field. The photosynthetic pigments which can be probed spectroscopically are imbedded in the membranes internal to these systems; they become oriented as a consequence of the entire system becoming oriented. To completely describe this partially ordered ensemble, it is necessary to consider two types of ordering effects:

(1). Incomplete alignment of the photosynthetic system in the magnetic field due to a finite magnetic susceptibility anisotropy.

(2). Inherent disorder present in the membranes. This disorder can arise from local imperfections in the membrane surface or from fluctuations in the orientation of the photosynthetic pigment being probed with respect

to the membrane.

The second effect makes the problem much more complex than traditional systems oriented in a magnetic field [3] or an electric field [4]. Our theory provides a general method for dealing with many types of unusual and complicated partially ordered ensembles.

In this chapter, I will extend the work begun in Ref. [5]. I will emphasize examples that illustrate the use of the orientational averaging theory.

II-2. GENERAL COMMENTS

We consider an ensemble of molecules that are spectroscopically identical and noninteracting. An observed response is, therefore, a superposition of the responses for the individual molecules. The superposition can be calculated by averaging a response function over an orientational distribution function. In what follows, I will be concerned only with a static ensemble of molecules whose independent molecular motion is negligible. The orientational averaging will then be done with a distribution function that is independent of time.

Before continuing, let me formally define two axis systems that will frequently be used in the ensuing discussions. First is the laboratory axis system (LAS); it is an axis system fixed in the laboratory reference frame. Any electromagnetic probe, such as the direction of the magnetic field used in EPR experiments, will be a constant vector in the LAS. I will label the LAS axes x, y, and z, and all vectors in LAS coordinates will be unprimed (e.g. the vector $\underline{V}$). The

second axis system is the molecular axis system (MAS); it is an axis system fixed with respect to the molecule being probed. I will label the MAS axes x', y', and z', and all vectors in the MAS will be primed (e.g. the vector $\underline{V}'$).

Many spectroscopic response functions depend only on the direction of one vector $\underline{V}'$ in the MAS. Examples include $\underline{V}'$ as the polarization vector of the electric field in absorption spectroscopy or $\underline{V}'$ as the direction of the magnetic field in EPR spectroscopy. The observed response when a one-vector response function is applicable can be written

$$\langle I \rangle = \int_0^{\pi} d\theta \int_0^{2\pi} d\phi \; I(\theta,\phi) D(\theta,\phi,\underline{\Delta}) \tag{1}$$

where $I(\theta,\phi)$ is the response of the system when $\underline{V}'$ has coordinates $|\underline{V}'|(\sin\theta\cos\phi, \sin\theta\sin\phi, \cos\theta)$ (i.e; $\underline{V}'$ is defined by the spherical angles θ and ϕ - see vector $\underline{V}_1'$ in Fig. II-1) in the MAS, $D(\theta,\phi,\underline{\Delta})$ is the probabilty that $\underline{V}'$ has those coordinates, and $\underline{\Delta} = (\Delta_1, \ldots, \Delta_k)$ is a set of parameters that describe the partial ordering. We call $D(\theta,\phi,\underline{\Delta})$ the density of states function. The core of our orientational averaging theory is the evaluation of $D(\theta,\phi,\underline{\Delta})$ from arbitrary models. The evaluation technique is easily applied to complicated problems like the one mentioned above.

Some spectroscopic response functions depend on the directions of two vectors $\underline{V}_1'$ and $\underline{V}_2'$ in the MAS which are perpendicular to each other and define directions of interest. For example, in a fluorescence polarization experiment, $\underline{V}_1'$ could be the polarization direction of the exciting light and $\underline{V}_2'$ could be the polarization direction of the

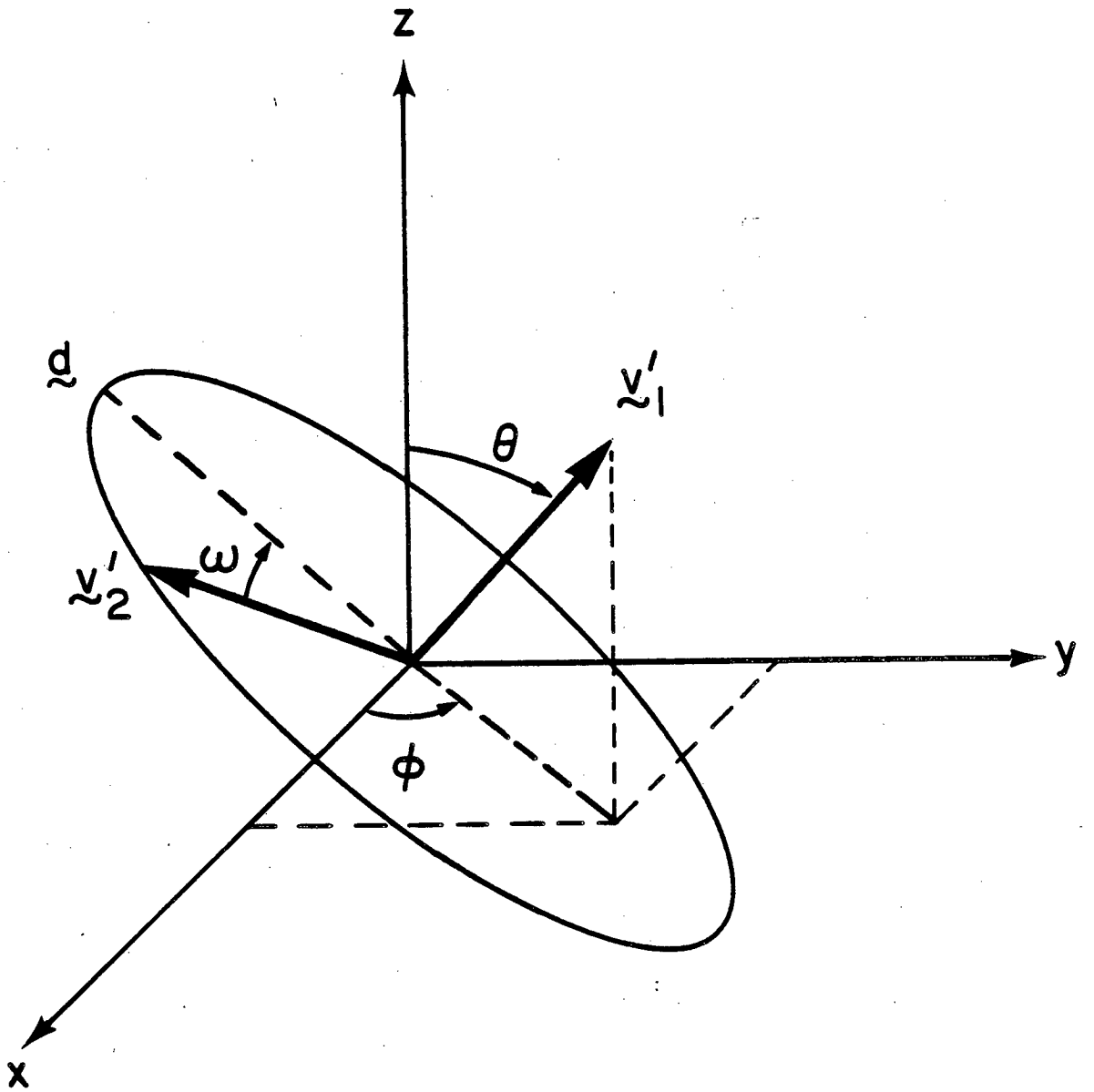

XBL 804-4110

Figure II-1: Definition of the angles θ, ϕ, and ω in the MAS (primes are omitted from the axis labels). θ and ϕ are the traditional spherical angles for the vector $\underline{V}_1'$; θ is the polar angle and ϕ is the azimuthal angle. ω is the angle between $\underline{V}_2'$ and an arbitrary (but fixed) direction $\underline{d}$ in the plane perpendicular to $\underline{V}_1'$.

detected fluorescence. In this case, we need a two-vector density of states function $P(\theta,\phi,\omega,\underline{\Delta})$ that is an extension of $D(\theta,\phi,\underline{\Delta})$ to simultaneously include the second vector. $P(\theta,\phi,\omega,\underline{\Delta})$ gives the probability that the location of $\underline{V}_2'$ is defined by ω when the spherical angles of $\underline{V}_1'$ in the MAS are θ and ϕ. This situation is illustrated in Fig II-1; by trigonometry, the coordinates of $\underline{V}_1'$ and $\underline{V}_2'$ are given by

$$\underline{V}_1' = \begin{pmatrix} \sin\theta\cos\phi \\ \sin\theta\sin\phi \\ \cos\theta \end{pmatrix} \tag{2}$$

and

$$\underline{V}_2' = \begin{pmatrix} \cos\theta\cos\phi\cos\omega + \sin\phi\sin\omega \\ \sin\phi\cos\theta\cos\omega - \cos\phi\sin\omega \\ -\sin\theta\cos\omega \end{pmatrix} \tag{3}$$

The observed response is

$$\langle I\rangle = \int_0^{\pi} d\theta \int_0^{2\pi} d\phi \int_0^{2\pi} d\omega \; I(\theta,\phi,\omega)P(\theta,\phi,\omega,\underline{\Delta}) \tag{4}$$

where $I(\theta,\phi,\omega)$ is the response when $\underline{V}_1'$ and $\underline{V}_2'$ are defined by Eqs. (2-3) in the MAS.

II-3. ONE-VECTOR PROBLEMS

The derivation of $D(\theta,\phi,\underline{\Delta})$ in Eq. (1) has been given in detail in Refs. [5] and [6]. A brief outline of the derivation should suffice

here. Consider a partially ordered set of MAS's such that each MAS is related to the LAS by $\underline{\alpha} = (\alpha_1, \ldots, \alpha_n)$ where $\alpha_1, \ldots, \alpha_n$ are n angles used in n rotations $R_1(\alpha_1), \ldots, R_n(\alpha_n)$ that rotate the LAS into the MAS. The average intensity is

$$\langle I \rangle = \int_{\alpha_1} \cdots \int_{\alpha_n} I(\underline{\alpha}) W(\underline{\alpha}, \underline{\Delta}) \, d\underline{\alpha} \tag{5}$$

where $I(\underline{\alpha})$ is the intensity function when the MAS is at orientation $\underline{\alpha}$, $W(\underline{\alpha}, \underline{\Delta})$ is a weighting function which gives the probability that the MAS has orientation $\underline{\alpha}$, and $\underline{\Delta} = (\Delta_1, \ldots, \Delta_k)$ is, as before, a set of parameters that describe the partial ordering. A coordinate transformation $(\alpha_1, \ldots, \alpha_n)$ to $(\theta, \phi, v_1, \ldots, v_{n-2})$ is performed using the constraint that $\underline{V}$ in the MAS is

$$\begin{aligned} \underline{V}' &= |\underline{V}'| (\sin\theta \cos\phi, \sin\theta \sin\phi, \cos\theta) \\ &= \left[\prod_{i=1}^{n} R_i(\alpha_i) \right] \underline{V} \end{aligned} \tag{6}$$

where $\underline{V}$ is the vector of interest in the LAS (see Appendix I for the convention used for rotation matrices). Application of the n dimensional change of variable theorem [5-7] yields

$$\begin{aligned} \langle I \rangle = \int_0^{\pi} \int_0^{2\pi} I(\theta,\phi) \, d\theta \, d\phi \int_{v_1} \cdots \int_{v_{n-2}} & W(\theta, \phi, v_1, \ldots, v_{n-2}, \underline{\Delta}) \\ & \times J(\theta, \phi, v_1, \ldots, v_{n-2}) \, d\underline{v} \end{aligned} \tag{7}$$

where J is the Jacobian of the transformation. By comparison with Eq. (1) we have

$$D(\theta,\phi,\underline{\Delta}) = \int_{v_1} \cdots \int_{v_{n-2}} W(\theta,\phi,v_1,\ldots,v_{n-2},\underline{\Delta}) \times J(\theta,\phi,v_1,\ldots,v_{n-2})d\underline{v} \quad (8)$$

A. EVALUATION OF $D(\theta,\phi,\underline{\Delta})$ FROM A MODEL

The spectroscopic simulation technique discussed above is based on the density of states function $D(\theta,\phi,\underline{\Delta})$ given in Eq. (8). I present here details of how $D(\theta,\phi,\underline{\Delta})$ is obtained in practice. The key step is to determine the set of n rotations $R_1(\alpha_1)$, ..., $R_n(\alpha_n)$ that generate the partially ordered ensemble of MAS's. The orientation of a given member of the ensemble is specified by $\underline{\alpha} = (\alpha_1, \ldots, \alpha_n)$. The density of states is determined by the weighting function $W(\underline{\alpha},\underline{\Delta})$ which gives the probability that a member of the ensemble has orientation $\underline{\alpha}$ (see Eq. (8)). Because it takes only three angles to specify the orientation of the MAS with respect to the LAS, one might ask why n would ever be greater than three. The answer is that the n rotations are chosen to utilize symmetry properties of the system and allow one to write down $W(\underline{\alpha},\underline{\Delta})$ by inspection. In contrast, if only three rotations, such as the Euler rotations, are used, it is not possible in general to construct $W(\underline{\alpha},\underline{\Delta})$ in a straightforward fashion. In fact the problem of constructing $W(\underline{\alpha},\underline{\Delta})$ becomes equivalent to the problem of finding $D(\theta,\phi,\underline{\Delta})$.

1. Density of states for a thin film

As an example, consider an ensemble of prolate cylindrical particles that are oriented by drying in a thin film. The LAS (xyz) is defined such that the xz plane is the plane of the film with its normal along the y axis. The MAS (x'y'z') will be taken with the z' axis along

the long axis of the cylinder. A reasonable model for this system is that the particles tend to align such that the angle between the long axis of the cylinder and the plane of the film, α_2, is zero. That is, the probability distribution in α_2 is

$$W_{DF}(\alpha_2,\underline{\Delta}) = \exp(-E(\alpha_2,\underline{\Delta})/kT) \tag{9}$$

where $E(\alpha_2,\underline{\Delta})$ is a potential energy function with a minimum at $\alpha_2 = 0$. The ensemble of MAS's can be generated by beginning with the MAS aligned with the LAS and applying the following three rotations: 1) a free rotation of α_1 about the z axis, 2) a rotation of α_2 weighted by Eq. (9) about the x axis, and 3) a free rotation of α_3 about the y axis. The probability that a particular member of the ensemble has orientation $\underline{\alpha} = (\alpha_1,\alpha_2,\alpha_3)$ is given by Eq. (9).

Let $\underline{V}'$ be the direction of interest in the MAS, then $D(\theta,\phi,\underline{\Delta})$ is the probility that $\underline{V}'$ has spherical angles θ and ϕ in the MAS. In Ref. [5], we assigned the z axis to the axis of the first rotation (as was done above) and showed that the Jacobian in Eq. (8) is

$$J = \sin\theta\,[|\partial V_z'(\underline{\alpha})/\partial\alpha_n|(v_1, \ldots, v_{n-2},\theta)] \tag{10}$$

and that Eq. (8) reduces to

$$D(\theta,\phi,\underline{\Delta}) = \frac{\sin\theta}{N}\int_{v_1}\cdots\int_{v_{n-2}} \frac{W(\underline{a},\underline{\Delta})\,d\underline{v}}{\left|\frac{\partial V_z(\underline{\alpha})}{\partial\alpha_n}\right|_{v_1, \ldots, v_{n-2},\theta}} \tag{11}$$

where N is a normalization constant,

$$\alpha_1 = -\phi + f_1(v_1, \ldots, v_{n-2},\theta)$$

$$\begin{aligned} \alpha_2 &= v_1 \\ &\cdot \\ &\cdot \\ &\cdot \\ \alpha_{n-1} &= v_{n-2} \\ \alpha_n &= f_2(v_1, \ldots, v_{n-2}, \theta) \end{aligned} \tag{12}$$

$|\partial V_z'(\underline{\alpha})/\partial\alpha_n|$ is the indicated partial derivative with $\alpha_1, \ldots, \alpha_n$ replaced by the transformed variables in Eq. (12), $f_1(v_1, \ldots, v_{n-2}, \theta)$ and $f_2(v_2, \ldots, v_{n-2}, \theta)$ are determined by the constraints in Eq. (6) and $d\underline{v}$ includes all the necessary volume elements. To illustrate, we will consider a polarized absorption experiment on a dried film with $\underline{V}$ in the LAS equal to $(\cos\psi, \sin\psi, 0)$. Application of Eq. (11) yields (see Appendix II)

$$D(\theta,\underline{\Delta}) = \frac{\sin\theta}{N}\int_{-\theta-\psi}^{\theta-\psi} \cos v_1 \, W_{DF}(v_1,\underline{\Delta}) \times \{[\sin v_1+\sin(\theta+\psi)][\sin(\theta-\psi)-\sin v_1]\}^{-1/2} dv_1 \tag{13}$$

Note that $D(\theta,\underline{\Delta})$ is axially symmetric. In fact, any density of states derived from a rotation scheme where the first rotation is unrestricted will be axially symmetric. The reason is that the only occurance of ϕ in Eqs. (11-12) is in the equation for α_1, and if the first rotation is unrestricted (i.e. $W(\alpha,\underline{\Delta})$ independent of α_1), $D(\theta,\underline{\Delta})$ will be independent of ϕ.

2. Three-Rotation Density of States - Evaluation by Chebyshev Quadrature

The integral in Eq. (13) must be evaluated numerically, a task which is complicated by the singularities of the integrand at the

endpoints. All density of states calculations that we have attempted have similar singularities, but the problem can be circumvented. By making the substitution

$$v_1(x) = \sin^{-1}(x \sin\theta \cos\psi - \sin\psi \cos\theta) \tag{14}$$

Eq. (13) can be transformed to

$$D(\theta,\underline{\Delta}) = \frac{\sin\theta}{N} \int_{-1}^{1} W_{DF}(v_1(x),\underline{\Delta})(1-x^2)^{-1/2}dx \tag{15}$$

the function $(1-x^2)^{-1/2}$ is the kernal for Chebyshev quadrature and, therefore, Eq. (15) is trivial to evaluate by numerical techniques. The result to Qth order quadrature is

$$D(\theta,\underline{\Delta}) = \frac{\pi\sin\theta}{QN} \sum_{i=1}^{Q} W_{DF}(v_1(x_i),\underline{\Delta}) \tag{16}$$

where

$$x_i = \cos\left(\frac{\pi(2i-1)}{2Q}\right) \tag{17}$$

The dried film model is an example of a zxy rotation scheme. If one picks the z axis as the axis of the first rotation, the only possible three-rotation schemes are zxy, zyx, zyz, and zxz. Furthermore, zxy and zyz are related to zyx and zxz by a simple exchange of x and y, which means that the only two unique three-rotation schemes are zxy and zyz. We will now consider all possible three-rotation density of states, but first it is convenient to introduce a general notation for density of states functions. The notation is

$$D^{RS}_{v,\psi}[\theta,\phi,W] \tag{18}$$

where RS is the rotation scheme (e.g. zyz, zxy, zxyz, etc.), v is the type of $\underline{V}$ field vector [v=1 for $\underline{V}=(\cos\psi, \sin\psi, 0)$, v=2 for $\underline{V}=(\cos\psi, 0, \sin\psi)$, and v=3 for $\underline{V}=(0, \cos\psi, \sin\psi)$], ψ is the angle of the $\underline{V}$ field vector, and W is the weighting function. As an example, the density of states for dried films in Eq. (16) is denoted by

$$D(\theta,\underline{\Delta}) = D^{zxy}_{1,\psi}[\theta,W_{DF}] \tag{19}$$

We find that all three-rotation density of states can be reduced to Chebyshev quadrature integrals. Analagous the Eq. (16), we write in the new notation

$$D^{RS}_{v,\psi}[\theta,\phi,\underline{\Delta}] = \frac{1}{N}\sum_{i=1}^{Q} W(\alpha_1(\theta,\phi,x_i),\alpha_2(\theta,x_i),\alpha_3(\theta,x_i),\underline{\Delta}) \tag{20}$$

where x_i is given by Eq. (17) and N is a normalization constant. In Table II-I we quote the functional forms of $\alpha_1(\theta,\phi,x_i)$, $\alpha_2(\theta,x_i)$, and $\alpha_3(\theta,x_i)$ for rotation schemes equal to zyz and zxy and v equal to 1, 2, and 3.

3. Four-Rotation Density of States

Next, we proceed to the density of states for models that require four rotations. In general, these density of states functions are much more difficult to calculate, and we will treat only the axially symmetric $D(\theta,\underline{\Delta})$; i.e. the case when $W(\underline{\alpha},\underline{\Delta})$ is independent of α_1. As will be explained later, it is straightforward to extend our results to cases that lack axial symmetry. We also make the simplifying assumption

Table II-I: The functional forms of $\alpha_1(\theta,\phi,x_i)$, $\alpha_2(\theta,x_i)$, and $\alpha_3(\theta,x_i)$ in Eq. (20). The normalization constant in Eq. (20) is chosen such that

$$\int_0^{\pi/2} d\phi \int_0^{\pi/2} d\theta \, D^{RS}_{v,\psi}[\theta,\phi,W] = 1;$$

Q is chosen to insure convergence of the numerical integration formula (Q=25 is usually sufficient).

a. Both the + and - forms of $\alpha_3(\theta,x)$ must be included in the sum in Eq. (20).

b. These formulas are inconvenient when the denominators are zero; instead use

$$D^{zyz}_{2,\pi/2}[\theta,\phi,W] = D^{zyz}_{3,\pi/2}[\theta,\phi,W]$$
$$= \frac{\sin\theta}{N} \int_0^{\pi/2} D\alpha_3 W(\alpha_1,\alpha_2,\alpha_3,\underline{\Delta})$$

where $\alpha_1 = \phi$ and $\alpha_2 = \theta$.

c. These formulas are inconvenient when the denominators are zero; instead use

$$D^{zxy}_{1,\pi/2}[\theta,\phi,W] = D^{zxy}_{3,0}[\theta,\phi,W]$$
$$= \frac{\sin\theta}{N} \int_0^{\pi/2} d\alpha_3 W(\alpha_1,\alpha_2,\alpha_3,\underline{\Delta})$$

where $\alpha_1 = \pi/2 - \phi$ and $\alpha_2 = \theta - \pi/2$.

Table II-I (part 1)

RS	v	$\alpha_2(\theta,x)$	$\alpha_3(\theta,x)$	
zyz	1	$\cos^{-1}[\sin\theta\sqrt{(1-x)/2}\,]$	$\psi\pm\cos^{-1}(\frac{\cos\theta}{\sin\alpha_2})$	a
zyz	2	$\cos^{-1}(x\cos\psi\sin\theta+\sin\psi\cos\theta)$	$\cos^{-1}(\frac{\cos\theta-\sin\psi\cos\alpha_2}{\cos\psi\sin\alpha_2})$	b
zyz	3	$\cos^{-1}(x\cos\psi\sin\theta+\sin\psi\cos\theta)$	$\sin^{-1}(\frac{\cos\theta-\sin\psi\cos\alpha_2}{\cos\psi\sin\alpha_2})$	b
zxy	1	$\sin^{-1}(x\cos\psi\sin\theta-\sin\psi\cos\theta)$	$\sin^{-1}(\frac{\cos\theta+\sin\psi\sin\alpha_2}{\cos\psi\cos\alpha_2})$	c
zxy	2	$\sin^{-1}[\sin\theta\sqrt{(1-x)/2}\,]$	$\pm\psi+\sin^{-1}(\frac{\cos\theta}{\cos\alpha_2})$	a
zxy	3	$\sin^{-1}(x\sin\psi\sin\theta-\cos\psi\cos\theta)$	$\cos^{-1}(\frac{\cos\theta+\cos\psi\sin\alpha_2}{\sin\psi\cos\alpha_2})$	c

TABLE II-I (part 2)

RS	v	$\alpha_1(\theta,\phi,x)$
zyz	1	$-\phi+\cos^{-1}(\lvert\cot\alpha_2\cot\theta\rvert)$
zyz	2	$-\phi+\sin^{-1}\left(\left\lvert\frac{\cos\psi\sin\alpha_3}{\sin\theta}\right\rvert\right)$
zyz	3	$-\phi+\sin^{-1}\left(\left\lvert\frac{\cos\psi\cos\alpha_3}{\sin\theta}\right\rvert\right)$
zxy	1	$-\phi+\sin^{-1}\left(\left\lvert\frac{\cos\psi\cos\alpha_3}{\sin\theta}\right\rvert\right)$
zxy	2	$-\phi+\sin^{-1}(\lvert\tan\alpha_2\cot\theta\rvert)$
zxy	3	$-\phi+\sin^{-1}\left(\left\lvert\frac{\sin\psi\sin\alpha_3}{\sin\theta}\right\rvert\right)$

that the weighting function can be factored to

$$W(\underline{\alpha}) = W_1(\alpha_4)W_2(\alpha_2,\alpha_3) \tag{21}$$

This assumption is not crucial, but it is applicable to the density of states that have concerned us [8]; furthermore, it leads to a simplification of the formulas.

Let us consider an example - we will calculate $D^{zxyz}_{1,\psi}[\theta,W_1W_2]$. Application of Eq. (11) yields (see Appendix III)

$$D^{zxyz}_{1,\psi}[\theta,W_1W_2] = \frac{\sin\theta}{N}\int_0^{2\pi} dv_2 W_1(v_2) \int_{-\theta-\psi+v_2}^{\theta-\psi+v_2} \cos v_1$$
$$\times W_2[v_1,\alpha_3(v_1,v_2,\theta)]\{[\sin v_1+\sin(\theta+\psi-v_2)]$$
$$\times [\sin(\theta-\psi+v_2)-\sin v_1]\}^{-1/2}dv_1 \tag{22}$$

The v_1 integral together with the $\sin\theta$ is identical to Eq. (13) except that the ψ in Eq. (13) is replaced by $\psi-v_2$, there is no normalization constant, and W_{DF} is replaced be W_2. Because the normalization constant in Eq. (13) is independent of ψ, we can write

$$D^{zxyz}_{1,\psi}[\theta,W_1W_2] = \frac{1}{N}\int_0^{2\pi} dv_2 W_1(v_2) D^{zxy}_{1,\psi-v_2}[\theta,W_2] \tag{23}$$

We now utilize the symmetry properties of $W_1(v_2)$ and $D^{zxy}_{1,\psi}[\theta,W_2]$ to simplify Eq. (23). Because partial ordering is induced by some force, the sign of whose direction is arbitrary, $W_1(v_2)$ is periodic with period π and symmetric about $\pi/2$; i.e. $W_1(v_2) = W_1(v_2+\pi)$ and $W_1(v_2) = W_1(\pi-v_2)$. For weighting functions possessing these symmetry properties, the density of states has similar properties with respect to ψ; i.e.

$$D^{zxy}_{1,\psi}[\theta,W_2] = D^{zxy}_{1,\psi+\pi}[\theta,W_2] \tag{24}$$

and

$$D^{zxy}_{1,\psi}[\theta,W_2] = D^{zxy}_{1,\pi-\psi}[\theta,W_2] \tag{25}$$

Finally, using these symmetry properties, Eq. (23) reduces to

$$D^{zxyz}_{1,\psi}[\theta,W] = \frac{2}{N}\int_0^{\pi/2} d\mu\; D^{zxy}_{1,\mu}[\theta,W_2][W_1(\psi-\mu)+W_1(\psi+\mu)] \tag{26}$$

Equation (26) may not appear to be simpler than Eq. (23), but the extent of integration is decreased from the interval 0 to 2π to the interval 0 to $\pi/2$. When numerical integration techniques are used this reduction will save computer time.

In Table II-II, we present many four-rotation density of states functions. Five characteristics of these functions are: 1) If the field has no component along the axis of the last rotation, the density of states can always be written as an integral over a three-rotation density of states analagous to Eq. (26). 2) If the field is along the axis of the last rotation, the last rotation is superfluous and the density of states is identical to the density of states function for the first three rotations. 3) If the field has a nonzero component along the axis of the last rotation and a nonzero component along another axis, evaluation of the density of states becomes very complicated. We do not consider this case. 4) These formulas are formally valid for nonaxially symmetric systems, except that new functional forms for α_1 in Table I must be used. These functional forms (which we have not evaluated) can be found from the constraints in Eq. (6). 5) When only the second

Table II-II: Functional form of many density of states functions for ensembles generated by four rotations. The normalization constant is chosen such that

$$\int_0^{\pi/2} d\theta \int_0^{\pi/2} d\phi \; D^{RS}_{v,\psi}[\theta,\phi,W] = 1;$$

W_1 and W_2 are the weighting functions for the last rotation, and the second and third rotations respectively (see text); the three-rotation density of states functions can be evaluated by use of Eq. (20) and Table II-I.

a. These are the values of Ψ for which the formula is valid.

TABLE II-II

RS	v	ψ[a]	$D^{RS}_{v,\psi}[\theta,\phi,W]$
zyzy	1	$\pi/2$	$D^{zyz}_{1,\pi/2}[\theta,\phi,W_2]$
zyzy	2	all	$\frac{1}{N}\int_0^{\pi/2} d\mu\, D^{zyz}_{2,\mu}[\theta,\phi,W_2][W_1(\mu-\psi)+W_1(\pi-\mu-\psi)]$
zyzy	3	0	$D^{zyz}_{1,\pi/2}[\theta,\phi,W_2]$
zyzx	1	0	$D^{zyz}_{1,0}[\theta,\phi,W_2]$
zyzx	2	0	$D^{zyz}_{1,0}[\theta,\phi,W_2]$
zyzx	3	all	$\frac{1}{N}\int_0^{\pi/2} d\mu\, D^{zyz}_{3,\mu}[\theta,\phi,W_2][W_1(\mu-\psi)+W_1(\pi-\mu-\psi)]$
zxyx	1	0	$D^{zxy}_{1,0}[\theta,\phi,W_2]$
zxyx	2	0	$D^{zxy}_{1,0}[\theta,\phi,W_2]$
zxyx	3	all	$\frac{1}{N}\int_0^{\pi/2} d\mu\, D^{zxy}_{3,\mu}[\theta,\phi,W_2][W_1(\mu-\psi)+W_1(\pi-\mu-\psi)]$
zxyz	1	all	$\frac{1}{N}\int_0^{\pi/2} d\mu\, D^{zxx}_{1,\mu}[\theta,\phi,W_2][W_1(\mu-\psi)+W_1(\pi-\mu-\psi)]$
zxyz	2	$\pi/2$	$D^{zxy}_{2,\pi/2}[\theta,\phi,W_2]$
zxyz	3	$\pi/2$	$D^{zxy}_{2,\pi/2}[\theta,\phi,W_2]$

rotation is weighted, the v_2 integral can be rewritten as a complete elliptical integral [5]. When computer time is limited, this approach can save computer time [7].

B. LINEAR DICHROISM

Reference [9] gives examples of calculations for several types of spectroscopies whose response functions depend on only one vector. The examples include linear dichroism, circular dichroism, and magnetic resonance. In this section, I will give a detailed example for the use of density of states functions in the analysis of linear dichroism. I will try to emphasize calculation techniques. Much of this section has already been presented in Ref. [10].

1. Theory

The dichroic ratio R of an absorption band is defined as the ratio of integrated absorption bands measured with light polarized parallel, $\underline{E}_H$, and perpendicular, $\underline{E}_V$, to a given direction; i.e. $R = A_H/A_V$ where A_H and A_V are the integrated absorbances. Most reported forms of linear dichroism can be related to R by simple algebra. One notable exception is for experiments that directly measure $A_H - A_V$ [11-13] and normalize by dividing by A_r which is the absorbance of the corresponding randomly oriented sample. We call this form the dichroic polarization L, defined as $L = (A_H-A_V)/A_r$. When the laboratory reference frame is axially symmetric, L can be related to R, but in the general nonaxially symmetric case, L cannot be related to R. Therefore, we also derive formulas for L.

We define two density of states functions $D_H(\theta,\phi,\underline{\Delta})$ and $D_V(\theta,\phi,\underline{\Delta})$.

These are the density of states functions for $\underline{E}_H$ and $\underline{E}_V$ in the MAS. These electric fields will interact with the transition moment $\underline{\mu}$ which is fixed with respect to the MAS; that is, a unit vector $\hat{\mu} = (\mu_x, \mu_y, \mu_z)$ in the direction of the transition moment $\underline{\mu}$ is a constant vector in the MAS. Using the density of states formalism, we can now develop a new approach to the theory of linear dichroism.

We begin by calculating A_H. The absorbance of a transition moment $\underline{\mu}$ interacting with a polarized field $\underline{E}$ is proportional to $(\underline{\mu}\cdot\underline{E})^2$. For a partially ordered ensemble interacting with $\underline{E}_H$, the absorbance is

$$A_H = \frac{K}{N} \int_0^{\pi} d\theta \int_0^{2\pi} d\phi \; (\hat{\mu}\cdot\underline{E})^2 D_H(\theta,\phi,\underline{\Delta}) \tag{27}$$

where $\underline{E} = |\underline{E}|(\sin\theta\cos\phi, \sin\theta\sin\phi, \cos\theta)$, $\mu = (\mu_x,\mu_y,\mu_z)$ is a constant vector (see Fig. II-2), K is an experimental constant which includes such parameters as extinction coefficient, concentration, and path length, and N is a normalization constant. Throughout this section, we use unnormalized density of states functions; the N in the denominator given by

$$N = \int_0^{\pi} d\theta \int_0^{2\pi} d\phi \; D_H(\theta,\phi,\underline{\Delta}) \tag{28}$$

provides the required normalization. As above, $D_H(\theta,\phi,\underline{\Delta})$ is periodic with period π and symmetric about $\pi/2$ with respect to both θ and ϕ. Using only these symmetry properties, Eq. (27) reduces to

$$A_H = K'(\mu_x^2[T_H(\underline{\Delta})-F_H(\underline{\Delta})]+\mu_y^2 F_H(\underline{\Delta})+\mu_z^2[1-T_H(\underline{\Delta})]) \tag{29}$$

where K' is a new constant,

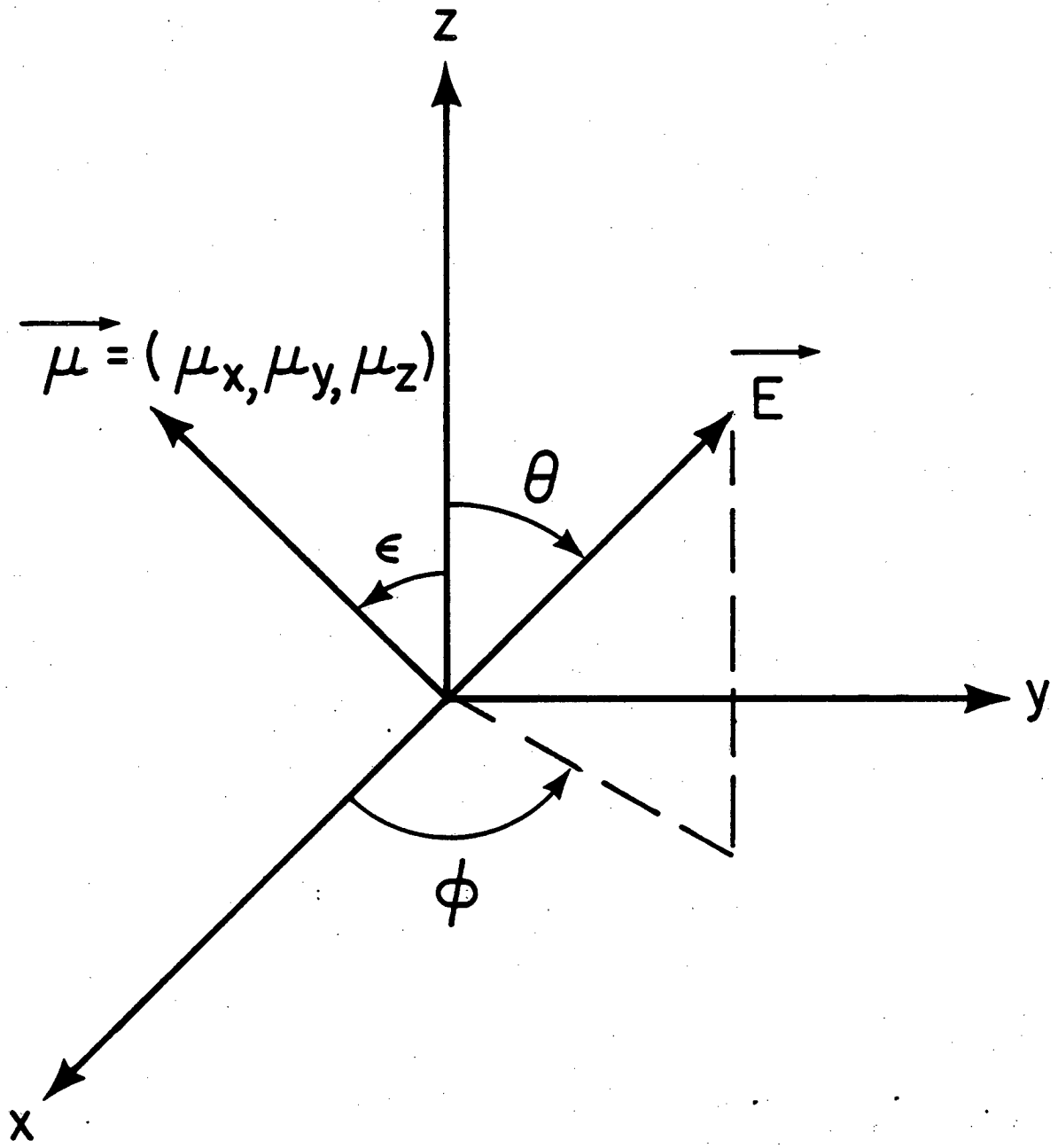

Figure II-2: Arrangement of $\underline{\mu}$ and $\underline{E}$ in the MAS. θ and ϕ are the spherical angles of $\underline{E}$.

$$T_H(\underline{\Delta}) = \int_0^{\pi/2} d\theta \sin^2\theta \int_0^{\pi/2} d\phi\, D_H(\theta,\phi,\underline{\Delta})/N_H(\underline{\Delta}) \tag{30}$$

$$F_H(\underline{\Delta}) = \int_0^{\pi/2} d\theta \sin^2\theta \int_0^{\pi/2} d\phi \sin^2\phi\, D_H(\theta,\phi,\underline{\Delta})/N_H(\underline{\Delta}) \tag{31}$$

and

$$N_H(\underline{\Delta}) = \int_0^{\pi/2} d\theta \int_0^{\pi/2} d\phi\, D_H(\theta,\phi,\underline{\Delta}) \tag{32}$$

In a random sample, $A_H = A_r$, $D_H(\theta,\phi,\underline{\Delta}) = \sin\theta$, $T_H(\underline{\Delta}) = 2/3$, and $F_H(\underline{\Delta}) = 1/3$. Using these facts, we find that $K' = 3A_r$ and Eq. (29) for the ordered sample becomes

$$A_H = 3A_r(\mu_x^2[T_H(\underline{\Delta})-F_H(\underline{\Delta})]+\mu_y^2 F_H(\underline{\Delta})+\mu_z^2[1-T_H(\underline{\Delta})]) \tag{33}$$

An analogous expression holds for A_V where we define $T_V(\underline{\Delta})$, $F_V(\underline{\Delta})$, and $N_V(\underline{\Delta})$ using $D_V(\theta,\phi,\underline{\Delta})$. The dichroic ratio is thus given by

$$R = \frac{A_H}{A_V} = \frac{\mu_x^2[T_H(\underline{\Delta})-F_H(\underline{\Delta})]+\mu_y^2 F_H(\underline{\Delta})+\mu_z^2[1-T_H(\underline{\Delta})]}{\mu_x^2[T_V(\underline{\Delta})-F_V(\underline{\Delta})]+\mu_y^2 F_V(\underline{\Delta})+\mu_z^2[1-T_V(\underline{\Delta})]} \tag{34}$$

and the dichroic polarization is given by

$$\begin{aligned} L = (A_H-A_V)/A_r = 3\{&\mu_x^2[T_H(\underline{\Delta})-T_V(\underline{\Delta})+F_V(\underline{\Delta})-F_H(\underline{\Delta})] \\ &+\mu_y^2[F_H(\underline{\Delta})-F_V(\underline{\Delta})]+\mu_z^2[T_V(\underline{\Delta})-T_H(\underline{\Delta})]\} \end{aligned} \tag{35}$$

Equations (34) and (35) take simpler forms when the density of states depends only on θ and $\underline{\Delta}$, which happens whenever the molecular

reference frame is axially symmetric. Equations (30) and (31) become

$$T_H(\underline{\Delta}) = \int_0^{\pi/2} d\theta \sin^2\theta D_H(\theta,\underline{\Delta}) \Big/ \int_0^{\pi/2} d\theta D_H(\theta,\underline{\Delta}) \tag{36}$$

and

$$F_H(\underline{\Delta}) = \tfrac{1}{2}T_H(\underline{\Delta}) \tag{37}$$

The dichroic ratio reduces to

$$R = \frac{T_H(\underline{\Delta})+\mu_z^2[2-3T_H(\underline{\Delta})]}{T_V(\underline{\Delta})+\mu_z^2[2-3T_V(\underline{\Delta})]} \tag{38}$$

If the laboratory reference frame is also axially symmetric and $\underline{E}_H$ is along the symmetry axis

$$A_r = \tfrac{1}{3}(A_H + 2A_V) \tag{39}$$

When Eq. (39) holds, L is given by $3(A_H-A_V)/(A_H+2A_V)$. In this form L can easily be related to R. If $\underline{E}_H$ is not along a laboratory symmetry axis, Eq. (39) is no longer valid but we can still write

$$L = \tfrac{3}{2}\{[T_V(\underline{\Delta})-T_H(\underline{\Delta})](3\mu_z^2-1)\} \tag{40}$$

We choose the z axis to be the axis of symmetry in the MAS. The angle between the z axis and the transition moment $\underline{\mu}$ is (see Fig. II-2) $\varepsilon = \cos^{-1}\mu_z$. From Eq. (38)

$$\varepsilon = \cos^{-1}\left[\frac{1}{3+\dfrac{2(1-R)}{RT_V(\underline{\Delta})-T_H(\underline{\Delta})}}\right]^{1/2} \tag{41}$$

We now consider some special cases of Eq. (38). One type of perfect ordering is where all the molecular z axes line up with the laboratory z axis. If linear dichroism is measured with $\underline{E}_H = (0,0,1)$ and $\underline{E}_V = (1,0,0)$, we have $D_H(\theta) = \delta(\theta)$, $D_V(\theta) = \delta(\pi/2 - \theta)$, $T_H(\theta) = 0$ and $T_V(\theta) = 1$ where δ is the Dirac delta function. Substitution into Eq. (38) gives the result first derived by Fraser [14]

$$R = 2\cot^2\varepsilon \tag{42}$$

The opposite extreme is a random sample where $D_H(\theta) = D_V(\theta) = \sin\theta$ and $T_H = T_V = 2/3$. The dichroic ratio is 1; i.e. there is no linear dichroism. In the general partially ordered case, a calculation of $T_H(\underline{\Delta})$ and $T_V(\underline{\Delta})$ is sufficient to interpret the linear dichroism.

2. An Example: Rhodopseudomonas sphaeroides in Stretched Film

In this section, I will apply the above theory to an example. Most reports of dichroic ratios are ratios of the peak absorbances and not the integrated absorbances. As long as the parallel and perpendicular lineshapes do not differ too much, the ratio of peak absorbances is a close approximation to the "true" dichroic ratio. We will ignore this difficulty. Another difficulty arises from band overlap of several transitions making it difficult to measure the dichroic ratio for a particular transition. In this example, I avoid this problem by analyzing a relatively pure transition.

The plan of attack for analyzing a linear dichroism experiment is the same for all systems. First, from a characterization of the absorption spectrum, one decides which bands are pure enough for an analysis. Second, from consideration of the symmetry properties of the

system, one calculates $D_H(\theta,\phi,\underline{\Delta})$ and $D_V(\theta,\phi,\underline{\Delta})$. Last, the formulas in the last section are used to extract all of the possible structural information.

Two papers by Rafferty and Clayton [15,16] describe the linear dichroism spectra of reaction centers of Rhodopseudomonas sphaeroides in stretched films. The reaction center particles contain four bacteriochlorophyll a molecules and two bacteriopheophytin a molecules which all contribute to a complicated absorption spectrum [17]. We choose to study the 860nm transition because it is believed to be a pure transition of P860, which is a Bacteriochlorophyll a dimer that functions as the primary electron donor in Rhodopseudomonas sphaeroides [18].

We assume, as did Rafferty and Clayton [15,16], that the reaction center particles possess an axis of symmetry which tends to align with the stretch direction. As a first approximation, this partially ordered ensemble can be generated by the following rotation scheme (see Fig. II-3): 1) a free rotation of α_1 about the laboratory z axis, 2) a weighted rotation of α_2 about the laboratory y axis, and 3) a free rotation of α_3 about the laboratory z axis. The second rotation is weighted by the probability that the symmetry axis of the particle tilts by α_2 from the plane of the film. Having no justification for anything else, we choose to weight the second rotation by a Gaussian

$$W_G(\beta,\Delta_G) = \exp(-\alpha_2^2/\Delta_G^2) \tag{43}$$

where Δ_G is the only parameter for the density of states function and it describes the width of the Gaussian for the stretched film. We call this model the symmetric uniaxial model (Note: to retain correct symmetry

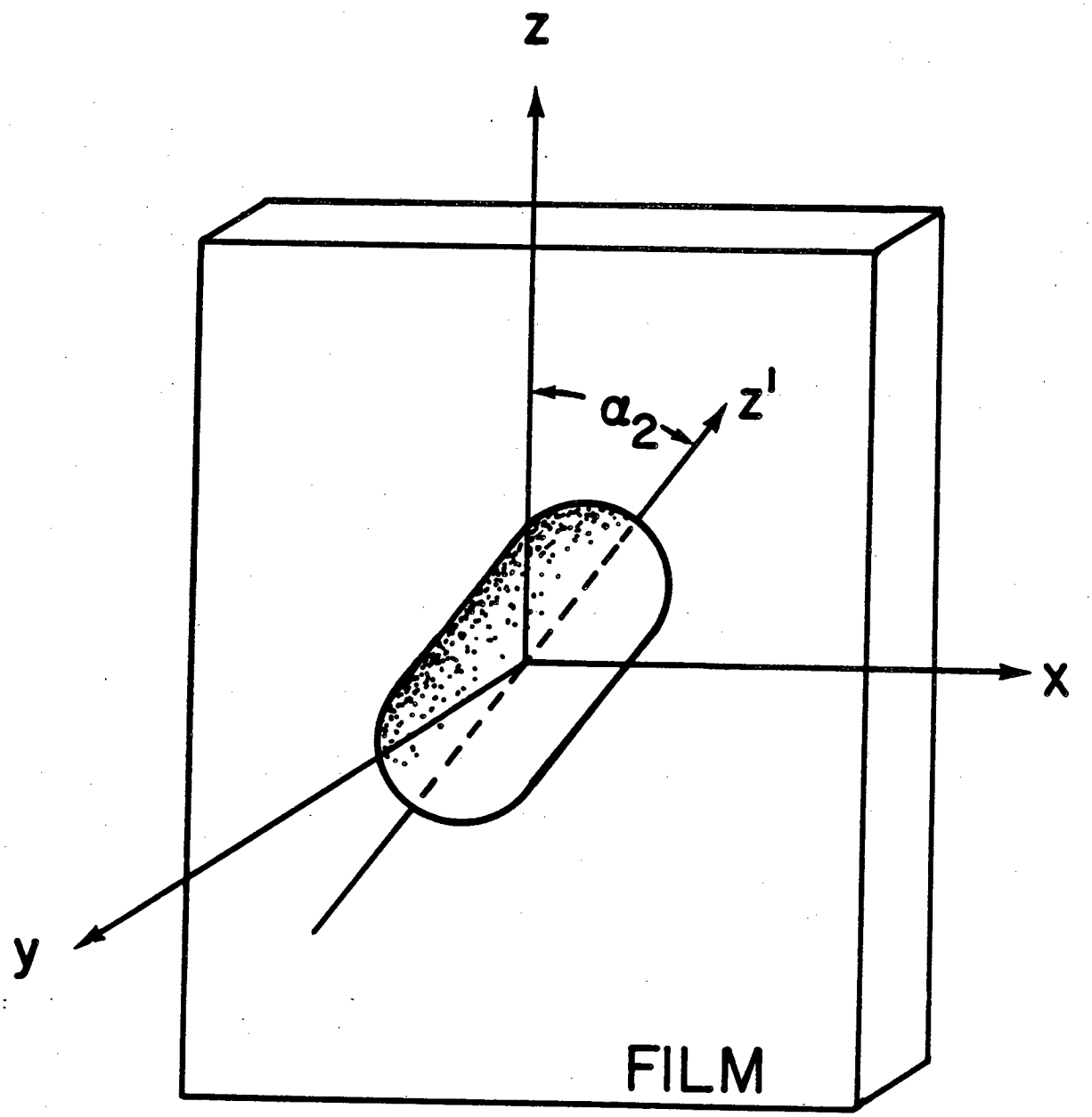

Figure II-3: Orientation of macromolecular structure in a stretched film. z' defines the symmetry axis of the macromolecular structure, and α_2 is the angle between z' and the stretch direction along the the laboratory z axis.

properties, we use Eq. (43) up to $\alpha_2 = \pi/2$ and extend to other values using the fact that $W_G(\alpha_2, \Delta_G) = W_G(\pi-\alpha_2, \Delta_G)$ and $W_G(\alpha_2, \Delta_G) = W_G(\pi+\alpha_2, \Delta_G)$).

Because the first rotation is unweighted, the density of states function is axially symmetric. In the notation of section A

$$D_H(\theta,\Delta_G) = D^{zyz}_{3,\pi/2}[\theta,W_G] \tag{44}$$

and

$$D_V(\theta,\Delta_G) = D^{zyz}_{1,0}[\theta,W_G] \tag{45}$$

$D_H(\theta,\Delta_G)$ and $D_V(\theta,\Delta_G)$ for several values of Δ_G and $T_H(\Delta_G)$ and $T_V(\Delta_G)$ are plotted in Figs. II-4 to II-6. The dichroic ratio, R, as calculated from Eq. (38) is plotted in Fig. II-7 versus the angle between the symmetry axis of the particle and the transition moment.

At 860 nm, Rafferty and Clayton [15,16] measure R = 2.28 which means $\epsilon < 43^o$. The curves in Fig. II-7 with $\Delta_G > 1.0$ radian never reach 2.28; thus we must have $\Delta_G < 1.0$ radian. We can narrow the limit on Δ_G further by considering the value of R = 0.48 at 597 nm. If we assume 597 nm to be a pure transition, we find Δ_G must be less than 0.75 radians. In reality, the 597 nm transition is not a pure transition, but this means that it must contain at least one transition whose R value is not greater than 0.48. Therefore, the limit of 0.75 radians on Δ_G is a conservative upper limit. Rafferty and Clayton [15,16] did experiments on films that were stretched to different extents. In one such film, they determined R at 860nm to be as high as 2.50. An R of 2.50 means that ϵ must be less than 42^o. Returning to the film where R = 2.28, we find that because the $\Delta_G < 0.30$ radians curves in Fig. II-7 do not go

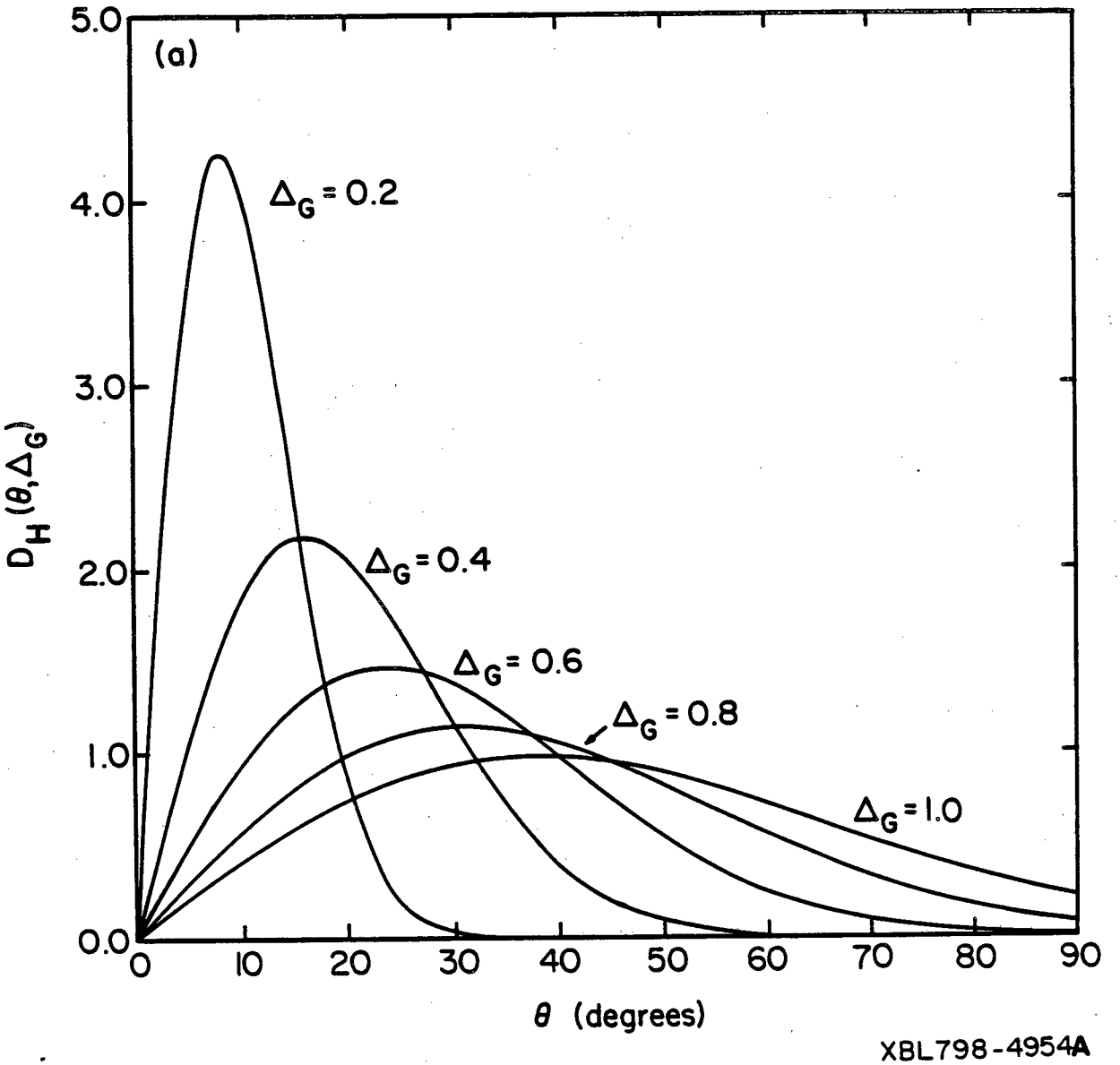

Figure II-4: $D_H(\theta,\Delta_G)$ for the symmetric uniaxial model for several values of Δ_G in radians.

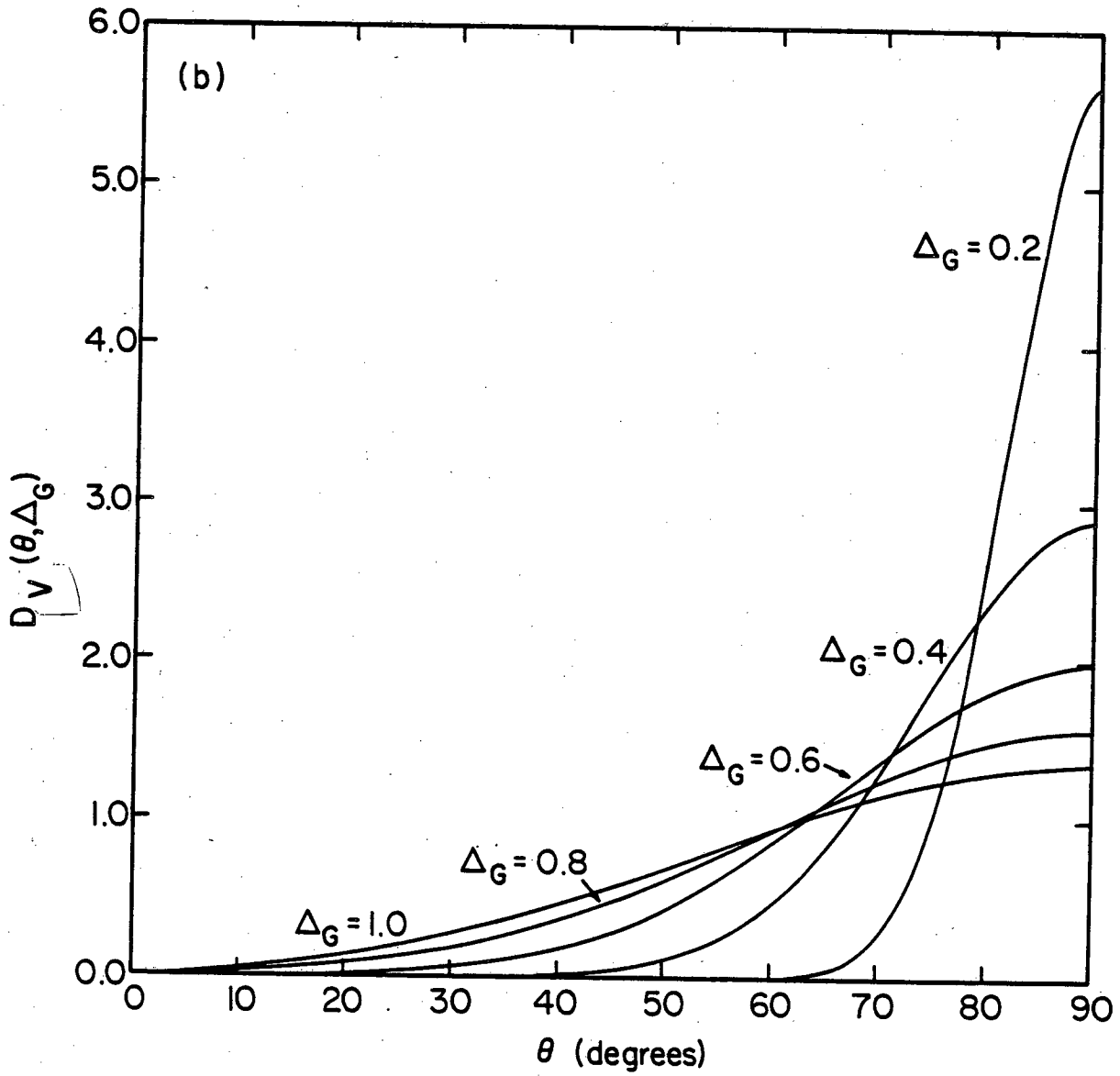

Figure II-5: $D_V(\theta,\Delta_G)$ for the symmetric uniaxial model for several values of Δ_G in radians.

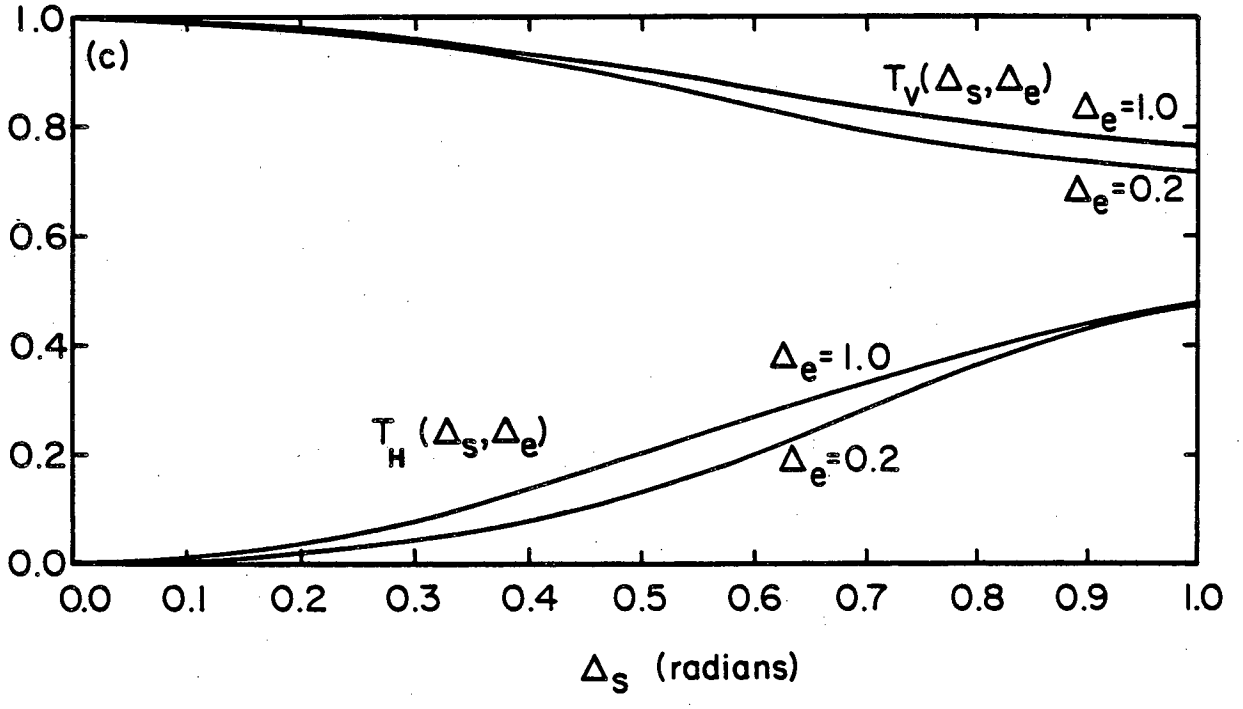

XBL798-4950A

Figure II-6: $T_H(\Delta_G,\Delta_e)$ and $T_V(\Delta_G,\Delta_e)$ for the symmetric uniaxial model (Δ_e = 1.0) and the elliptic uniaxial model with Δ_e = 0.2.

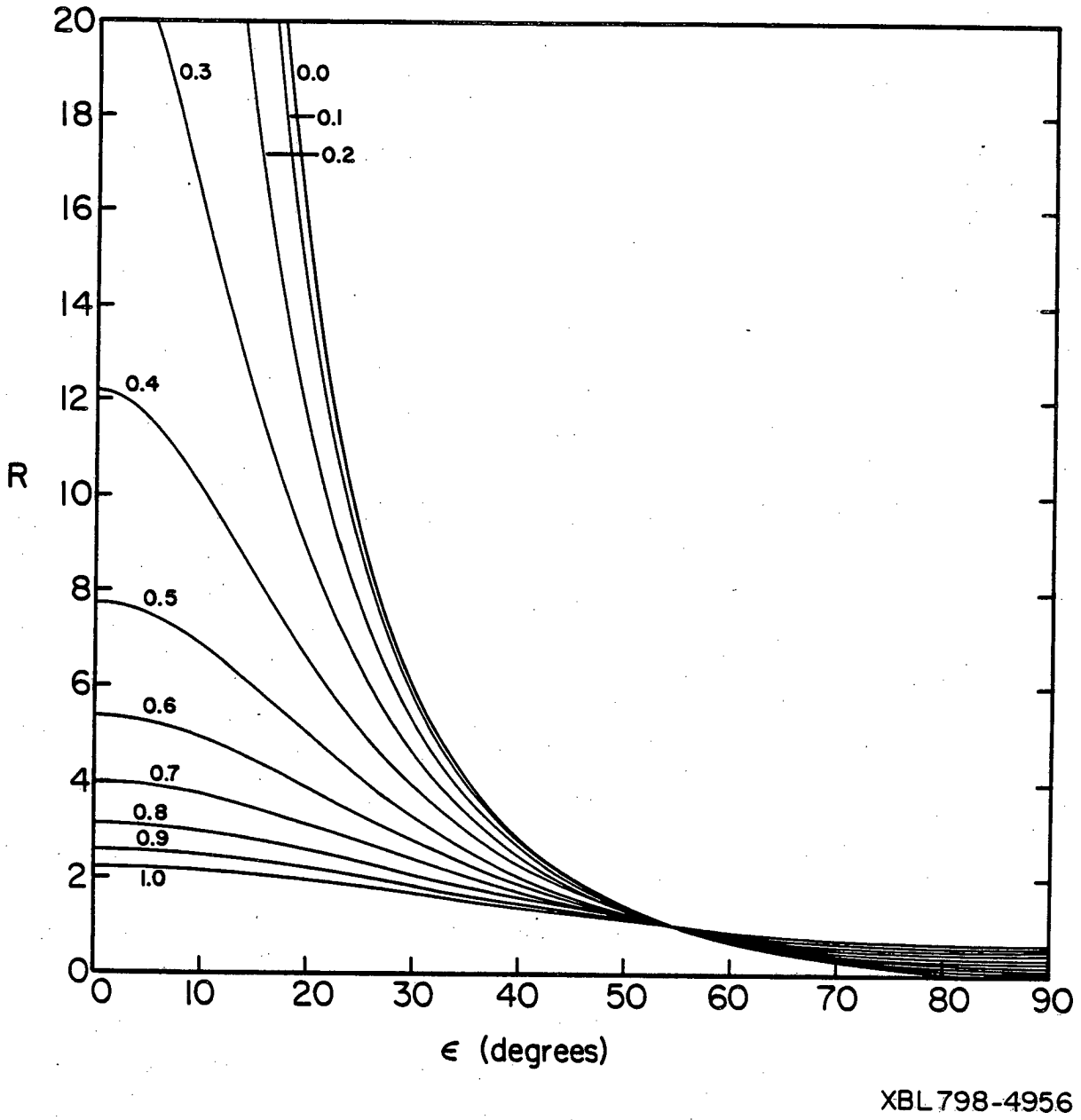

Figure II-7: Dichroic ratio R versus angle ϵ between the transition moment $\underline{\mu}$ and the symmetry axis of the molecular reference frame. The plots are for the symmetric uniaxial model with several values of Δ_G in radians.

below 42^o until R > 2.28, we must have Δ_G > 0.30 radians. The final most conservative limits on Δ_G are

$$0.30 \text{ radians} < \Delta_G < 0.75 \text{ radians} \tag{46}$$

From Eq. (41), the limits on ϵ are

$$29^o < \epsilon < 42^o \tag{47}$$

Perhaps the symmetric uniaxial model is an oversimplification, because it neglects the anisotropy of the unstretched film; i.e., it neglects the possibility that the particle symmetry axes lie in the plane of the unstretched film. We will therefore consider a more sophisticated model. Instead of giving equal weights to all symmetry axes that lie on the circle in Fig. II-8a, we now use the model illustrated in Fig. II-8b where all symmetry axes that lie on an ellipse have equal weights. Upon stretching, it is more likely that the tilt of the particle symmetry axis away from the laboratory z axis is in the plane of the film than out of the plane of the film. Therefore, the ratio of the ellipse axes Δ_e = b/a is less than 1. This model can be generated by the same rotation scheme (zyz) but the total weighting function is changed to

$$W_{EG}(\alpha_2,\alpha_3,\Delta_G,\Delta_e) = \exp(-x^2/\Delta_G{}^2) \tag{48}$$

where

$$x = \tan^{-1}\{\tan\alpha_2[(\sin^2\alpha_3/\Delta_e{}^2) + \cos^2\alpha_3]^{1/2}\} \tag{49}$$

Despite the loss of axial symmetry in the laboratory reference frame, $D_H(\theta,\Delta_G,\Delta_e)$ and $D_V(\theta,\Delta_G,\Delta_e)$ are still axially symmetric. $T_H(\Delta_G,\Delta_e)$ and

Figure II-8: (a) Schematic representation of the symmetric uniaxial model. β is the half angle of the cone centered on the laboratory z axis. (b) Schematic representation of the elliptical uniaxial model. χ is the angle between the laboratory z axis and the line in the yz plane that points to the ellipse. a and b are the major and minor axes of the ellipse.

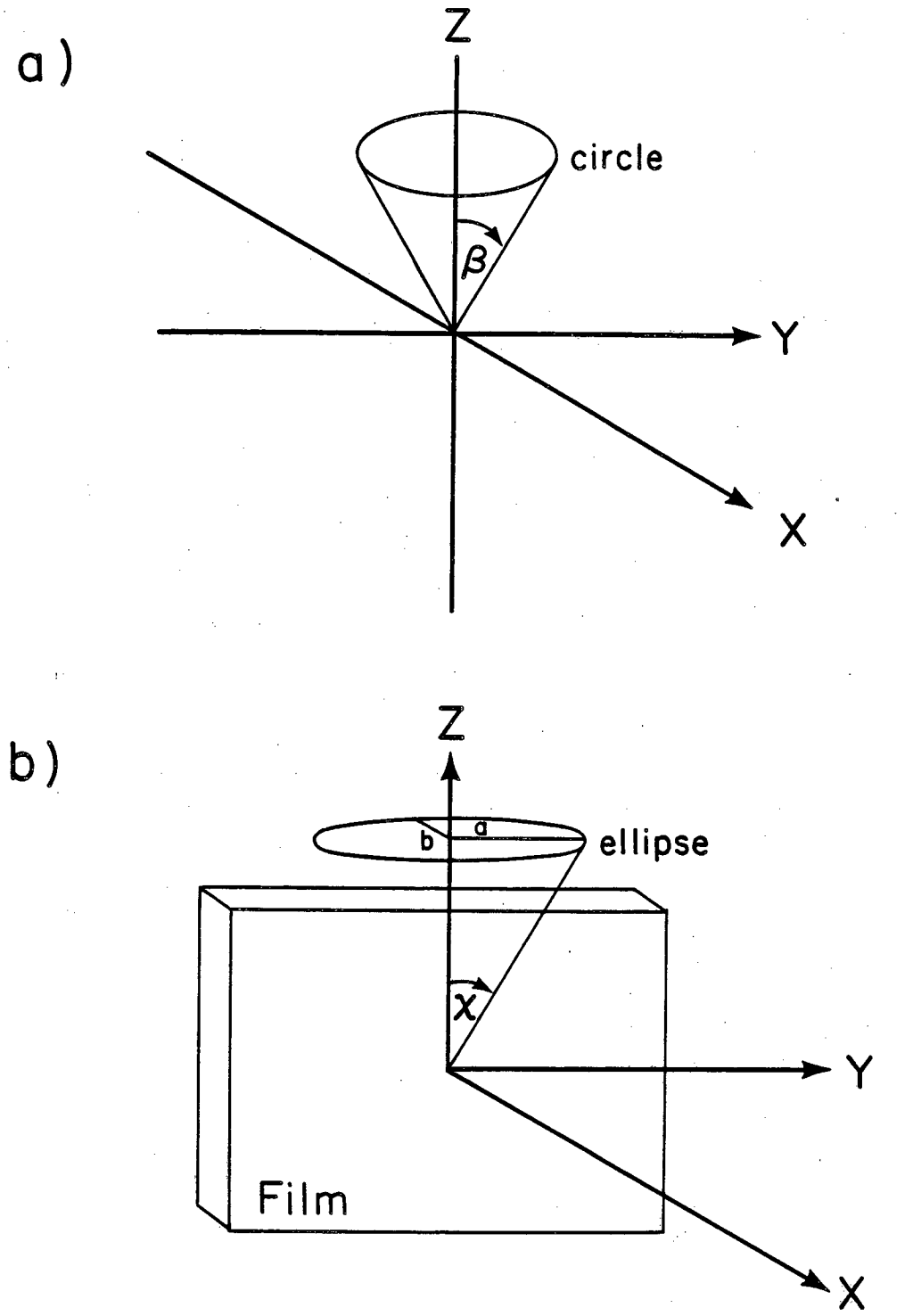

XBL796-4826

$T_V(\Delta_G,\Delta_e)$ for $\Delta_e = 1.0$ (symmetric uniaxial) and $\Delta_e = 0.2$ are plotted in Fig. II-6.

To use this new model, we pick a trial value for Δ_e and analyze the linear dichroism data just as we did with the symmetric uniaxial model. After doing this for all values of $\Delta_e < 1.0$, we find that the limits on ϵ in Eq. (47) are independent of Δ_e. Thus, Eq. (47) is consistent with this more sophisticated model.

Rafferty and Clayton [15,16] calculated ϵ to be 40.8^o by assuming that an extrapolated value of R = 2.68 at 860nm corresponds to perfect order. This value falls within our limits, but if their extrapolation is not valid, the range of ϵ in Eq. (47) provides a more realistic interpretation of their data. The question can be resolved by using $D_H(\theta,\Delta_G,\Delta_e)$ and $D_V(\theta,\Delta_G,\Delta_e)$ to analyze other types of experiments and thereby pin down Δ_G and Δ_e. Reference [10] gives several more examples on the use of density of states functions for analyzing linear dichroism data.

II-4. TWO-VECTOR PROBLEMS

The derivation of $P(\theta,\phi,\omega,\underline{\Delta})$ is very similar in theory to the derivation of $D(\theta,\phi,\underline{\Delta})$. The main difference is the coordinate transformation. Beginning from Eq. (5), we perform a new transformation $(\alpha_1, \ldots, \alpha_n)$ to $(\theta, \phi, \omega, v_1, \ldots, v_{n-3})$ under the constraints that $\underline{V}_1'$ and $\underline{V}_2'$ in the MAS are

$$\underline{V}_1' = \left[\prod_{i=1}^{n} R_i(\alpha_i)\right]\underline{V}_1 \qquad (50)$$

$$\underline{V}_2' = [\prod_{i=1}^{n} R_i(\alpha_i)]\underline{V}_2 \tag{51}$$

where $\underline{V}_1$ and $\underline{V}_2$ are the two vectors of interest in the LAS and $\underline{V}_1'$ and $\underline{V}_2'$ are given by Eqs. (2-3).

The details of the coordinate transformation are presented in Appendix IV (see also Ref. [19]). If we take the z axis to be the axis of the first rotation, the two-vector density of states function is

$$P(\theta,\phi,\omega,\underline{\Delta}) = \frac{\sin^2\theta\sin\omega}{N} \int_{v_1} \cdots \int_{v_{n-3}} W_1[-\phi+f_4(v_1,\ldots,v_{n-3},\theta,\omega)]$$
$$\times W_{n-1}[f_2(v_1,\ldots,v_{n-3},\theta,\omega)]W_n[f_3(v_1,\ldots,v_{n-3},\theta,\omega)]$$
$$\times \frac{\prod_{i=2}^{n-2} W_i(v_{i-1})dv_{i-1}}{\left|\frac{\partial V_{1z}}{\partial\alpha_{n-1}}\frac{\partial V_{2z}}{\partial\alpha_n} - \frac{\partial V_{1z}}{\partial\alpha_n}\frac{\partial V_{2z}}{\partial\alpha_{n-1}}\right|} \tag{52}$$

Here, W_i is the weighting function for the ith rotation, f_2, f_3, and f_4 are defined in Appendix IV, and N is a normalization constant. Equation (52) is an extension of Eq. (11) for the one-vector density of states function. We note that if the first rotation is unweighted ($W_1(\alpha_1) = 1$), we have an axially symmetric distribution. If we have a randomly oriented system, it can be shown that $P(\theta,\phi,\omega,\underline{\Delta})$ = constant x sin θ.

When the partially ordered ensemble can be generated with three rotations, there is no need for the dummy variables v_1, ..., v_{n-3} in Eq. (3) of Appendix IV and Eq. (52) will not involve any integration. In such a case, Eq. (52) simplifies to

$$P(\theta,\phi,\omega,\underline{\Delta})=\sin\theta\ W[\alpha_1(\theta,\phi,\omega),\alpha_2(\theta,\omega),\alpha_3(\theta,\omega),\underline{\Delta}] \quad (53)$$

where $W[\alpha_1,\alpha_2,\alpha_3,\underline{\Delta}]$ is the product of the weighting functions for the three rotations. The two-vector density of states is thus determined by finding the functional forms of $\alpha_1(\theta,\phi,\omega)$, $\alpha_2(\theta,\omega)$, and $\alpha_3(\theta,\omega)$. These functional forms for all possible three-rotation schemes and combinations of $\underline{V}_1$ and $\underline{V}_2$ are listed in Table II-III. We do not include $\alpha_1(\theta,\phi,\omega)$, therefore Table II-III is restricted to axially symmetric two-vector density of states functions.

AN EXAMPLE: FLUORESCENCE POLARIZATION

To illustrate the density of states approach to analysis of two-vector problems, we will work through a hypothetical example. The example is a fluorescence polarization study of a fluorophore attached to a macromolecular structure which can be oriented in a stretched film. This example is shown in Fig. II-3 with the lab z axis as the stretch direction. We can use the symmetric uniaxial model discussed in section 2B above. Thus the ensemble can be generated by a zyz rotation scheme and the weighting function is given by Eq. (43).

To calculate the two-vector density of states function, we need to know the two vectors $\underline{V}_1$ and $\underline{V}_2$ in the LAS. Fluorescence polarization experiments are typically done with the configuration shown in Fig II-9. A sample is excited with light that is polarized in the z direction and propagating along the y axis and fluorescence is detected along the x axis, the fluorescence intensities F_{zz} and F_{zy} are measured with an analyzing polarizer oriented either along the z axis or along the y axis

Table II-III: The functional forms of $\alpha_2(\theta,\omega)$ and $\alpha_3(\theta,\omega)$ in Eq. (51). When ± appears in an equation for $\alpha_2(\theta,\omega)$ or $\alpha_3(\theta,\omega)$, both terms must be included; i.e, $P(\theta,\omega,\underline{\Delta}) = \sin\theta\,(W[\alpha_{2+}(\theta,\omega), \alpha_{3+}(\theta,\omega), \underline{\Delta}] + W[\alpha_{2-}(\theta,\omega), \alpha_{3-}(\theta,\omega), \underline{\Delta}])$.

a. Use these formulas if the denominators are not equal to zero.

b. Use these formulas if the denominators in the previous column equal zero.

c. In these cases, any value of α_3 can be used, because for any physically realizable model $W[\alpha_2,\alpha_3,\underline{\Delta}]$ will be independent of α_3 when the denominators in the previous column equal zero.

TABLE II-III (part 1)

RS	$\underline{V}_1$	$\underline{V}_2$	$\alpha_2(\theta,\omega)$
zyz	$(\cos\psi,\sin\psi,0)$	$(0,0,1)$	$\cos^{-1}(\sin\theta\cos\omega)$
zyz	$(\cos\psi,0,\sin\psi)$	$(0,1,0)$	$\cos^{-1}(\cos\theta\sin\psi\pm\cos\psi\sin\theta\sin\omega)$
zyz	$(0,\cos\psi,\sin\psi)$	$(1,0,0)$	$\cos^{-1}(\cos\theta\sin\psi\pm\cos\psi\sin\theta\sin\omega)$
zyz	$(0,0,1)$	$(\cos\psi,\sin\psi,0)$	θ
zyz	$(0,1,0)$	$(\cos\psi,0,\sin\psi)$	$\cos^{-1}(\sin\theta\sin(\psi\pm\omega))$
zyz	$(1,0,0)$	$(0,\cos\psi,\sin\psi)$	$\cos^{-1}(\sin\theta\sin(\psi\pm\omega))$
zxy	$(\cos\psi,\sin\psi,0)$	$(0,0,1)$	$\sin^{-1}(\cos\theta\sin\psi\pm\cos\psi\sin\theta\sin\omega)$
zxy	$(\cos\psi,0,\sin\psi)$	$(0,1,0)$	$\sin^{-1}(\sin\theta\cos\omega)$
zxy	$(0,\cos\psi,\sin\psi)$	$(1,0,0)$	$\sin^{-1}(\cos\theta\cos\psi\pm\sin\psi\sin\theta\sin\omega)$
zxy	$(0,0,1)$	$(\cos\psi,\sin\psi,0)$	$\sin^{-1}(\sin\theta\sin(\psi\pm\omega))$
zxy	$(0,1,0)$	$(\cos\psi,0,\sin\psi)$	$\pi/2-\theta$
zxy	$(1,0,0)$	$(0,\cos\psi,\sin\psi)$	$\sin^{-1}(\sin\theta\cos(\psi\pm\omega))$

TABLE II-III (part 2)

RS	$\underline{V}_1$	$\underline{V}_2$	$\alpha_3(\theta,\omega)^a$	$\alpha_3(\theta,\omega)^b$
zyz	$(\cos\psi,\sin\psi,0)$	$(0,0,1)$	$\psi-\cos^{-1}(\pm\cos\theta/\sin\alpha_2)$	0^c
zyz	$(\cos\psi,0,\sin\psi)$	$(0,1,0)$	$\sin^{-1}(\sin\theta\cos\omega/\sin\alpha_2)$	$\pi/2-\omega$
zyz	$(0,\cos\psi,\sin\psi)$	$(1,0,0)$	$\cos^{-1}(\sin\theta\cos\omega/\sin\alpha_2)$	ω
zyz	$(0,0,1)$	$(\cos\psi,\sin\psi,0)$	$\psi\pm\omega$	$\psi\pm\omega$
zyz	$(0,1,0)$	$(\cos\psi,0,\sin\psi)$	$\sin^{-1}(\cos\theta/\sin\alpha_2)$	0^c
zyz	$(1,0,0)$	$(0,\cos\psi,\sin\psi)$	$\cos^{-1}(\cos\theta/\sin\alpha_2)$	0^c
zxy	$(\cos\psi,\sin\psi,0)$	$(0,0,1)$	$\cos^{-1}(\sin\theta\cos\omega/\cos\alpha_2)$	ω
zxy	$(\cos\psi,0,\sin\psi)$	$(0,1,0)$	$\psi-\sin^{-1}(\pm\cos\theta/\cos\alpha_2)$	0^c
zxy	$(0,\cos\psi,\sin\psi)$	$(1,0,0)$	$\sin^{-1}(\sin\theta\cos\omega/\cos\alpha_2)$	$\pi/2-\omega$
zxy	$(0,0,1)$	$(\cos\psi,\sin\psi,0)$	$\cos^{-1}(\cos\theta/\cos\alpha_2)$	0^c
zxy	$(0,1,0)$	$(\cos\psi,0,\sin\psi)$	$\pi/2-\psi\pm\omega$	$\pi/2-\psi\pm\omega$
zxy	$(1,0,0)$	$(0,\cos\psi,\sin\psi)$	$\sin^{-1}(\cos\theta/\cos\alpha_2)$	0^c

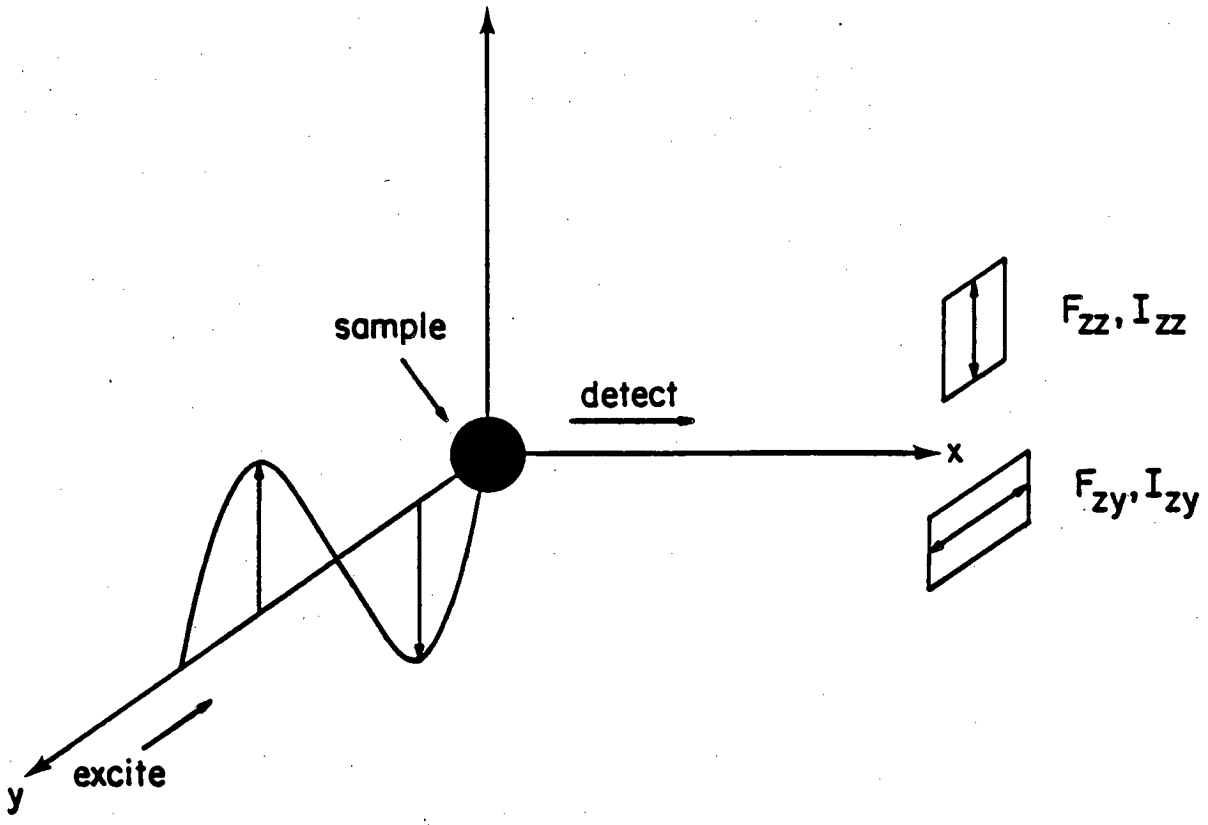

XBL 804-4108

Figure II-9: Experimental set up for a polarization experiment with exciting light polarized along the z axis. The axis system shown is the LAS.

respectively. We take $\underline{V}_1$ to be the polarization direction of the exciting light and $\underline{V}_2$ to be the polarization direction of the detected fluorescence. Thus, for F_{zz} and F_{zy}, $\underline{V}_1$ is along the laboratory z axis while $\underline{V}_2$ is along either the laboratory z or y axes. It is also possible to excite with a different polarization, such as along the laboratory x axis (see Fig. II-10), and correspondingly measure F_{xz} and F_{xy} (here $\underline{V}_1 = \hat{x}$ and $\underline{V}_2 = \hat{z}$ or $\hat{y}$). In a randomly distributed sample, F_{xz} and F_{xy} do not provide any new information because $F_{zy} = F_{xz} = F_{xy}$. In an ordered sample, the z direction and the x direction will not be equivalent (unless the y axis is an axis of symmetry in the LAS); thus F_{zy}, F_{xz}, and F_{xy} will all be different and, in principle, will provide more information.

Having established a partially ordered system and decided on $\underline{V}_1$ and $\underline{V}_2$, we can now calculate the density of states functions. We will need one density of states function for each measured quantity; i.e. one density of states function for each of F_{zz}, F_{zy}, F_{xz}, and F_{xy}. We begin with F_{zz}. Because $\underline{V}_1 = \underline{V}_2$, we need only a one-vector density of states function. We call this density of states function $D_{zz}(\theta,\Delta_G)$. $D_{zz}(\theta,\Delta_G)$ is equal to $D_H(\theta,\Delta_G)$ presented in section 2B-2 and plotted in Fig. II-4. F_{zy}, F_{xz}, and F_{xy} all need two-vector density of states functions. Because our hypothetical example can be generated with three rotations, the appropriate two-vector density of states functions are easily found by proper use of Eq. (53) and Table II-III. We call these density of states functions $P_{zy}(\theta,\omega,\Delta_G)$, $P_{xz}(\theta,\omega,\Delta_G)$, and $P_{xy}(\theta,\omega,\Delta_G)$. A plot of $P_{xz}(\theta,\omega,\Delta_G)$ for $\Delta_G = 0.5$ radians is shown in Fig II-11.

The next step is to find the response function for fluorescence polarization. In the dipole approximation, the response function in a

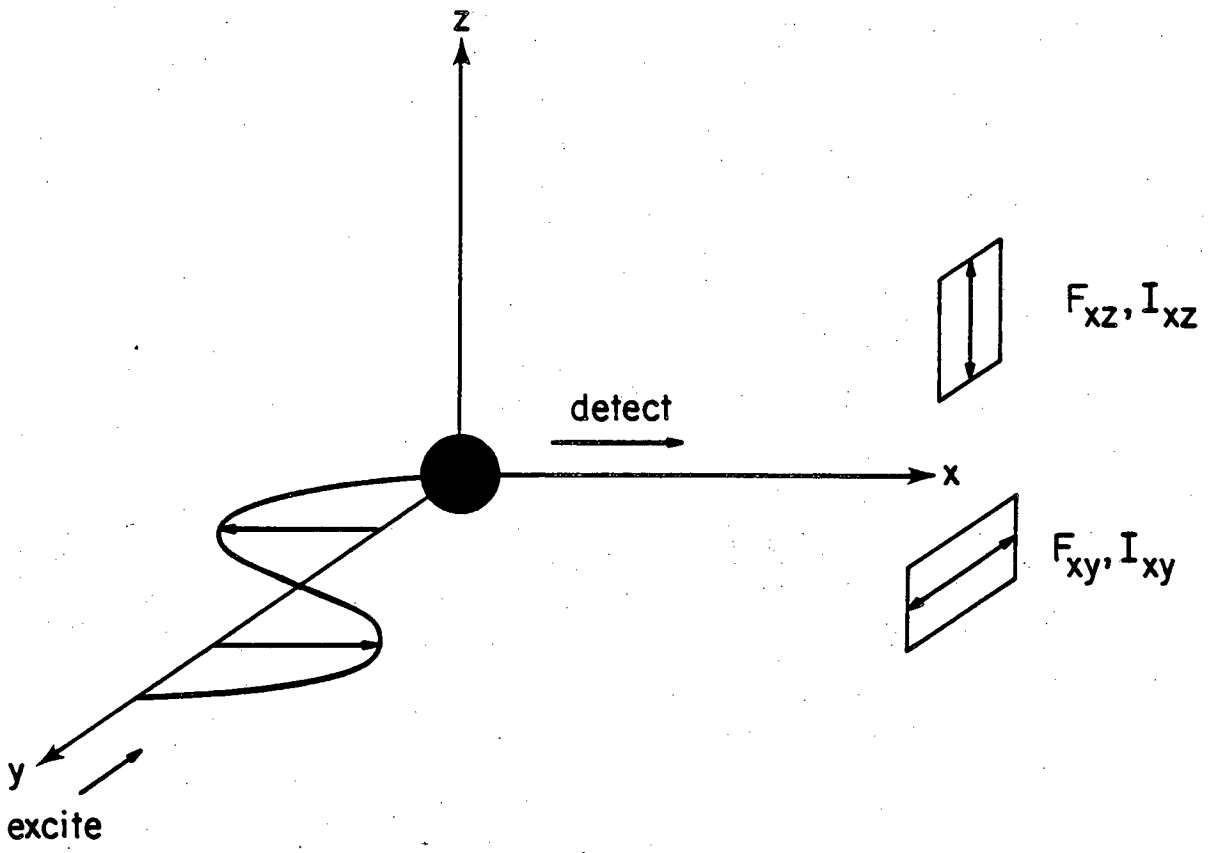

XBL 804-4109

Figure II-10: Experimental setup for a polarization experiment with exciting light polarized along the x axis. The axis system shown is the LAS.

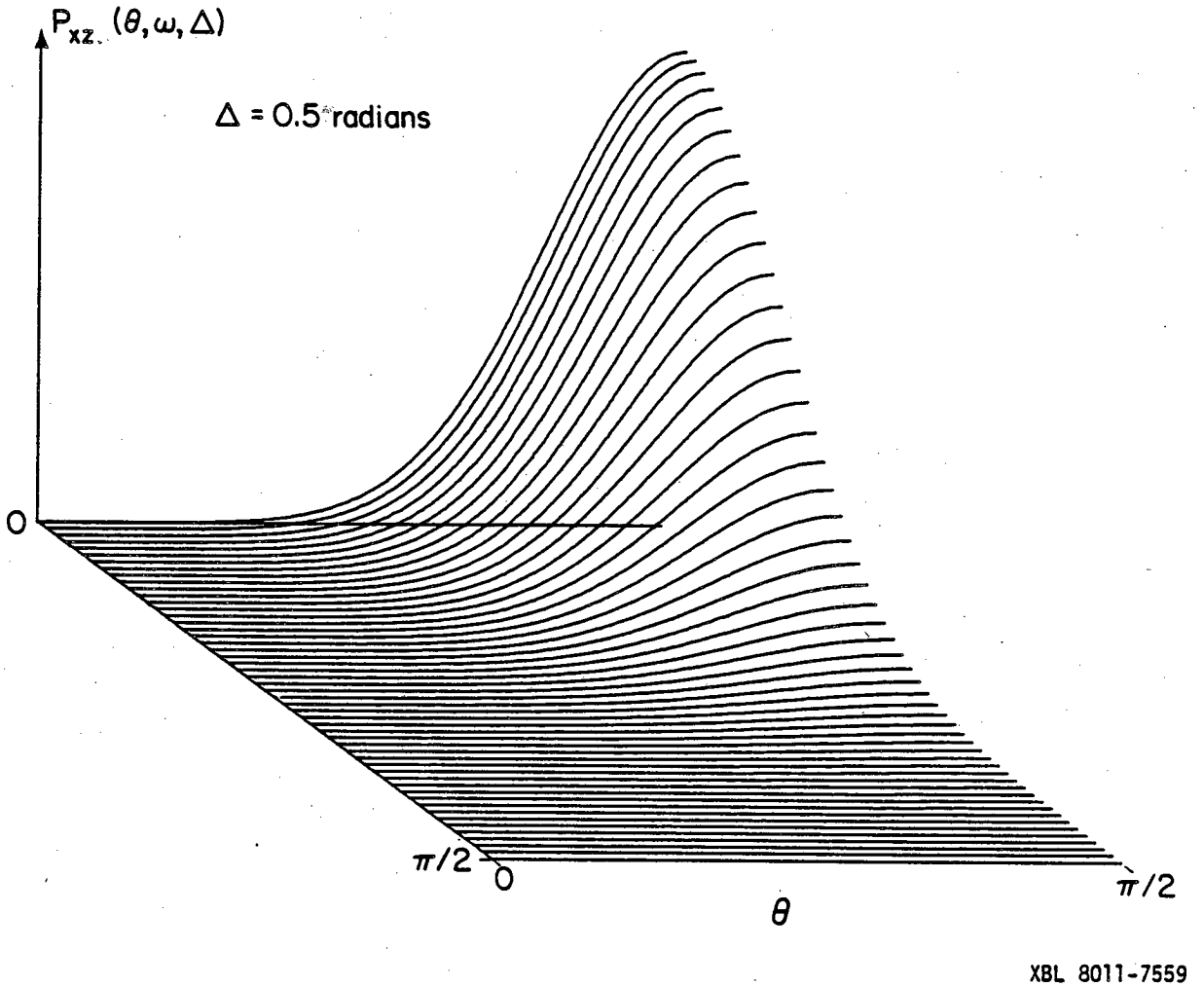

Figure II-11: Plot of the two vector density of states $P_{xz}(\theta,\omega,\Delta_G)$ for Δ_G = 0.5 radians.

static noninteracting ensemble of molecules is

$$I(\theta,\phi,\omega) = K^2(\hat{\mu}_1\cdot\underline{V}_1)^2(\hat{\mu}_2\cdot\underline{V}_2)^2 \tag{54}$$

where $\hat{\mu}_1 = (x_1,y_1,z_1)$ is a unit vector along the absorption dipole moment, $\mu_2 = (x_2,y_2,z_2)$ is a unit vector along the emission dipole moment, $\underline{V}_1$ is the polarization direction of the exciting light, $\underline{V}_2$ is the polarization direction of the detected fluorescence, and K^2 is a constant. Equation (54) can be reduced to

$$I(\theta,\phi,\omega) = \underline{V}_1\cdot\underline{\underline{T}}\cdot\underline{V}_2 \tag{55}$$

where $\underline{\underline{T}}$ is given by the dyad

$$\underline{\underline{T}} = K\hat{\mu}_2:\hat{\mu}_1 = K\begin{pmatrix} x_2 \\ y_2 \\ z_2 \end{pmatrix}(x_1\ y_1\ z_1) = K\begin{pmatrix} x_1x_2 & y_1x_2 & z_1x_2 \\ x_1y_2 & y_1y_2 & z_1y_2 \\ x_1z_2 & y_1z_2 & z_1z_2 \end{pmatrix} \tag{56}$$

To calculate F_{zz}, we substitute Eq.(55) with $\underline{V}_2 = \underline{V}_1$ and $\underline{V}_1$ given by Eq. (2) into Eq. (1) using $D_{zz}(\theta,\Delta_G)$. For the moment, we will retain the general tensor elements of $\underline{\underline{T}}$ (e.g. T_{xx}, T_{xy}, etc.) rather than the specific tensor elements of Eq. (56). The partial ordering in our example is induced by exerting a mechanical stretch on the film. Utilizing the symmetry properties of $D_{zz}(\theta,\Delta_G)$, expanding Eq. (1), and integrating over ϕ results in

$$\begin{aligned} F_{zz} = (1/8)(&8T_{zz}^2+\alpha[8T_{xx}T_{zz}+4(T_{xz}+T_{zx})^2+8T_{yy}T_{zz}+4(T_{yz}+T_{zy})^2 \\ &-16T_{zz}^2]+\beta[3T_{xx}^2+3T_{yy}^2+2T_{xx}T_{yy}+(T_{xy}+T_{yx})^2-8T_{xx}T_{zz} \\ &-4(T_{xz}+T_{zx})^2-8T_{yy}T_{zz}-4(T_{yz}+T_{zy})^2+8T_{zz}^2]) \end{aligned} \tag{57}$$

where

$$\alpha = \int_0^{\pi/2} d\theta \, \sin^2\theta \, D_{zz}(\theta,\Delta_G) \tag{58}$$

$$\beta = \int_0^{\pi/2} d\theta \, \sin^4\theta \, D_{zz}(\theta,\Delta_G) \tag{59}$$

and $D_{zz}(\theta,\Delta_G)$ is normalized such that

$$\int_0^{\pi/2} d\theta \, D_{zz}(\theta,\Delta_G) = 1 \tag{60}$$

After incorporation of the elements of $\underline{\underline{I}}$ from Eq. (56) into Eq. (57), we arrive at

$$\begin{aligned} F_{zz} = {} & (K/8)[8z_1^2z_2^2+4\alpha(z_1^2+z_2^2-10z_1^2z_2^2+4z_1z_2\cos\varepsilon) \\ & +\beta(-5z_1^2-5z_2^2+35z_z^2z_2^2-20z_1z_2\cos\varepsilon+2\cos^2\varepsilon+1)] \end{aligned} \tag{61}$$

where ε is the angle between $\hat{\mu}_1$ and $\hat{\mu}_2$. F_{zy}, F_{xy}, and F_{xz} are calculated by inserting Eq. (55) with $\underline{V}_1'$ and $\underline{V}_2'$ given by Eqs. (2) and (3) into Eq. (4) using the appropriate density of states function. Expanding Eq. (4) and evaluating the integral over ϕ yields

$$\begin{aligned} F_{ij} = {} & (1/8)(4(T_{xz}^2+T_{yz}^2)+\alpha_{ij}[4(T_{xy}^2+T_{yx}^2+T_{xz}^2-T_{yz}^2)-(T_{xy}+T_{yx})^2 \\ & +(T_{xx}-T_{yy})^2]+\gamma_{ij}[4(T_{xx}-T_{zz})^2+4(T_{yy}-T_{zz})^2-2(T_{xx}-T_{yy})^2 \\ & +2(T_{xy}+T_{yx})^2-4(2T_{xz}T_{zx}+2T_{yz}T_{zy}+T_{xy}^2+T_{yx}^2+T_{xz}^2+T_{yz}^2)] \\ & +\xi_{ij}[4(T_{xz}+T_{zx})^2+4(T_{yz}+T_{zy})^2-(T_{xy}+T_{yx})^2 \\ & +(T_{xx}-T_{yy})^2-4(T_{xx}-T_{zz})^2-4(T_{yy}-T_{zz})^2]) \end{aligned} \tag{62}$$

where

$$\gamma_{ij} = \int_0^{\pi/2} d\theta \int_0^{\pi/2} d\omega \, \sin^2\theta\cos^2\omega \, P_{ij}(\theta,\omega,\Delta_G) \tag{63}$$

$$\xi_{ij} = \int_0^{\pi/2} d\theta \int_0^{\pi/2} d\omega \, \sin^4\theta\cos^2\omega \, P_{ij}(\theta,\omega,\Delta_G) \tag{64}$$

$P_{ij}(\theta,\omega,\Delta_G)$ is normalized such that

$$\int_0^{\pi/2} d\theta \int_0^{\pi/2} d\omega \, P_{ij}(\theta,\omega,\Delta_G) = 1 \tag{65}$$

i = x, y, or z and j = y or z. Here α_{zy} is given by Eq. (58) but α_{xy} and α_{xz} are given by

$$\alpha_{xj} = \int_0^{\pi/2} d\theta \, \sin^2\theta \, D_{xx}(\theta,\Delta_G) \tag{66}$$

where $D_{xx}(\theta,\Delta_G)$ is the one-vector density of states function for a vector along the laboratory x axis. Inserting the tensor elements of Eq. (56) into Eq.(62), we obtain

$$\begin{aligned} F_{ij} = (1/8)[&(4z_1^2-4z_1^2z_2^2)+\alpha_{ij}(3-2\cos^2\varepsilon-7z_1^2-3z_2^2+5z_1^2z_2^2+4z_1z_2\cos\varepsilon) \\ &+\gamma_{ij}(4\cos^2\varepsilon-2z_1^2+2z_2^2-2+30z_1^2z_2^2-24z_1z_2\cos\varepsilon) \\ &+\xi_{ij}(5z_1^2+5z_2^2-35z_1^2z_2^2-1-2\cos^2\varepsilon+20z_1z_2\cos\varepsilon)] \end{aligned} \tag{67}$$

Fluorescence polarization data are generally in the form of ratios to eliminate the experimental constant K. From the four quantities F_{zz}, F_{zy}, F_{xz}, and F_{xy} we can construct three ratios. For example

$$P_1 = \frac{F_{zz} - F_{zy}}{F_{zz} + F_{zy}} \tag{68}$$

and P_2 and P_3 are derived from P_1 by replacing F_{zy} by F_{xz} and F_{xy} respectively. In an ordered sample, one can measure P_1, P_2, and P_3. In a random sample $P_1 = P_2 = P_3 = P$, but it is worth measuring P, because it provides an independent measure of the parameter ϵ (see below). We therefore find four measurable quantities P_1, P_2, and P_3 from an ordered sample and P from a random sample as data to determine the four parameters z_1, z_2, ϵ, and Δ_G in Eqs. (61) and (67). In our hypothetical example, we will use the following data: $P = 0.14 \pm 0.02$, $P_1 = 0.50 \pm 0.04$, $P_2 = -0.52 \pm 0.04$, and $P_3 = -0.26 \pm 0.04$.

In the random sample ($\alpha = 2/3$, $\beta = 8/15$, $\gamma = 1/3$, and $\xi = 4/15$), Eqs. (61) and (67) reduce to

$$P = \frac{3\cos^2\epsilon - 1}{\cos^2\epsilon + 3} \tag{69}$$

From the data, we find $\epsilon = 45.0^o \pm 1.5^o$

In the ordered sample, we use Eqs. (58-59), (63-64), and (66) to calculate α, β, $\alpha_{xz} = \alpha_{xy}$, γ_{zy}, γ_{xy}, γ_{xz}, ξ_{xy}, ξ_{zy}, and ξ_{xz} for several values of Δ_G; in our example, we calculated these values for Δ_G between 0 and 1 radian at increments of 0.05 radians. A simple computer program is then written to enumerate through all possible values of z_1 and z_2 (z_1 and z_2 are between 0 and 1). For each set of z_1 and z_2, the ratios P_1, P_2, and P_3 are calculated for each value of Δ_G considered. Any set of z_1, z_2, and Δ_G where P_1, P_2, and P_3 all fall within the experimental error of the measured ratios is an acceptable solution. The set of all solutions define z_1, z_2 and Δ_G complete with uncertainties. Carrying out this procedure for our hypothetical data results in

$$z_1 = 0.22 \pm 0.08 \tag{70}$$

$$z_2 = 0.70 \pm 0.03 \tag{71}$$

$$\Delta_G = 0.35 \pm 0.10 \text{ radians} \tag{72}$$

It is important to emphasize that we have measured Δ_G in this example. That is, we did not need to know the distribution function to carry out the above analysis; we needed only a model which enabled us to parametrically represent the the distribution function with Δ_G.

II-5. DISCUSSION

Spectroscopic studies of partially ordered ensembles can be used to probe information not available from the corresponding studies on randomly oriented ensembles. Three types of parameters (type I, type II, and type II) that can be measured are:

(I). Spectroscopically inherent structural parameters which relate molecular properties to the MAS. To illustrate, consider Eqs. (61), (67), and (68) for fluorescence polarization; these expressions contain the spectroscopically inherent structural parameters z_1, z_2, and ϵ. These parameters describe the projection of $\hat{\mu}_1$ and $\hat{\mu}_2$ on the z axis of the MAS (z_1 and z_2) and the angle between $\hat{\mu}_1$ and $\hat{\mu}_2$ (ϵ). In contrast, Eq. (69) for the random system contains only ϵ. Therefore, an experiment on an ordered sample is required to probe z_1 or z_2.

(II). Fundamental molecular parameters which describe quantum mechanical interactions at the molecular level. Examples include the polarizability tensor in Raman spectroscopy [19] and the elements of the spin

Hamiltonian matrix in EPR

(III). Order parameters which describe the partial ordering. In the density of states method, this information is contained in $\underline{\Delta}$. In complicated systems, such as biological systems, $\underline{\Delta}$ is often of much interest.

The importance of these three types of parameters makes studies on partially ordered ensembles highly desirable. We believe that the density of states approach provides a useful technique for extracting these parameters. In this section, I will contrast the density of states approach to other methods that exist in the literature [20,21] and point out the advantages of our method.

When analyzing a spectroscopic response of a partially ordered ensemble, one is faced with evaluating an integral like Eq. (1) or (4). To evaluate such an expression, one needs to know the spectroscopic response function and the distribution function of the partially ordered ensemble. The spectroscopic response function is usually determined through quantum mechanical analysis; if this analysis can not be done with much precision (such as in the case of Resonance Raman [22]), a quantitative analysis of the results will not be possible. If a suitable spectroscopic response function is known, one is left with determining the distribution function. Sometimes the distribution function can be written down. An example would be alignment in a magnetic field of a molecule with a known magnetic susceptibility anisotropy [3]. But, more often one is faced with one of the following difficulties: 1) A formula for the distribution function can be written down, but parameters in the formula (e.g. the magnetic susceptibility [3]) are not known. 2) The partial ordering is very complex, (e.g.

biological systems) and rigorous ordering formulas cannot be written down. In both of these cases, the problem of analyzing spectroscopic data in partially ordered systems is reduced to the problem of determining the distribution function.

A mathematically elegant method of dealing with the distribution function has been presented by Hentschel et. al. [20] and McBrierty [21]. They began by writing the average intensity as

$$\langle I \rangle = \int_0^{2\pi} d\alpha \int_{-1}^{+1} d\cos\beta \int_0^{2\pi} d\gamma \; p(\alpha,\beta,\gamma) I(\alpha,\beta,\gamma) \tag{73}$$

where $p(\alpha,\beta,\gamma)$ is the distribution function, here defined as the probability that the MAS of a member of the ensemble is related to the LAS by the Euler angles α,β, and γ (for a discussion of Euler angles, see Arfken [23], page 179), and $I(\alpha,\beta,\gamma)$ is the response function for orientation α,β, and γ. The distribution function is handled by expanding it in terms of the Wigner rotation matrix elements (denoted here by M)

$$p(\alpha,\beta,\gamma) = \sum_l \sum_m \sum_n p_{lmn} M^l_{mn}(\alpha,\beta,\gamma) \tag{74}$$

where

$$p_{lmn} = \frac{2l+1}{8\pi^2} \int_0^{2\pi} d\alpha \int_{-1}^{+1} d\cos\beta \int_0^{2\pi} d\gamma \; p(\alpha,\beta,\gamma) M^l_{mn}(\alpha,\beta,\gamma) \tag{75}$$

is the lmn^{th} moment of the distribution function. The problem of determining $p(\alpha,\beta,\gamma)$ is thus reduced to determining the moments of the expansion. If the ensemble is axially symmetric, p_{lmn} is zero unless m =

n = 0. In other words

$$p(\beta) = \sum_{l} p_{l00} M^{l}_{00}(0,\beta,0) \tag{76}$$

and the problem of determining $p(\alpha,\beta,\gamma)$ is further reduced to determining only the moments p_{l00}.

When Eq. (74) (or Eq. (76) in axially symmetric cases) is substituted into Eq. (73), the average response is written in terms of the moments p_{lmn}. Due to symmetry, this substitution often leads to simplified formulas with most of the p_{lmn} moments not entering the expression for $\langle I \rangle$. For example, in linear dichroism, the resulting expresssion for $\langle I \rangle$ depends only on the $l = 2$ moments. If the distribution function is axially symmetric, the resulting expression will depend only on p_{200}. p_{200} is related to the traditional linear dichroism order parameter S [24] by

$$S = (1/3)(3\langle \cos^2\beta \rangle - 1) = (8\pi/5)p_{200} \tag{77}$$

where $\langle \cos^2\beta \rangle$ is the ensemble average of $\cos^2\beta$. In this extreme case, the effect of partial ordering introduces only a single parameter S. In general, more than the $l = 2$ moments will survive. For example, if $I(\alpha,\beta,\gamma)$ is given by Eq. (55), both $l = 2$ and $l = 4$ moments survive [19] or, if $I(\alpha,\beta,\gamma)$ is the response function for a magnetic resonance experiment (EPR of NMR), all moments may survive [5,6,9].

In summary, the disadvantages of the moment expansion method are: (1). If an experiment is planned to measure parameters of type I or II, it is necessary to know all the surviving moments or to be able to fit the data using the surviving moments as parameters. In the case of

linear dichroism in an axially symmetric system, only one moment survives and the situation may not be too bad. In general, however, the survival of many moments may preclude the possibility of a meaningful analysis. It is difficult even to place limits on these moments, because they are merely mathematical projections of an unknown distribution function onto the Wigner rotation matrix elements.

(2). If type I and II parameters are known, it is possible to measure type III parameters with an experiment on an ordered system. At best, the result will be to measure some of the moments. If only a few moments are determined, they may be of little value for describing the distribution function especially if the expansion in Eq. (74) is slowly convergent. Even if many moments can be determined, one would like to construct a model, calculate $p(\alpha,\beta,\gamma)$, and see if the calculated moments agree with the measured moments. However, no general method for constructing $p(\alpha,\beta,\gamma)$ from a model that involves a rotation scheme of four or more rotations has been described.

The density of states approach overcomes these two problems. One way to think of the difference between our approach and the moment expansion approach is that we represent the distribution function in terms of the parameter $\underline{\Delta}$ instead of the moments p_{lmn}. The major benefits afforded by adopting our approach are:

(1). If an experiment is planned to measure type I or II parameters, it is necessary to know the magnitude of $\underline{\Delta}$ instead of the moments p_{lmn}. It is easier to estimate the magnitude of $\underline{\Delta}$ then to estimate the magnitude of the moments p_{lmn}, because $\underline{\Delta}$ may often be restricted from physical considerations. With most models for partial ordering, the number of parameters needed in $\underline{\Delta}$ will usually be less than the number of moments

needed.

(2). If type I and II parameters are known and used to probe the distribution function, one may obtain $\underline{\Delta}$. The $\underline{\Delta}$ parameter in conjunction with the rotation scheme and weighting functions gives a complete definition of the distribution function. In fact, if one knows $\underline{\Delta}$, one could calculate all the moments p_{lmn} [9,19]. Furthermore, each Δ_i is related is related to some physical property of the ensemble and, as such, is a quantity of interest [10,8].

(3) Our approach solves the general problem of calculating distribution functions from complicated models. As such, it is straightforward to interpret data in light of a specific model.

(4). The fact that we average orientations in the MAS instead of the LAS sometimes makes our approach more efficient. For example, Ref. [10] gives an example of a system where the distribution function is axially symmetric in the MAS but not in the LAS.

The one-vector [5,9,10] and two-vector [19] density of states functions provide a new approach to the analysis of spectroscopic properties in partially ordered ensembles. This approach displays several advantages over the traditional moment expansion approach. These advantages are particularly apparent in two cases: 1) in systems where many moments are required, and 2) in systems where the partial ordering is complex (e.g. biological systems). In these two cases, most work has either attempted the cumbersome moment expansion method [25,26] or resorted to only a qualitative analysis [27]. As a result, spectroscopic studies on these types of ordered samples is probably an underexplored area. We hope the density of states approach will enable greater exploration in these areas.

II-6. REFERENCES

1. J. Breton, J. F. Becker, and N. E. Geacintov, Biochem. Biophys. Res. Commun. 54, 1403 (1973).
2. G. Paillotin, A. Vermeglio, and J. Breton, Biochim. Biophys. Acta 545, 249 (1979).
3. R. S. Knox and M. A. Davidovich, Biophys. J. 24, 689 (1978).
4. A. D. Buckingham, Proc. Phys. Soc. B, 344 (1956).
5. R. Friesner, J. A. Nairn, and K. Sauer, J. Chem. Phys. 71, 358, 5388 (1979).
6. R. Friesner, "Theoretical Studies of the Light Reactions in Photosysnthesis", PhD Thesis, University of California, Berkeley, LBL-8953 (1979).
7. R. E. Williamson and H. F. Trotter, Multivariable Mathematics, Prentice-Hall, Inc., Englewood Cliffs, N. J. (1974).
8. H. A. Frank, R. Friesner, J. A. Nairn, G. C. Dismukes, and K. Sauer, Biochim. Biophys. Acta 547, 484 (1979).
9. R. Friesner, J. A. Nairn, and K. Sauer, J. Chem. Phys. 72, 221 (1980).
10. J. A. Nairn, R. Friesner, H. A. Frank, and K. Sauer, Biophys. J. 32, 733 (1980).
11. I. Chabay, E. C. Hsu, and G. Holzwarth, Chem. Phys. Lett. 15, 211 (1972).
12. R. Gale, A. J. McCaffery, and R. Shatwell, Chem. Phys. Lett. 17, 416 (1972).
13. R. S. Stein, J. Appl. Polymer Sci. 5, 96 (1961).
14. R. D. B. Fraser, J. Chem. Phys. 21, 1511 (1953).

15. C. N. Rafferty and R. K. Clayton, Biochim. Biophys. Acta 545, 106 (1979).

16. C. N. Rafferty and R. K. Clayton, Biochim. Biophys. Acta 502, 51 (1978).

17. S. C. Straley, W. W. Parson, D. C. Mauzerall, and R. K. Clayton, Biochim. Biophys. Acta 305, 597 (1973).

18. W. W. Parson and R. J. Cogdell, Biochim. Biophys. Acta 416, 105 (1975).

19. J. A. Nairn, R. Friesner, and K. Sauer, J. Chem. Phys. 74, 5398 (1981).

20. R. Hentschel, J. Schlitter, H. Silescu, and H. W. Spiess, J. Chem. Phys. 68, 56 (1978).

21. V. J. McBrierty, J. Chem. Phys. 61, 872 (1974).

22. J. Behringer, in Raman Spectroscopy (ed. H. A. Szymanski), Plenum Press, New York, 168 (1967).

23. G. Arfken, Mathematical Methods for Physicists, Acadmic Press, New York, (1970).

24. R. Zbinden, in Infrared Spectroscopy of High Polymers, Academic Press, New York, 166 (1964).

25. L. L. Chapoy and D. B. DuPre, J. Chem. Phys. 69, 519 (1978).

26. L. L. Chapoy and D. B. DuPre, J. Chem. Phys. 70, 2550 (1979).

27. N. E. Geacintov, F. Van Nostrand, J. F. Becker, and J. B. Tinkel, Biochim. Biophys. Acta 267, 65 (1972).

CHAPTER III

PICOSECOND FLUORESCENCE LIFETIME SYSTEM

III-1. INTRODUCTION

Fluorescence lifetimes reported in these studies where measured using the single-photon timing apparatus diagrammed in Fig. III-1. This set up is a modification of an earlier system [1-3] to include a synchronously pumped, mode-locked dye laser. The output pulses of this laser have a full-width-half-maximum (FWHM) of about 10 ps; with these pulses, we can push single-photon timing to the limit of its resolution capabilities. In this chapter, I will describe the single-photon timing apparatus and discuss the techniques used for numerical anaylsis of our data.

III-2. THE EXCITATION SOURCE

The excitation pulse in the single-photon timing apparatus is provided by a Spectra Physics synchronously pumped, mode-locked dye laser. The pump laser is a Spectra Physics SP 171 argon ion laser which is mode locked acoustooptically [4]. The acoustooptic mode locking crystal is driven by a Spectra Physics SP 362 Ultrastable Mode Locker. The output pulses of the argon ion laser have a FWHM of about 150 ps and the output is at 514 nm. The output of the argon ion laser is used to pump a modified Spectra Physics SP 375 dye laser. The dye laser cavity

Figure III-1: Block diagram of the single-photon timing system used for picosecond lifetime measurements. Abbreviations: ADC, analog-to-digital converter; BS, beam splitter; CFD, constant fraction discriminator; F1, neutral density filter; F2, interference filter; LEV. DISC., level discriminator; MCA, multichannel analyzer; M.L., mode locker; P.D., photomultiplier; P.M., photodiode; TAC, time-to-amplitude converter.

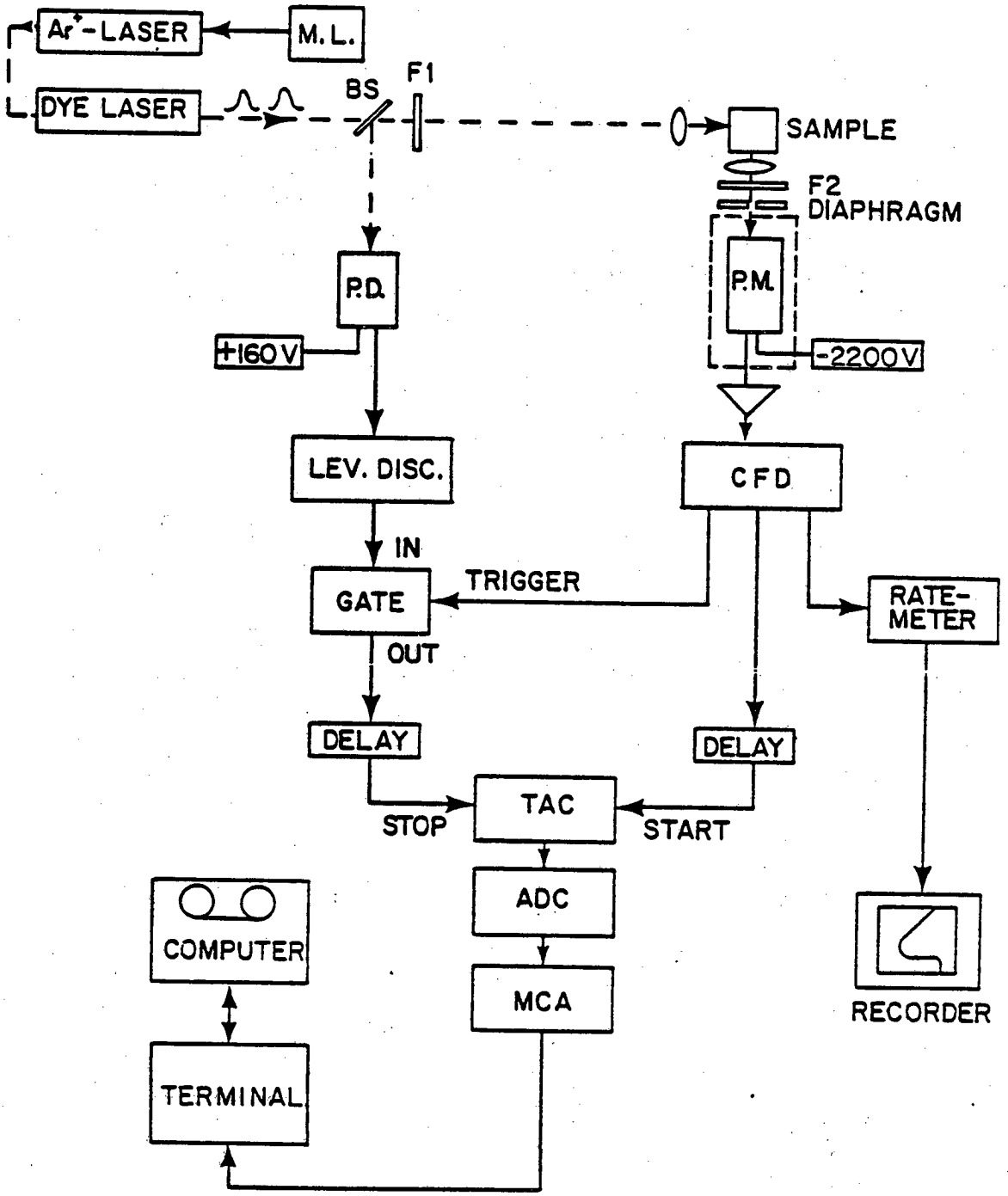

PHOTON TIMING SYSTEM

XBL 811-4422

has been extended to match the cavity length of the argon ion laser. In a similar configuration, dye laser pulses of less than 1 ps have been obtained using the laser dye rhodamine 6G [5,6]. The dramatic shortening of the dye laser pulses as compared to the argon ion laser pulses is due to a partial reduction of the pump-pulse induced population inversion by stimulated emission which is induced by simultaneous transit of the dye pulse through the dye stream [7,8].

Pulse widths from the dye laser are measured by the technique of zero-background, second harmonic generation [9]. The setup used for pulse width measurement is shown in Fig. III-2. The laser beam is divided into two beams by a beam splitter. One beam traverses a fixed path length while the path length of the other beam is variable. The two beams are recombined by focusing onto a thin potassium dihydrogen phosphate, KDP, crystal which has been cut to the phase matching angle [10]. When two pulses overlap in the crystal, one photon from each beam can combine, resulting in a UV photon which leaves the crystal along the bisector of the two input beams. Measuring the UV intensity along the bisector while changing the variable path length results in an autocorrelation function for the laser pulse.

We can obtain pulse widths with a FWHM of 1.5 ps at 620 nm by using rhodamine 6G, pumping at the threshold of lasing (about 750 mW argon pump power), and carefully matching the cavity lengths of the two lasers. For the fluorescence lifetime experiments, it was more convenient to run the dye laser above threshold and pump with about 950 mW argon ion power. A typical autocorrelation function for an excitation pulse used in fluorescence lifetime studies is shown in Fig. III-3. The spike in the center is a coherence spike and it occurs in the

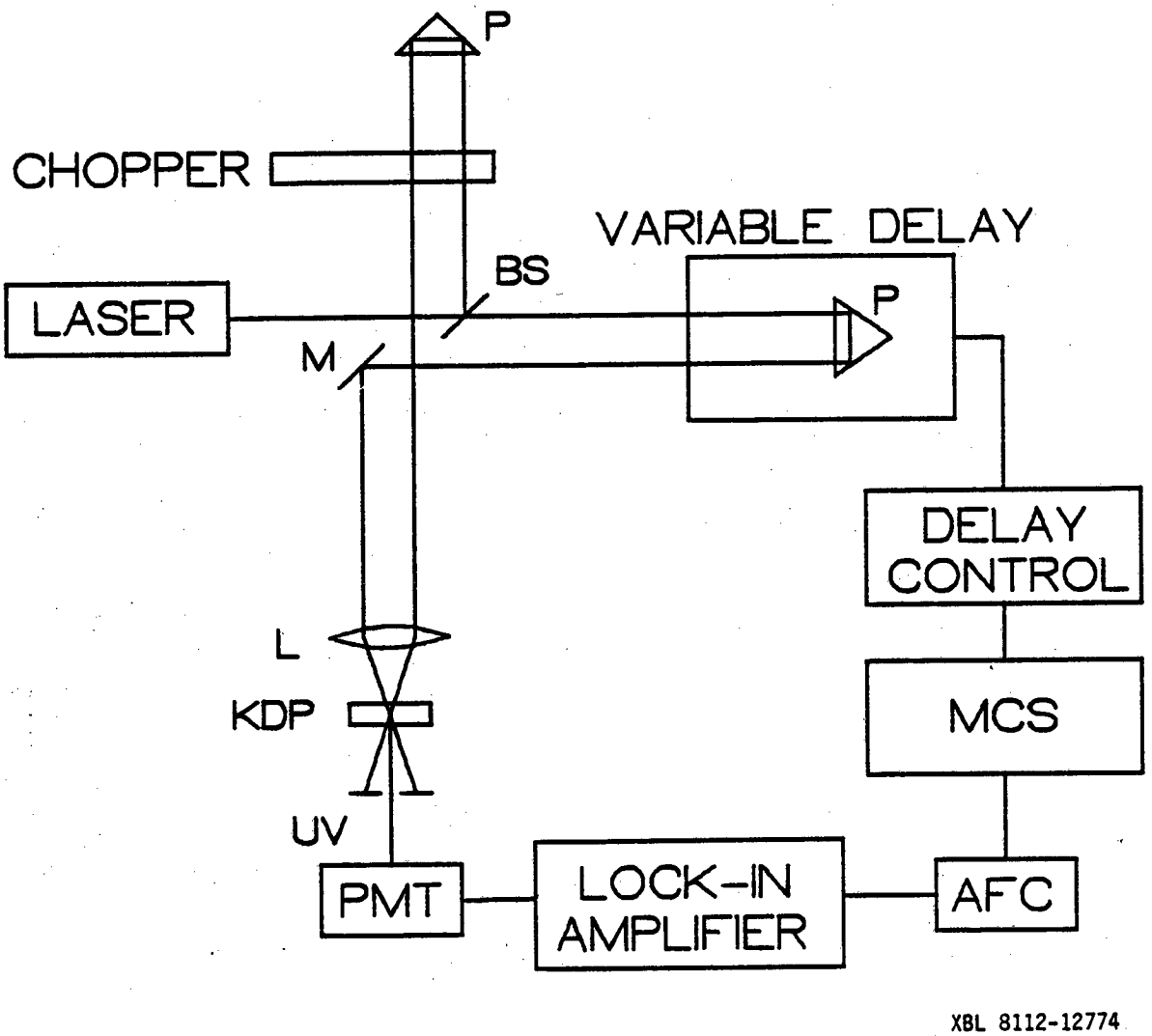

Figure III-2: Block diagram of zero-background, second harmonic generation system used to measure pulse widths. Abbreviations: AFC, analog to freguency converter; BS, beam splitter; KDP, second harmonic generating crystal; L, lens; M, mirror; MCS, multichannel scaler; P, right angle prism; PMT, photomultiplier.

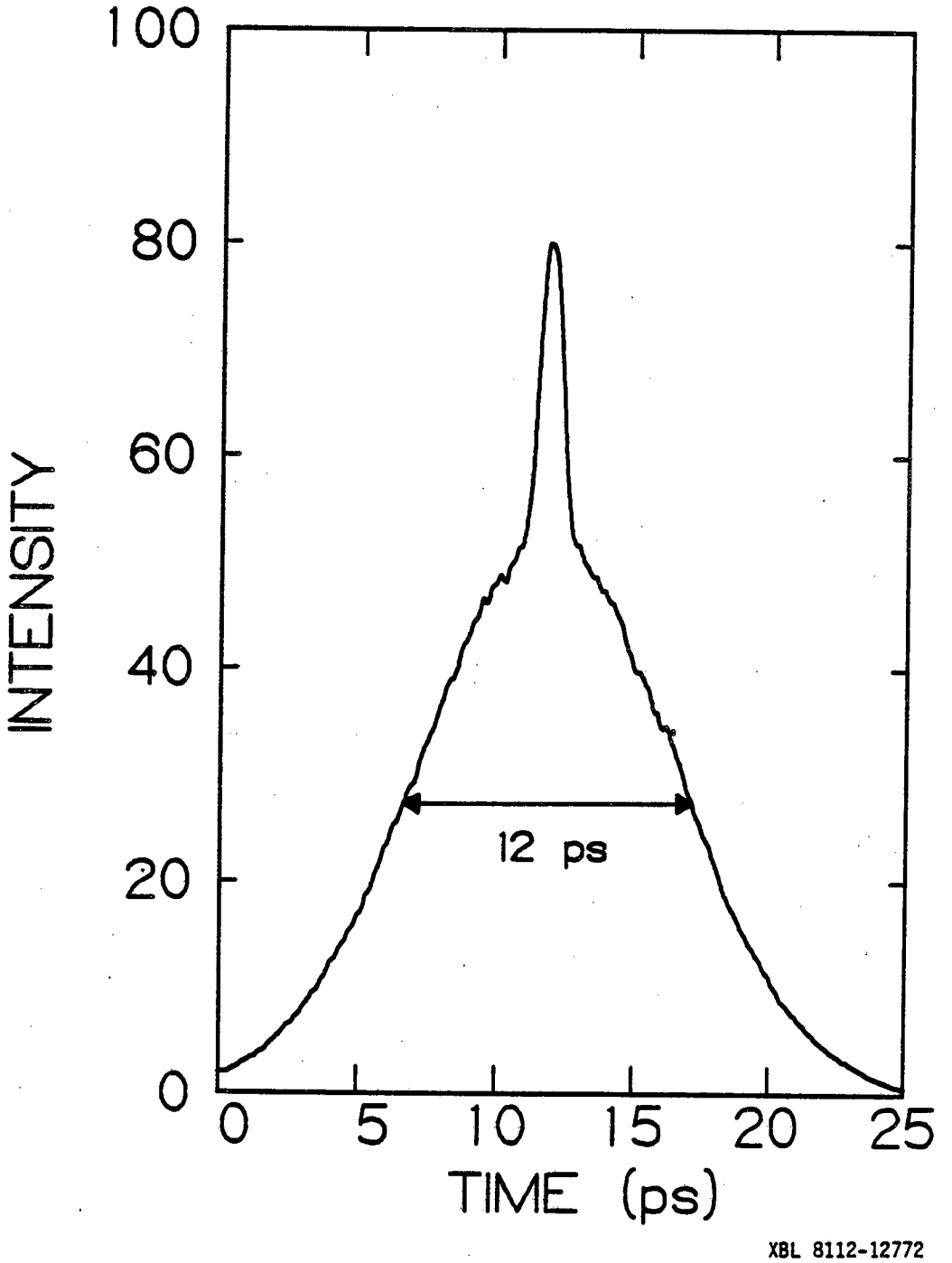

Figure III-3: Autocorrelation function for the output pulse of the synchronously pumped, mode-locked dye laser when in the configuration used for fluorescence experiments.

autocorrelation function of a pulse that has fine structure under the pulse envelope. The presence of fine structure indicates incomplete mode-locking; the result is a broadening of the pulse width [11]. The FWHM of the autocorrelation trace is 12 ps. To find the width of the laser pulse, we need to know the laser pulse shape; we assume that the laser pulse has a Gaussian envelope. An autocorrelation function of a Gaussian pulse has a FWHM that is $\sqrt{2}$ times the FWHM of the Gaussian. Thus, we estimate the FWHM of our laser pulse to be about 8 ps. The assumption of a Gaussian pulse shape is a conservative assumption because other pulse shapes (e.g. Lorentzian) lead to division of the FWHM of the autocorrelation function by factors larger than $\sqrt{2}$ [12].

III-3. SINGLE-PHOTON TIMING ELECTRONICS

Conventional single-photon timing systems start a voltage ramp in a time-to-amplitude converter (TAC) (We use a Canberra 2043 TAC) upon each excitation pulse and stop the voltage ramp when a fluorescence photon is detected. The resultant height of the voltage ramp is proportional to the time between the start and the stop pulse. The recording of many such events results in a histogram which is equivalent to the fluorescence intensity versus time [13]. Because the repetition rate of our laser (82 MHz or 12 ns pulse separation) is too high for the TAC to start a voltage ramp on each laser pulse, we have adopted a reverse single-photon timing scheme. In our system, we start the TAC with a fluorescence photon and stop the TAC with the next laser flash. The jitter of the time between laser pulses is sufficiently low (< 5ps) that

we do not sacrifice resolution in this mode of operation.

Fluorescence photons are detected by a RCA 31034A photomultiplier. The output of the photomultiplier is amplified and input to a constant fraction discriminator [1,2]. One output of the constant fraction discriminator provides a pulse to the TAC resulting in the start of the voltage ramp. Two other outputs trigger the gate box (see below) and feed a count ratemeter; the count ratemeter was used to monitor the fluorescence intensity during an experiment. Laser pulses are detected by a Texas Instruments TIED 55 photodiode mounted in a transmission line housing similar to the one described by Steinmetz [14]. The output of the photodiode triggers a level discriminator whose output provides a pulse to the TAC which stops the voltage ramp. Before reaching the TAC, the output of the level discriminator passes through the gate box.

The function of the gate box is to prevent pulses from the level discriminator from reaching the TAC except when a fluorescence photon has been detected. Fluorescence data taken before installation of the gate box showed large oscillations with a period of about 2 ns (See Fig. III-4). The oscillations appear to be due to perturbations in the TAC circuitry caused by the presence of a pulse from the level discriminator every 12 ns. Insertion of the gate box eliminated most of the oscillations. Remaining oscillations were attributable to the slowness of an ORTEC 462 TAC which was used in early versions of the single-photon timing system. The faster Canberra 2043 TAC eliminated these last oscillations. All data presented here were taken with the Canberra TAC and the gate box; the results are free from instrumental oscillations. Reference [15] has more details on the gate box and other features in this system.

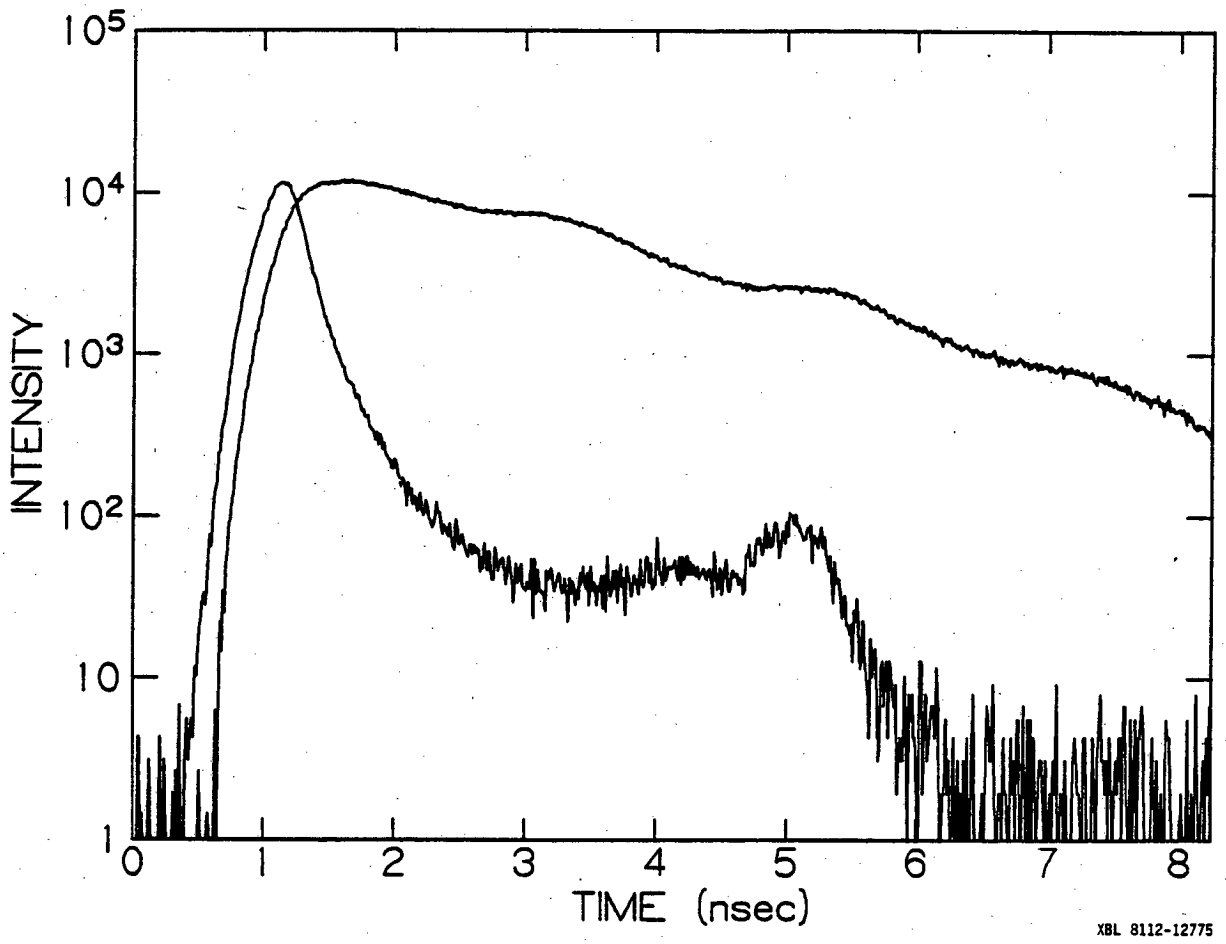

Figure III-4: Fluorescence decay measured without gate box between level discriminator and TAC. Fluorescent sample has a lifetime of about 2 ns.

The output of the TAC is converted into a channel number by a Northern 1024 analog-to-digital converter and stored locally in a 1024 channel Northern NS636 multichannel analyzer. We collected data until the peak channel had at least 10000 counts. The contents of the Northern NS636 was transferred to a VAX 11/780 computing system for data analysis.

III-4. NUMERICAL ANALYSIS

A fluorescence lifetime determination involves measurement of both E(t) and F(t). E(t) is the response of our system, and it is measured with a scattering solution in the sample cell. F(t) is the fluorescence decay curve, and it is measured with a fluorescent sample in the sample cell (See Fig. III-1). F(t) is related to E(t) by the convolution integral

$$F(t) = \int_0^t du\, E(u)I(t-u) \qquad (1)$$

where I(t) is the actual fluorescence decay law. It is the actual decay law, I(t), that is sought in a fluorescence lifetime experiment. When the width of E(t) is not negligible compared to the width of F(t), I(t) is only obtainable by deconvolution techniques. Our deconvolution techniques will be described in this section.

The two most popular methods for numerical deconvolution of Eq. (1) found in the literature are non-linear least squares (NLLS) [16-18] and method of moments (MOM) [19-23]. In each method, one assumes a form

of I(t) which contains adjustable parameters. A common I(t), and the I(t) that I will discuss here, is a sum of exponentials

$$I(t) = \sum_{i=1}^{N} \alpha_i \exp(-t/\tau_i) \tag{2}$$

where α_i is the amplitude and τ_i is the lifetime of the ith component. The yield of the ith component given by

$$\phi_i = \alpha_i \tau_i \tag{3}$$

is equal to the number of photons emitted in the ith phase. In NLLS, a non-linear least square minimization routine [16,17] is used to minimize the least squares residual

$$S = \sum_{j=1}^{NPTS} (F_j(t)-C_j(t))^2/F_j(t) \tag{4}$$

where NPTS is the number of data points and $F_j(t)$ and $C_j(t)$ are the jth points in the fluorescence data (after the dark counts have been subtracted out), and the calculated reconvolution using a particular set of α_i and τ_i. In photon counting data, the signal to noise ratio is proportional to the square root of the number of counts. The factor $1/F_j(t)$, therefore, weights the squared deviation at the jth point by $1/\sigma^2$ where σ is the standard deviation of the jth point; this factor is the appropriate weighting factor for a least squares residual [18]. MOM is based on the fact that the 2N parameters α_i and τ_i in an N exponential decay law can be calculated from the first 2N moments of E(t) and F(t). Here, the kth moment is defined as

$$M(k) = \int_0^\infty dt\ t^{k-1}F(t) \tag{5}$$

In general, F(t) and E(t) data are collected only to some finite time, T_f, and all of the work in MOM is determining cutoff corrections to the moments. Formally, we have

$$\begin{aligned} M(k) &= \int_0^{T_f} dt\ t^{k-1}F(t) + \int_{T_f}^\infty dt\ t^{k-1}F(t) \\ &= M_0(k) + \delta M(k) \end{aligned} \tag{6}$$

where $M_0(k)$ is the kth moment calculated from the available data and $\delta M(k)$ is the cutoff correction. Because E(t) is normally zero by time T_f, $\delta M(k)$ for E(t) is assumed to be zero. Isenberg et. al. [19-23] describe a self consistency approach to evaluating $\delta M(k)$ for F(t) in the case where I(t) is a sum of exponentials.

With high signal-to-noise ratio data free from instrument artifacts, both NLLS and MOM work well when I(t) contains one or two exponentials. We found that any discrepancy between the two methods was due to problems with the data and not to an inherent superiority of either NLLS or MOM over the other method. Besides collecting enough data for a high signal to noise ratio and removing all instrument artifacts, two more subtle problems needed to be dealt with before NLLS and MOM would agree consistently. First, because E(t) is recorded at the excitation wavelength and F(t) is recorded at the fluorescence wavelength, one might expect different transit times through the photomultiplier when recording E(t) and F(t). The different transit times would be due to the different energies of the incident photons. To

account for this effect, we shift E(t) in time; we use the shift that yields the best fit as determined by the least squares residual. When an E(t) at 620 nm and an F(t) at 680 nm are recorded one after another, the shift with an RCA C31034A photomultiplier is fairly constant at about +10 ps. When the recording of E(t) and the recording of F(t) is separated by more than 30 minutes, the optimal shift varies from about -15 ps to +30 ps. This variation is probably due to long term drifts in some system transit time property. Allowing the shift to vary freely enabled us to get good fits even when the recording of E(t) and F(t) are separated by 2 hours.

The second problem we encountered concerned how much data to include in the analysis. If too few points are included, it is obvious that inferior fits will result due to a lack of information. We also found that if too many points out to long times are included, inferior fits can also result. The problem here seems to be due to including points with few counts and a low signal-to-noise ratio. In all results reported here, we were careful to avoid this problem by limiting the anaysis range to include only points with a signal-to-noise ratio greater than 10.

When fits to three exponentials were sought, both NLLS and MOM worked and agreed, but NLLS achieved solutions faster than MOM and was less likely to result in computer errors when approaching the solution. For convenience, we have adopted NLLS as our standard method.

All data analysis is done by the program FLORFIT and its associated subroutines. This program is capable of deconvolution by NLLS [16-18], MOM [19-23], or exponential series method [24]. FLORFIT is largely an implementation of the methods described in the cited references. One

major change was necessary due to the 12 ns pulse separation time in our excitation source. When some of the exponential components have long lifetimes (> 2 ns), all fluorescence from a particular excitation pulse will not have decayed to zero by the next excitation pulse. The surviving fluorescence contributes a non-random background in F(t) which needs to be subtracted out.

The expected background can be calculated for a particular set of α_i and τ_i. First, consider an E(t) and F(t) collected up to time T_f. For $t < T_f$, F(t) due to a single excitation pulse is given by Eq. (1). For I(t) given by a sum of exponentials

$$F(t) = \int_0^t du\ E(u)\alpha_i \exp(-(t-u)/\tau_i) \tag{7}$$

where, here and below, a sum over i is understood. For $t > T_f$, we note that E(t) should have decayed to zero (i.e. $E(t) = 0$ for $t > T_f$). By Eq. (1), F(t) for $t > T_f$ is

$$\begin{aligned} F(t) &= \exp(-(t-T_f)/\tau_i) \int_0^{T_f} du\ E(u)\alpha_i \exp(-(T_f-u)/\tau_i) \\ &= \exp(-(t-T_f)/\tau_i) F_i(T_f) \end{aligned} \tag{8}$$

where $F_i(T_f)$ is the measured fluorescence at time T_f due to the ith component.

Now look at $t < T_f$ and add in the fluorescence from previous pulses using Eq. (8). The result is

$$F(t) = \int_0^t du E(u)\alpha_i \exp(-(t-u)/\tau_i) + F_i(T_f)\exp(-(t+T_p-T_f)/\tau_i) +$$

$$+ F_i(T_f)\exp(-(t+2T_p-T_f)/\tau_i) + \ldots \quad (9)$$

where T_p is the pulse separation time - about 12 ns for our laser. Evaluating the infinite series results in

$$F(t) = \int_0^t du E(u)\alpha_i \exp(-(t-u)/\tau_i) + C_i\exp(-t/\tau_i) \quad (10)$$

where

$$C_i = F_i(T_f)/[\exp((T_p-T_f)/\tau_i)-\exp(-T_f/\tau_i)] \quad (11)$$

From the second term in Eq. (10), we see that the expected background decays as a sum of exponentials with the same lifetimes as the fluorescence decay and amplitudes given by C_i. If τ_i is short, $F_i(T_f)$ is small and C_i is near zero, but if $\tau_i > 2$ ns, C_i is no longer negligible. To correct for the long-lifetime background, we use the following procedure: 1) An initial set of α_i and τ_i is found, usually by a normal fit with no long lifetime background subtractions. 2) The current set of α_i and τ_i is used to calculate C_i, and a long-lifetime background is subtracted from F(t). 3) The new F(t) is used to find a new set of α_i and τ_i. 4) Steps 2 and 3 are repeated until the lifetimes no longer change. The convergence normally takes two or three cycles.

The program FLORFIT is capable of fitting to an I(t) decay law that is not a sum of exponentials. The numerical procedures are much slower due to a loss of some simplifications that result when using exponential decay laws. Also, the procedure for long-lifetime background subtraction must be altered because the above method is based on I(t) given by a sum of exponentials.

III-5. CONCLUSION

The picosecond laser, single-photon timing electronics, and computer software described above represent a system that pushes current single-photon timing techniques to their limits of resolution. Based on deconvolutions of simulated data that are convoluted using one real E(t) and deconvoluted using another E(t), we estimate that we can resolve fluorescence lifetimes as short as 25 ps. The limiting factor is a broadening of E(t) due to jitter in the electronics. The most probable source of jitter is the photomultiplier and constant fraction discriminator combination which is used to detect photons. Application of newly developed static crossed field photomultipliers to single-photon timing should reduce this jitter and result in even higher resolution [25].

III-6. REFERENCES

1. B. Leskovar, C. C. Lo, P. R. Hartig, and K. Sauer, Rev. Sci. Instr. 47, 1113 (1976).
2. P. R. Hartig, K. Sauer, C. C. Lo, and B. Leskovar, Rev. Sci. Instr. 47, 1122 (1976).
3. G. T. Brewington, "Studies of Photosynthetic Membranes Using Chlorophyll Fluorescence Lifetimes", PhD Thesis, Univ. California, Berkeley (LBL-9795) (1979).
4. D. von der Linde, Appl. Phys. 2, 281 (1973).
5. C. P. Ausschnitt and R. K. Jain, Appl. Phys. Lett. 32, 727 (1978).
6. J. P. Heritage and R. K. Jain, Appl. Phys. Lett. 32, 101 (1978).
7. H. A. Haus, IEEE J. Quantum Electron. QE-11, 323 (1975).
8. N. J. Frigo, T. Daly, and H. Mahr, IEEE J. Quantum Electron. QE-13, 101 (1977).
9. E. P. Ippen and C. V. Shank, Appl. Phys. Lett. 27, 488 (1975).
10. J. A. Giordmaine, Phys. Rev. Lett. 8, 19 (1962).
11. H. A. Haus, C. V. Shank, and E. P. Ippen, Optics Comm. 15, 29 (1975).
12. P. W. Smith, M. A. Dugay, and E. P. Ippen, in Progress in Quantum Electronics (eds. J. J. Sanders and S. Stenholm), Vol. 3, 105 (1974).
13. W. R. Ware, in The Creation and Detection of the Excited State (ed. A. A. Lamola), Vol 1A, 213 (1971).
14. L. L. Steinmetz, Rev. Sci. Instr. 50, 582 (1979).
15. B. Turko, J. A. Nairn, and K. Sauer, in preparation.
16. K. Levenberg, Quart. Appl. Math. 2, 164 (1944).

17. D. W. Marquardt, J. Soc. Indust. Appl. Math. 11, 431 (1963).

18. A. Grinvald and I. Z. Steinberg, Anal. Biochem. 59, 583 (1974).

19. I. Isenberg and R. D. Dyson, Biophys. J. 9, 1337 (1969).

20. R. D. Dyson and I. Isenberg, Biochem. 10, 3233 (1971).

21. I. Isenberg, J. Chem. Phys. 59, 5696 (1973).

22. I. Isenberg, J. Chem. Phys. 59, 5708 (1973).

23. I. Isenberg, Biophys. J. 13, 1090 (1973).

24. W. R. Ware, L. J. Doemeny, and T. L. Nemzek, J. Phys. Chem. 77, 2038 (1973).

25. V. J. Koester, Anal. Chem. 51, 458 (1979).

CHAPTER IV

F_0, F_{max} AND INTENSITY DEPENDENT FLUORESCENCE DECAY KINETICS IN SPINACH CHLOROPLASTS AND ALGAE AT ROOM TEMPERATURE

IV-1. INTRODUCTION

It has been known for a long time that the state of the photosystem II reaction center affects the room-temperature fluorescence emission of chloroplasts in higher plants and algae. This emission is usually attributed to photosystem II chlorophyll [1-3]. In the all-open state (electron acceptor Q all oxidized), the fluorescence yield, F_0, is low and the average lifetime is short. In the all-closed state (electron acceptor Q reduced), photochemistry is blocked and the fluorescence yield, F_{max}, is 3 to 5 times greater than F_0 [4,5]. A simple model of the photosynthetic unit (See reference [6] and discussion section of this chapter) predicts that when photochemistry, which has a quantum yield of about 0.95 [7,8], is blocked, the fluorescence yield should increase 20 fold. This apparent discrepancy could occur for two reasons. First, either photosystem I chlorophyll or chlorophyll that is not connected to any photosystem could contribute a constant background fluorescence present in both F_0 and F_{max} [9,10]. Second, there may be a new radiationless deactivation mechanism in the closed reaction center which does not occur in the open reaction center [11-13]. Recently, it was proposed that variable fluorescence results from recombination between the primary electron acceptor and the primary electron donor of photosystem II and that this charge recombination repopulates the

excited singlet state of chlorophyll [14-20]. An analogous process leading to triplet or ground state chlorophyll molecules could provide a mechanism for radiationless deactivation in closed reaction centers. Fluorescence decay kinetic studies provide a direct method for distinguishing between these two models.

The experiments described in this chapter investigate the fluorescence decay kinetics in spinach chloroplasts, pea chloroplasts, and whole algae for various states of the photosystem II reaction center. We find three exponential decay components in the all-open state (F_0 level) as well as for the all-closed state (F_{max} level). The slowest component has a lifetime of 1 to 2 ns and exhibits a dramatic increase in yield as Q becomes reduced. Under the same conditions the lifetime of this component shows a small change. Two faster phases (< 700 ps) are present and they show minor lifetime and yield changes between F_0 and F_{max}. The intensity dependence of the fluorescence decay kinetics shows how the three components change at intermediate states between all-open and all-closed. Our results support the model that variable fluorescence is due to charge recombination between the primary electron acceptor and the primary electron donor in photosystem II. A working model for the interpretation of fluorescence lifetimes is presented in Chapter V.

IV-2. MATERIALS AND METHODS

Broken spinach chloroplasts were isolated by the method described in reference [21]. Fresh spinach leaves, grown either in a growth chamber or in a green house, were ground for 10 sec in 50 mM HEPES-NaOH

buffer (pH 7.5) with 0.4 M sucrose and 10 mM NaCl followed by centrifugation for 2 min at 2000 xg. After one wash with fresh grinding buffer, the chloroplasts were kept for 20 min at $0^{o}C$ in 10 mM HEPES-NaOH buffer (pH 7.5) with 0.1 M sucrose and 10 mM NaCl. After a centrifugation for 5 min at 2000 xg, the pellet was resuspended in 10 mM HEPES-NaOH buffer (pH 7.5) with 0.1 M sucrose, 5 mM $MgCl_2$, and 5 mM NaCl. For experiments in the absence of magnesium, $MgCl_2$ was omitted from the resuspending buffer. The chlorophyll concentration was adjusted to 18 µg chlorophyll/ml by dilution with the resuspending buffer. For experiments at the F_0 level, we added 1.25 mM ferricyanide as electron acceptor, 1.25 mM ferrocyanide to control the redox potential, and 2.5 µg/ml gramicidin D as uncoupler. The latter was added to prevent the slow formation of a pH gradient across the thylakoid membrane which has been reported to cause a decline in the fluorescence yield [22]. The chloroplast sample was rapidly stirred in a 1 cm x 1 cm cuvette and each sample was replaced every 10 min if more data accumulation was needed. For experiments at the F_{max} level, we added 12.5 µM DCMU and 2 mM hydroxylamine hydrochloride. To close the reaction centers, the sample was illuminated with about 10 flashes of saturating intensity immediately before the lifetime measurement.

Chlorella pyrenoidosa, strain UTEX 1230, and Chlamydomonas reinhardtii, strain UTEX 89, were grown as described [23,24] and diluted with growth medium to give a chlorophyll concentration of 18-20 µg/ml. The measurements were carried out in a 0.7 cm x 1 cm cuvette. For F_0 measurements the sample was flowed at a rate of 6 ml/min - the effective sample replacement volume was approximately 0.15 ml. For F_{max} measurements the algae were incubated for 10 min with 20 µM DCMU and

10 mM hydroxylamine hydrochloride, preilluminated with several flashes of saturating intensity, and not flowed. All cuvettes were painted black except for a window for the exciting beam and a window in the direction of the photomultiplier. This masking was necessary to eliminate an apparent broadening of the excitation pulse shape due to reflections from the cuvette surfaces.

The single-photon timing fluorescence lifetime system and methods of numerical analysis are described in Chapter III.

III-3. RESULTS

1. Separation of three components in F_0 and F_{max}

In Fig. IV-1 is plotted the fluorescence decay data, F(t), in spinach chloroplasts with all reaction centers open in the presence of Mg^{+2}. If the excitation intensity is high enough to induce a steady state level of closed reaction centers, the fluorescence yield will rise during the course of an experiment. We checked for this effect by continuously monitoring the fluorescence yield (photon count rate). The yield did not increase during the measurement. The fluorescence decay law was assumed to be a sum of exponentials (see Eq. (2) in Chapter III); the lifetimes and amplitudes were deconvolved using the numerical techniques described in Chapter III. We first tried a sum of two exponentials. A plot of the deviations between the best two-exponential fit and the data is plotted on a linear scale in the middle of Fig. IV-1. The ringing pattern near the peak of the data is above the noise level and indicates that the decay cannot be described by two

Figure IV-1: Fluorescence decay of spinach chloroplasts at 680 nm in the presence of 5 mM $MgCl_2$ at low excitation intensity (F_0 level). The curve labeled E(t) is the excitation profile, and it has a FWHM of 310 ps. The curves labeled F(t) are the experimental fluorescence decay data (noisy) and the best three-exponential fit (smooth). The lifetimes, τ, and the relative yields, ϕ, of the three components are indicated. The middle and bottom plots are the deviations between the best two- and three-exponential fits and the fluorescence data. The deviations plots are on a linear scale.

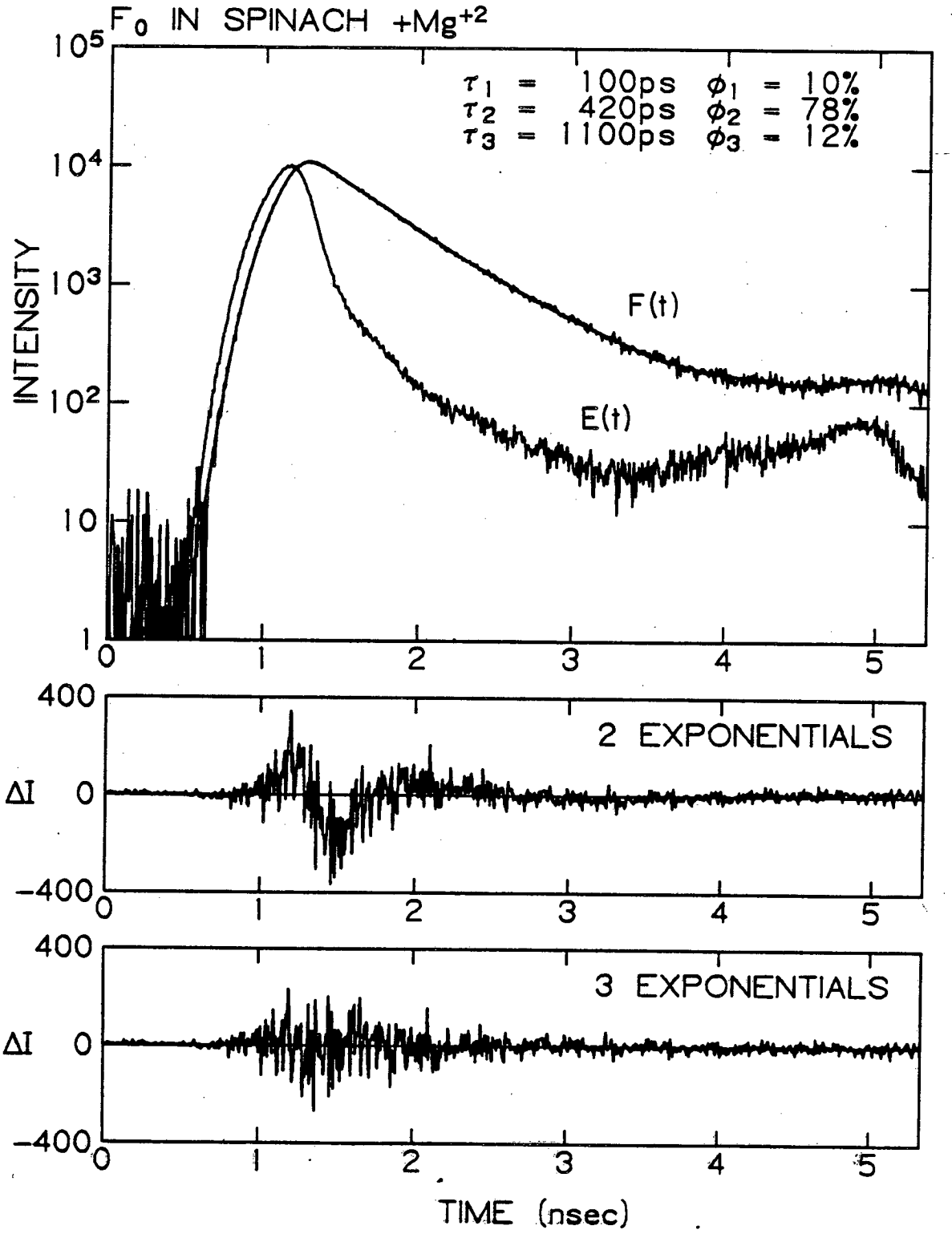
F_0 IN SPINACH +Mg^{+2}
τ_1 = 100ps ϕ_1 = 10%
τ_2 = 420ps ϕ_2 = 78%
τ_3 = 1100ps ϕ_3 = 12%
INTENSITY
F(t)
E(t)
2 EXPONENTIALS
3 EXPONENTIALS
ΔI
TIME (nsec)

XBL 811-4430

exponentials. The bottom of Fig. IV-1 illustrates that the deviations resulting from the best three-exponential fit contain only statistical noise. It is the best three-exponential fit that is the smooth line following F(t).

The fluorescence decay at the F_{max} level also requires a three-exponential fit to eliminate systematic errors in the deviations plot. The F_{max} data are plotted in Fig. IV-2. Because the fastest component is only a small amount of the total decay (approximately 1%), the two-exponential deviations resemble statistical noise. The finding of three components in F_0, however, led us to look for a third component in F_{max}. The bottom of Fig. IV-2 shows that the addition of the third fast component inproves the fit.

The results in Figs. IV-1 and IV-2 are for spinach chloroplasts in the presence of 5 mM $MgCl_2$. Elimination of $MgCl_2$ from the suspension buffer causes the grana membranes to unstack and alters the fluorescence properties of the chloroplasts [25,26]. The fluorescence results in the absence of $MgCl_2$ are given in Table IV-I. For both F_0 and F_{max} we needed a three-exponential decay law to fit the data. A detailed discussion of the magnesium effect is reserved for Chapter VI.

Table IV-I summarizes the results discussed above. This table includes the lifetime, τ, relative amplitudes, α, and yields, ϕ, of our best three-exponential fits. The amplitude, α, is the preexponential factor in Eq. (2) in Chapter III; the yield, which is proportional to $\alpha\tau$, represents the total fraction of the photons emitted in each phase. To compare our results with published experiments, we have included our best two-exponential fits and our τ_{mean} calculated from

Figure IV-2: Fluorescence decay of spinach chloroplasts at 680 nm in the presence of 5 mM $MgCl_2$ at the maximum fluorescence level, F_{max}. The chloroplasts were preilluminated with several saturating flashes following the addition of 12.5 μM DCMU and 2 mM hydroxlyamine hydrochloride. Other details are as in Fig. IV-1.

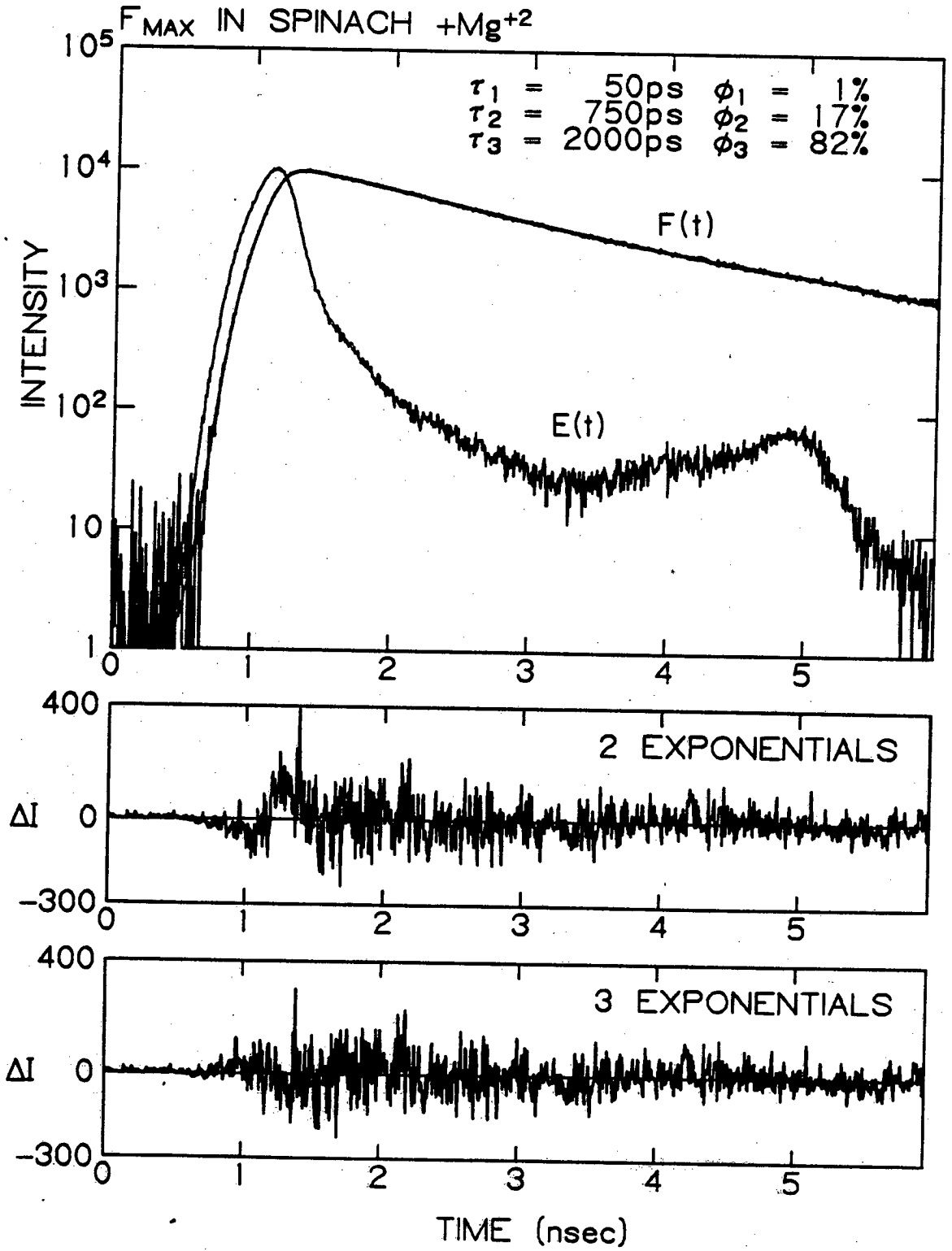
F_{MAX} IN SPINACH $+Mg^{+2}$
τ_1 = 50ps ϕ_1 = 1%
τ_2 = 750ps ϕ_2 = 17%
τ_3 = 2000ps ϕ_3 = 82%
F(t)
E(t)
INTENSITY
10^5
10^4
10^3
10^2
10
1
0 1 2 3 4 5
400
ΔI 0
-300
2 EXPONENTIALS
3 EXPONENTIALS
TIME (nsec)

XBL 811-4431

Table IV-I: Lifetimes and relative amplitudes of the exponential decay components in the fluorescence kinetics of spinach chloroplasts. Published values are indicated by the reference in the column at the right. In Ref. [32], the measurements under low salt were done without the addition of 5-10 mM monovalent cations. The techniques were single-photon counting [31,32], streak camera with high intensity single picosecond pulse [33], and phase fluorimetry [4,38]. The chloroplasts were isolated from spinach [31], pea [32,38], lettuce [4], or barley [33].

TABLE IV-I

Experimental conditions	3-exponential fit τ(ps)	α	ϕ	2-exponential fit τ(ps)	α		1-exponential fit τ_{mean}(ns)	
F_0	130	0.55	26%	250	0.92		0.55	[This study]
	360	0.41	55%	1100	0.08			
	1500	0.04	19%					
+5 mM NaCl								
				200	0.99	[31]	0.6	[4]
				500	0.01			
				410	0.96	[32]	0.4	[38]
				1460	0.04			
				160	0.77	[33]		
				600	0.23			
F_{MAX}	160	0.31	8%	410	0.76		1.04	[This study]
	530	0.53	47%	1500	0.24			
	1700	0.16	45%					
+5 mM NaCl								
				480	0.93	[31]	1.31	[4]
				2000	0.07			
				450	0.90	[32]	0.9	[38]
				1330	0.10			
				150	0.72	[33]		
				1060	0.28			
F_0	100	0.34	10%	320	0.80		0.47	[This study]
	420	0.63	78%	750	0.20			
	1200	0.03	12%					
+5 mM NaCl								
				320	0.99	[31]	0.7	[4]
+5 mM $MgCl_2$				>500	0.01			
				150	0.66	[33]	0.5	[38]
				620	0.34			
F_{MAX}	50	0.25	1%	790	0.37		1.73	[This study]
	750	0.26	17%	2000	0.63			
	2000	0.49	82%					
+5 mM NaCl								
				460	0.63	[32]	1.7	[4]
+5 mM $MgCl_2$				1340	0.37			
				130	0.52	[33]	1.35	[38]
				1290	0.48			

$$\tau_{mean} = \sum_{i=1}^{3} \alpha_i \phi_i \Big/ \sum_{i=1}^{3} \phi_i \qquad (1)$$

The remaining values in Table IV-I are results from earlier studies. In general, we find fairly good agreement with published results. The major new finding of our experiments is that one or two components do not adequately describe the data, while three components describe the data well. The picosecond resolution capabilities of our system enable us to detect the fast component with a lifetime of about 100 ps. The lifetime of the middle component is between 400 ps and 700 ps and the lifetime of the slow component is between 1.2 ns and 2.2 ns; each of these lifetimes depends on the conditions of the experiment. The yield of the slow component is extremely sensitive to the state of the reaction center of photosystem II.

It is not possible for the fast phase to be an artifact originating from a low level transmission of scattered excitation light through the 680 nm interference filter and Corning 2-59 cutoff filter (passes $\geq$ 640 nm) used in front of the photomultiplier. A typical F_0 measurement is collected at a photon count rate of about 2000 photons per second. Because about 10% of F_0 is fast phase, the fast phase accounts for about 200 photons per second. We determined that, with the excitation intensity used on an F_0 experiment, less than 5 photons per second of scattered light pass through our filter combination. This low level of scattered light could not cause the observation of a fast phase.

2. Fluorescence Decay Kinetics in Green Algae

Spinach chloroplasts were removed from spinach leaves by the

procedure described in the Materials and Methods section. There is a possibility that this treatment, which breaks the chloroplasts, affects the fluorescence decay kinetics of chlorophyll a. To test for such an effect, we measured the fluorescence decay kinetics in the green algae Chlamydomonas reinhardtii and Chlorella pyrenoidosa; these experiments were done on intact cells. In Figs. IV-3 and IV-4 are plotted the fluorescence data from green algae. The values for the lifetimes and yields are given in Table IV-II. As in broken chloroplasts, a good fit to the green algae data requires a three-exponential decay law. The three components are nearly identical to the three components we found in spinach except for a slightly larger contribution of the slow phase to the F_0 level.

3. Intensity Dependence of Fluorescence Decay Kinetics in Spinach Chloroplasts

Two extreme models of the photosynthetic antenna are the lake and puddle models. In the lake model, the antenna chlorophyll can transfer its energy to any one of many reaction centers. This model predicts that as reaction centers become progressively closed, there will be a gradual change in the fluorescence decay kinetics induced by an increased concentration of closed reaction centers. In the puddle model, each reaction center has an isolated chlorophyll antenna associated with it. In this model, as the reaction centers become progressively closed, there will be two classes of lifetimes - lifetimes associated with open reaction centers and lifetimes associated with closed reaction centers. Provided that we are able to resolve all of the fluorescence components, the puddle model predicts that as reaction centers become closed, there

Figure IV-3 Fluorescence decay of Chlamydomonas reinhardtii at 680 nm in the dark adapted state, $F_0(t)$, and in the state of maximum fluorescence, $F_{max}(t)$. The curve labeled E(t) is as in Fig. IV-1. The noisy experimental decays are superimposed with a smooth curve that is the best three-exponential fit. The deviations between the best fit and the experimental data are shown on a linear scale for F_0, middle, and F_{max}, bottom.

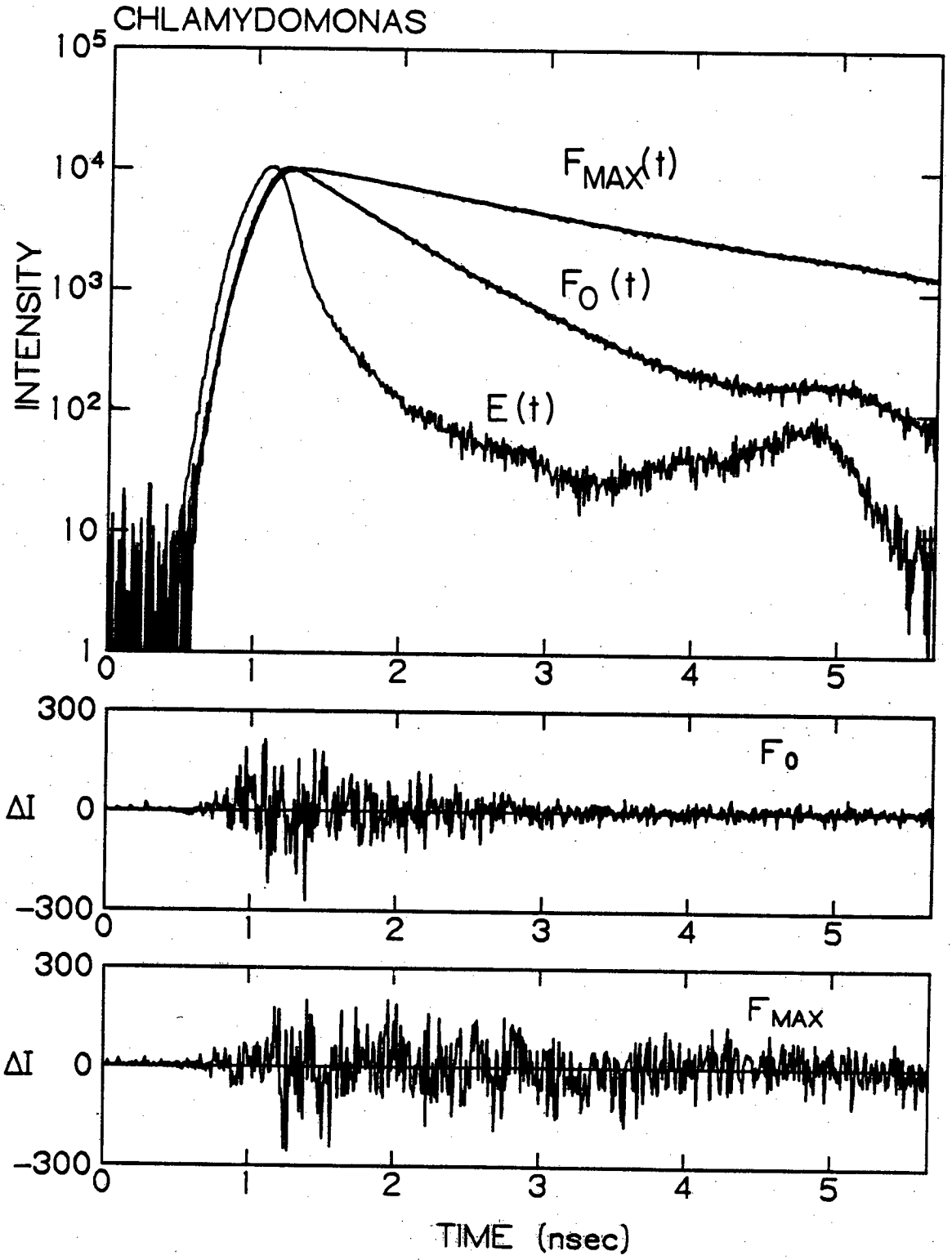
CHLAMYDOMONAS
INTENSITY
10^5
10^4
10^3
10^2
10
1
$F_{MAX}(t)$
$F_O(t)$
E(t)
0 1 2 3 4 5
300
ΔI 0
−300
F_O
0 1 2 3 4 5
300
ΔI 0
−300
F_{MAX}
0 1 2 3 4 5
TIME (nsec)

XBL811-4432

Figure IV-4: Fluorescence decay of Chlorella pyrenoidosa at 680 nm. Other details are as in Fig. IV-3.

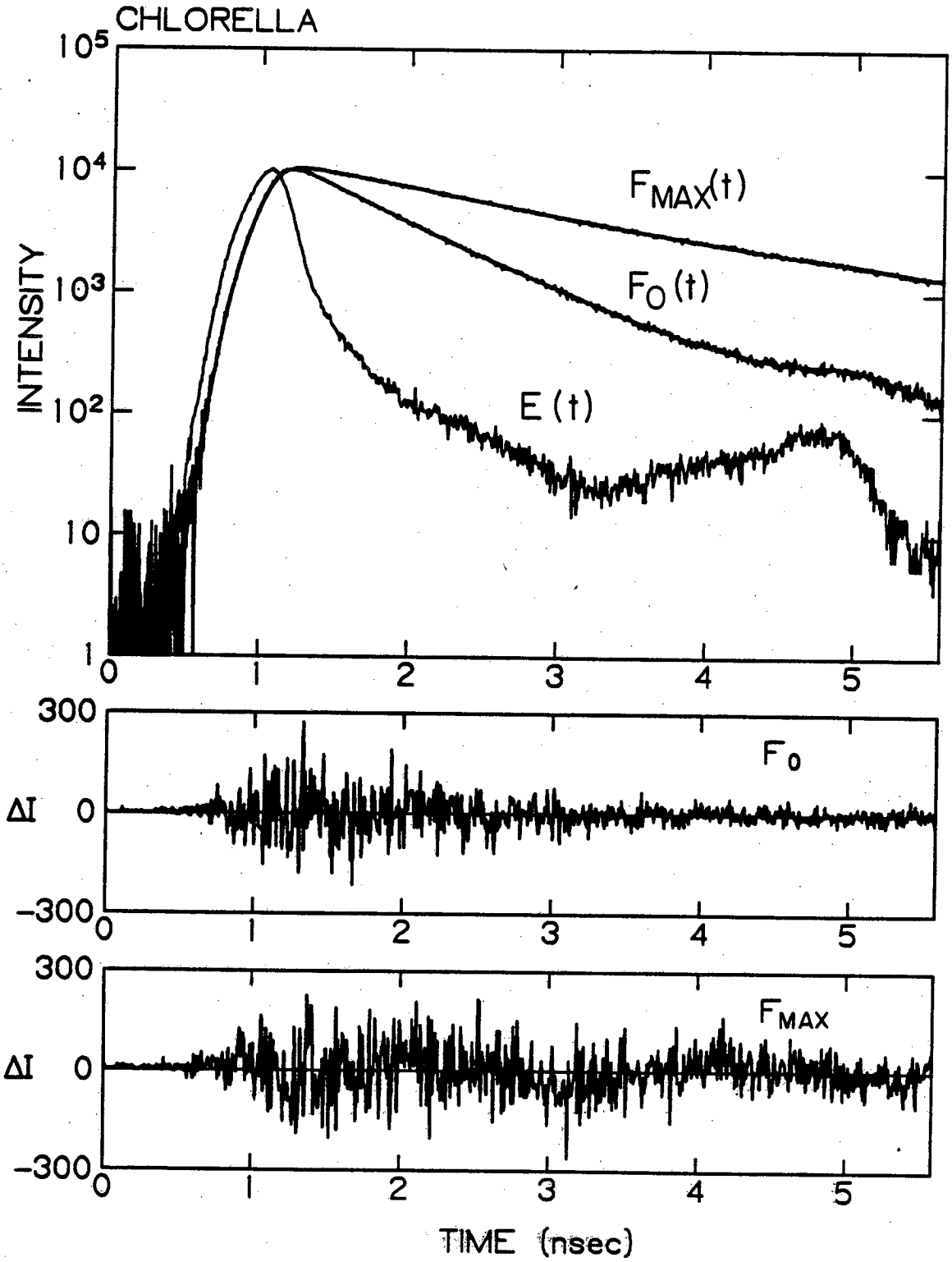
CHLORELLA
INTENSITY
10^5
10^4
10^3
10^2
10
1
$F_{MAX}(t)$
$F_0(t)$
E(t)
0
1
2
3
4
5
300
ΔI
0
-300
F_0
F_{MAX}
TIME (nsec)

XBL 811-4433

Table IV-II: Decay components for fluorescence decay kinetics in green algae (intact cells) and in spinach chloroplasts (broken chloroplasts in the presence of 5 mM $MgCl_2$). The fluorescence yields in this table are normalized for a total yield of F_0 equal to 100. Pea chloroplasts were isolated by the same procedure as for spinach chloroplasts, either from 11 day old seedlings grown in a growth chamber or from peas germanated for 7 days in the dark and illuminated by 50 intermittent light periods (1700 lux) of 2 min each followed by a dark period of 118 min [23,24]

Sample	Level	τ_1(ps)	ϕ_1	τ_2(ps)	ϕ_2	τ_3(ps)	ϕ_3	F_{max}/F_0
Chlamydomonas reinhardtii	F_0	70	8.0	390	44	750	48	3.8
	F_{MAX}	60	2.3	850	62	2300	310	
Chlorella pyrenodosa	F_0	60	2.0	390	30	840	68	3.0
	F_{MAX}	70	2.2	810	48	2100	250	
Spinach Chloroplasts	F_0	110	10	420	78	1200	12	4.0
	F_{MAX}	50	4.0	750	68	2000	330	
Pea Chloroplasts	F_0	50	6.0	340	65	680	29	5.1
	F_{MAX}	70	2.5	700	68	2200	440	
Iml-Pea Chloroplasts	F_0	80	14	510	35	2100	51	2.2
	F_{MAX}	90	9.0	660	50	2400	158	

will be a build-up of components due to closed reaction centers and a disappearance of components due to open reaction centers. It is not possible to discriminate between these models by looking only at the all-open and all-closed states. Thus, we have looked at the fluorescence decay kinetics in spinach chloroplasts as the reaction centers become increasingly closed.

The spinach chloroplast sample measured was in the buffer containing 5 mM $MgCl_2$ with the addition of 2 μg/ml of gramicidin D. The sample was stirred in a 1 cm x 1 cm cuvette. In Figs. IV-5 and IV-6 are plotted the lifetimes and yields, repectively, as the intensity is varied to progressively close reaction centers. The results at the lowest intensity and at the highest intensity are very similar to the F_0 and F_{max} results in the presence of 5 mM Mg^{+2} presented in Table IV-1. Thus, the data in Figs. IV-5 and IV-6 span the entire range from all-open reaction centers to all-closed reaction centers.

The major change in yields is a 30-fold increase in the slow phase. The yields of the fast and middle phases are nearly constant, which means that the slow phase accounts for nearly all of the variable fluorescence; i.e., all of the change in ϕ_{tot}.

The lifetime of the slow phase increases by a factor of only two, despite the enormous change in its yield. The middle phase lifetime also increases by a factor of two and the fast phase lifetime decreases somewhat. The change in the lifetime of the fast phase is less definite because of the difficulty of resolving this phase, especially near the all-closed state.

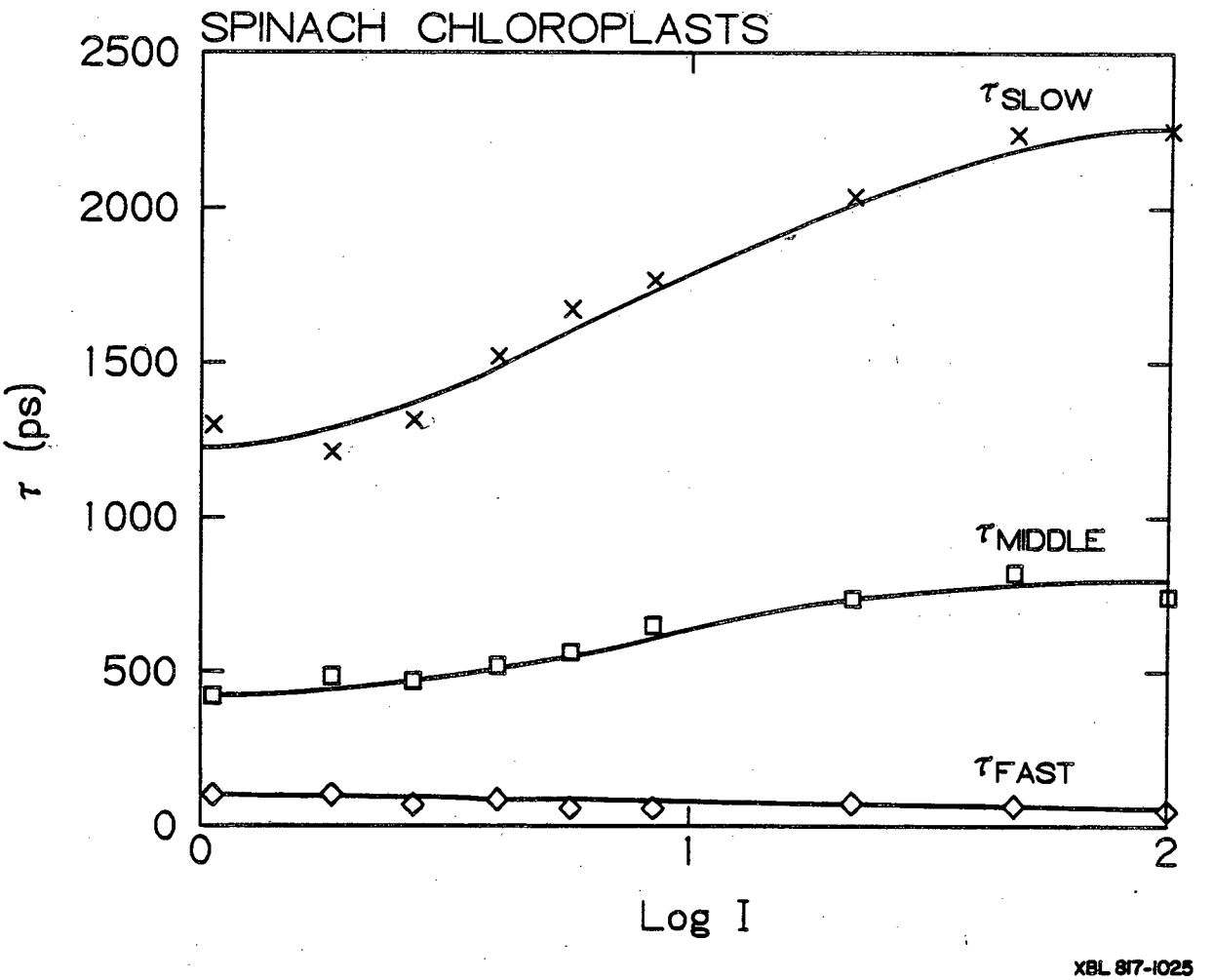

Figure IV-5: Lifetimes of the components of the fluorescence decay kinetics in spinach chloroplasts as a function of the laser intensity. Other experimental conditions as in Fig. IV-1.

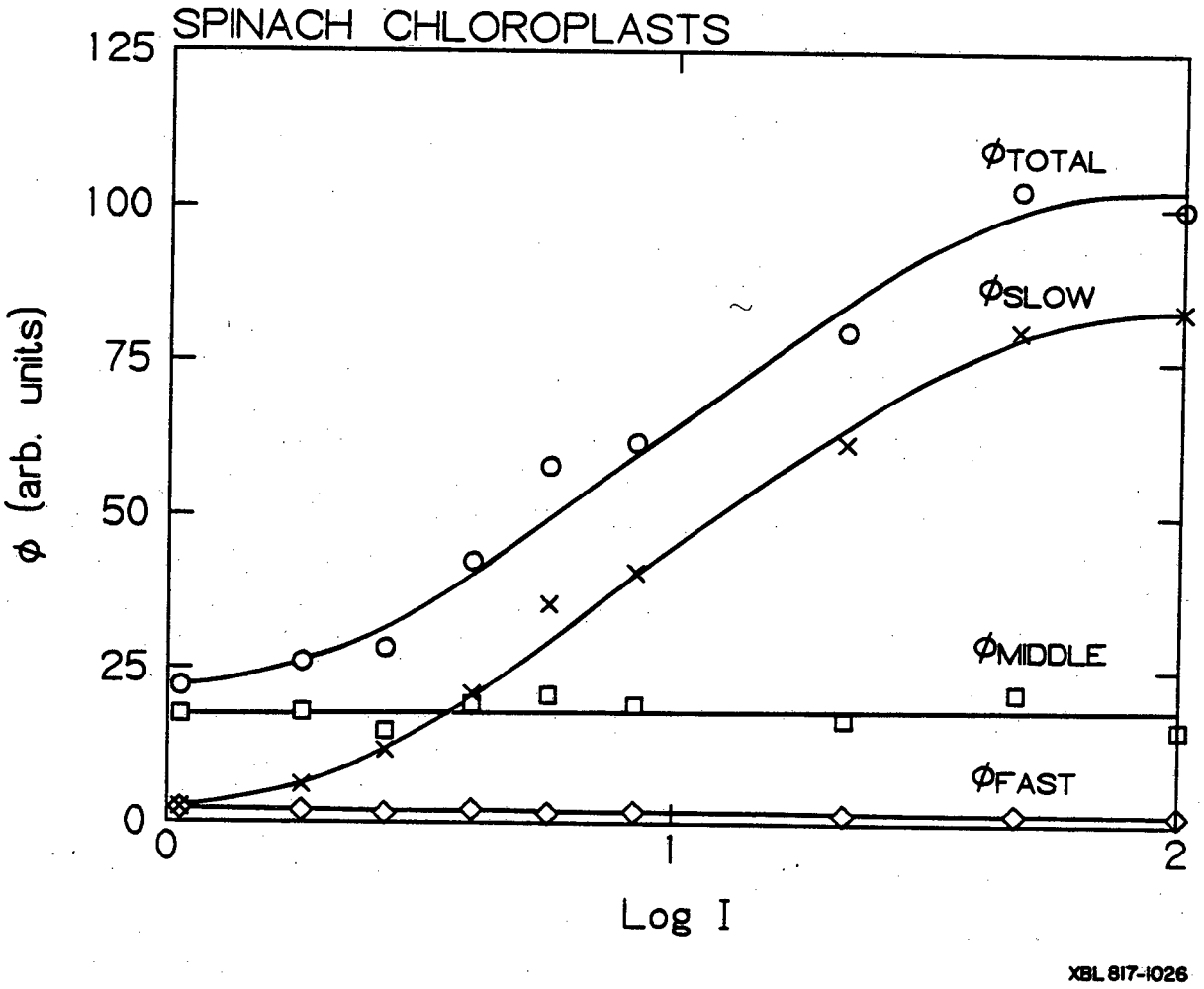

Figure IV-6: Yields of the components of the fluorescence decay kinetics in spinach chloroplasts as a function of the laser intensity. Other experimental conditions as in Fig. IV-1.

4. Intermittent-Light Pea Chloroplasts

Changes in the composition of the light-harvesting antenna chlorophyll might influence the fluorescence decay kinetics and may give insight into connections between photosynthetic units. To investigate this effect, we have measured the fluorescence decay in pea chloroplasts grown in intermittent light. These chloroplasts have intact photosystem I and photosystem II but are agranal and do not contain the light-harvesting chlorophyll a/b protein [27,28]. The values of the best three-exponential fits are given in Table IV-II. The major changes compared to normal pea chloroplasts (results also given in Table IV-II) are: (1) very little change in the lifetimes of the slow and middle phases between F_0 and F_{max}, and (2) a much smaller change in the yield of the slow component as the reaction centers become closed. The ratio $F_{max}/F_0 = 2.2$ is in good agreement with previous measurements [28].

IV-4. DISCUSSION

1. Comparison With Other Lifetime Measurements

The deconvolutions of our fluorescence decay kinetics indicate that three-exponential decays fit the experimental data within the statistical noise. The three components are found in intact cells of Chlorella and Chlamydomonas as well as in chloroplasts from spinach and peas; the three components are observed at both the F_0 and F_{max} levels. As demonstrated by the deviations plots in Figs. IV-1 and IV-2, a two-exponential decay is not sufficient to describe the fluorescence decay kinetics. We also are not able to fit our data with nonexponential decay

laws such as those used by Barber et al. [29].

A comparison of our findings with those published in the recent literature (See Table IV-I) shows that, apart from the number of resolved components, our results can be reconciled fairly well with the results of other workers. Compared to previous measurements from this laboratory [30,31] the time resolution and the deconvolution techniques have both been improved. These changes account, in part, for the different results presented in this paper. If our results are reduced to the best two-exponential fits, the fluorescence lifetimes and amplitudes are comparable to those measured by Beddard, et al. [32]. They used a fluorescence lifetime measuring system similar to ours.

Searle, et al. [33] excited chloroplast samples with a high laser pulse energy of about 2×10^{14} photons/cm^2 and monitored the fluorescence decay with a streak camera. These authors resolved two exponential components and the two components were affected by the addition of Mg^{+2} and the closing of photosystem II reaction centers in a similar way to the components of our two-exponential analysis. Their lifetimes, however, are considerably shorter than ours. The shortening was probably caused by singlet-singlet annihilation, which is induced by picosecond pulses having energies greater than 10^{13} photons/cm^2 [34,35]. We emphasize that the energy or our pulses, $2\text{-}4 \times 10^6$ photons/cm^2, is more than six orders of magnitude lower than the energy of pulses used in studies involving single picosecond pulses from a solid state laser. In addition, the time averaged intensity of the excitation during our measurements is similar to that used in conventional studies of the fluorescence yield.

Most of the fluorescence lifetime studies in the literature have

been done by phase fluorimetry. The lifetimes are generally calculated from the results by assuming that the fluorescence follows a single-exponential decay law. We find good agreement between lifetimes derived by phase fluorimetry and the mean lifetimes calculated from the best three-exponential fits in Table IV-I. The most complete phase fluorimetry studies have measured the lifetime as a function of light intensity. In each case, the lifetime was found to increase from about 0.4 ns at low intensity to about 2 ns at high intensity and to be proportional to the total yield [4,36-39]. To compare these results to our data, we have plotted in Fig. IV-7 the mean lifetime of the results plotted in Figs. IV-5 and IV-6 as a function of the total fluorescence yield. The nearly linear relation closely agrees with the phase fluorimetry results. This deceptively simple linear relation has influenced the conclusions of some authors about the fluorescence properties of chloroplasts.

2. A Model for the Origin of the Fluorescence

A simple model for the fluorescence lifetime and yield from an array of light-harvesting chlorophylls connected to photosystem II reaction centers, $P_{680}Q$ (cf. Ref. [5]), leads to the relations

$$\tau = 1/(k_F + k_D + K_{ic} + k_T[P_{680}Q]) \tag{2}$$

and

$$\Phi_F = k_F\tau \tag{3}$$

where k_F is the intrinsic rate constant for fluorescence, k_D is the sum of the rate constants for radiationless deactivation by internal

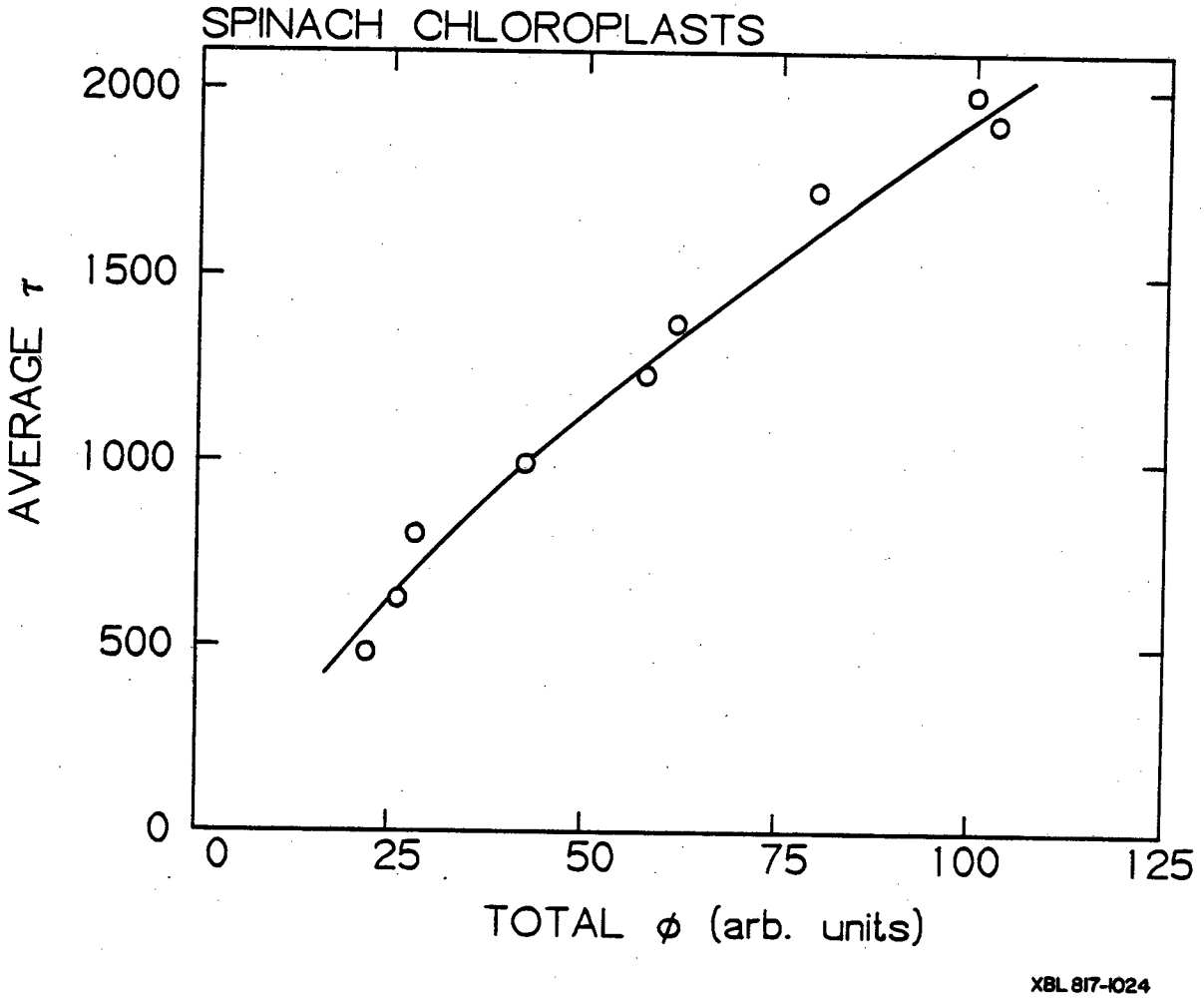

Figure IV-7: Average lifetime of the fluorescence decay as a function of total fluorescence yield. Average lifetime calculated from the data in Figs. IV-5 and IV-6.

conversion and spillover to photosystem I, k_{ic} is the rate constant for intersystem crossing, k_T is the second order rate constant for energy transfer to photosystem II reaction centers, and $[P_{680}Q]$ is the fraction of open photosystem II reaction centers. If all of the reaction centers are open, the fluorescence yield is at a minimum (F_0); if all reaction centers are closed, the fluorescence yield is at a maximum (F_{max}). It is easy to show [40] that based on this model, the maximum yield of photochemistry is given by

$$\phi_{Pmax} = \frac{F_{max} - F_0}{F_{max}} \tag{4}$$

A value of $\phi_{Pmax} \geq 0.95$ has been estimated from the quantum yield of the electron transport through photosystem II [6,7]. A slightly lower value of $\phi_{Pmax} = 0.935$ can be estimated from the minimum quantum yield of excitation losses by fluorescence of 2% [7] and by intersystem crossing of 4.5% [41]. These values give a predicted ratio F_{max}/F_0 of 20 and 15, respectively, which is not consistent with the ratio of 3 to 5 found for chloroplasts and algae (cf. Refs. [4], [5] and Table II).

One proposal to account for this discrepancy without modifying the simple model is that a portion of F_0 and F_{max} is fluorescence from chlorophyll that is not connected to the reaction center of photosystem II. Free chlorophyll or chlorophyll separated from the light-harvesting pigments could account for such a constant contribution to the fluorescence. It should have a long lifetime (2 to 5 ns), however, and we see no significant contribution from a constant long-lifetime background. Another source of constant fluorescence could be chlorophyll in photosystem I. Beddard *et al.* [32] have measured a

fluorescence lifetime of 110 ps for photosystem I particles, and this result is consistent with the lifetime of 80 ps attributed to photosystem I by Paschenko et al. [42]. These results suggest that our fast phase may be due to photosystem I. The spectrum of the fast phase is very similar to those of the other two components, all peaking around 680 nm, and shows only a slightly larger relative yield around 730 nm compared to 680 nm (data not shown). We conclude that some of the fast phase may be emission from chlorophyll a from the antenna pigments associated with photosystem I. These pigments have an emission spectrum similar to that of the pigments of photosystem II [2]. Apart from this assignment, the yield of the fast phase, being 10% or less of F_0, is much smaller than approximately 80% of F_0 that would have to be constant fluorescence to account for the above discrepancy.

Butler [13,40,43] and Duysens [11,12] account for the discrepancy between the measured and predicted ratio F_{max}/F_0 by assuming a new radiationless deactivation pathway in closed reaction centers. That is, the closed reaction center can still quench fluorescence. Duysens [11,12] has calculated the amount of quenching required in the closed reaction centers in order to observe only a 4 fold increase between F_0 and F_{max}. His model is adequate to describe this effect as well as the relation in Fig. IV-7, but it cannot explain our data in Figs IV-5 and IV-6.

In the tripartite model proposed by Butler et al. [13,40,43], excitation is transfered to photosystem II reaction centers from closely connected chlorophyll a proteins. Energy can reach the chlorophyll a proteins either by direct absorption or by energy transfer from remotely connected light-harvesting chlorophyll a/b proteins. Excitation reaching

a closed reaction center can undergo radiationless deactivation or be transferred back to the chlorophyll antenna where fluorescence is possible. A qualitative kinetic analysis of this scheme results in the following conclusions for photosystem II fluorescence: 1) When all reaction centers are open, the fluorescence would be dominated by two fast components whose lifetimes are close to the transfer times from the two different components of the photosystem II antenna to the reaction center. 2) When reaction centers are closed, the fast components would still be present, because transfer to the reaction center is still taking place, and a new slow component would arise reflecting the kinetics of back transfer from the reaction center to the antenna. This pattern is qualitatively identical to our observations, except that we see a small amount of slow fluorescence in F_0. The residual slow fluorescence could be due either to a dark level of closed photosystem II reaction centers or to kinetic competition between photochemistry and back transfer in open photosystem II reaction centers.

The results of Klimov et al. [14-20] suggest a mechanism for the processes occuring in the photosystem II reaction center that may control the back transfer of energy to the antenna discussed by Butler et al. [13,40,43]. In the model of Klimov et al. [14-20], a pheophytin molecule (Ph) functions as a primary electron acceptor in photosystem II between P_{680} and Q. Charge separation is always possible in a photosystem II reaction center. When Q is oxidized, a fast charge stabalization takes place

$$P^+_{680}Ph^-Q \longrightarrow P^+_{680}Ph\ Q^- \qquad (5)$$

But when Q is reduced, charge recombination can occur [14-20]

$$P^{+}_{680}Ph^{-}Q^{-} \longrightarrow P^{*}_{680}Ph\ Q^{-} \qquad (6)$$

The excited state may lead to fluorescence from the antenna or from the reaction center. Charge recombination to the ground state provides the new mechanism of radiationless deactivation in closed reaction centers postulated by Butler et al. [13,40,43] and Duysens [11,12]. Our data are consistent with Butler's tripartite model for energy transfer and with the processes in the reaction center described by Klimov et al. [14-20]

We conclude that the fast phase and the middle phase represent fluorescence resulting from excitation that is lost on its way from the light-harvesting pigments to the photosystem II reaction center and reflect the transfer times from the two different antenna proteins. Photosystem I fluorescence may account for some of the fast phase. We propose that the component, increasing from 1 ns when all reaction centers are open to 2.2 ns when all reaction centers are closed, reflects the kinetics of the charge recombination. The two fold increase in lifetime indicates some connection between photosystem II units. Our slow component is shorter than the 4 ns component reported by Shuvalov et al. [44]. We did not find in either chloroplasts or algae such a slow component of fluorescence.

In Chapter V, is presented a detailed analysis of a kinetic model for fluorescence emission. The model allows us to make some quantitative conclusions about the emission from the antenna chlorophyll proteins and about the connectedness between photosystem II units [45].

IV-5. REFERENCES

1. R. B. Park, K. E. Steinbeck, and P. V. Sane, Biochim. Biophys. Acta 253, 204 (1971).
2. N. K. Boardman, S. W. Thorne, and J. M. Anderson, Proc. Natl. Acad. Sci. USA 56, 586 (1966).
3. Govindjee and L. Yang, J. Gen. Physiol. 49, 763 (1966).
4. J.-M. Briantais, C. Vernotte, and I. Moya, Biochim. Biophys. Acta 325, 530 (1973).
5. B. M. Henkin and K. Sauer, Photochem. Photobiol. 26, 277 (1977).
6. M. Kamen, in Primary Processes in Photosynthesis, Academic Press, New York, 105 (1963).
7. B. Kok and G. Hoch, in Light and Life (eds: W. D. McElroy and B. Glass), Johns Hopkins, Baltimore, 397 (1961).
8. A. S. K. Sun and K. Sauer, Biochim. Biophys. Acta 234, 399, (1971).
9. R. K. Clayton, Biophys. J. 9, 60 (1969).
10. J. Lavorel and P. Joliot, Biophys. J. 12, 815 (1972).
11. L. N. M. Duysens, in Chlorophyll Organization and Energy Transfer in Photosynthesis, Ciba Found. Symp. 61, Elsevier/North Holland Press, Amsterdam, 323 (1979).
12. R. van Grondelle and L. N. M. Duysens, Plant Physiol. 65, 751 (1980).
13. W. L. Butler and M. Kitajima, Biochim. Biophys. Acta 376, 116 (1975).
14. V. V. Klimov, A. V. Klevanik, V. A. Shuvalov, and A. A. Krasnovsky, FEBS Lett. 82, 183 (1977).
15. A. V. Klevanik, V. V. Klimov, V. A. Shuvalov, and A. A. Krasnovsky,

Dokl. Akad. Nauk SSSR 236, 241 (1977).

16. V. V. Klimov, S. I. Allakhverdiev, and V. Z. Paschenko, Dokl. Akad. Nauk SSSR 236, 1204 (1978).

17. V. V. Klimov, S. I. Allakhverdiev, and A. A. Krasnovsky, Dokl. Akad. Nauk SSSR 249, 485 (1980).

18. V. V. Klimov, S. I. Allakhverdiev, S. Demeter, and A. A. Krasnovsky, Dokl. Akad. Nauk SSSR 249, 227 (1980).

19. V. V. Klimov, S. I. Allakhverdiev, S. I. Shutilova, and A. A. Krasnovsky, Sov. Plant Physiol. 27, 315 (1980).

20. V. V. Klimov, E. Dolan, and B. Ke, FEBS Lett. 112, 97 (1980).

21. B. Andersson, C. Sundby, and P.-A. Albertsson, Biochim. Biophys. Acta 599, 128 (1980).

22. J.-M. Briantais, C. Vernotte, M. Picaud, and G. H. Krause, Biochim. Biophys. Acta 548, 128 (1979).

23. R. C. Starr, in Methods in Enzymology, XXIII (ed. San Pietro), Academic Press, New York, 36 (1971).

24. N. Sueoka, Proc Natl. Acad. Sci. USA 46, 83 (1960).

25. N. Murata, Biochim. Biophys. Acta 189, 171 (1969).

26. E. L. Gross and S. H. Prasher, Arch. Biochem. Biophys. 164, 460 (1974).

27. J. H. Argyroudi-Akoyunglou and G. Akoyunoglou, Plant Physiol. 46, 247 (1970).

28. P. A. Armond, C. J. Arntzen, J.-M. Briantais, and C. Vernotte, Arch. Biochem. Biophys. 175, 54 (1976).

29. J. Barber, G. F. W. Searle, and C. J. Tredwell, Biochim. Biophys. Acta 501, 174 (1978).

30. K. Sauer and G. T. Brewington, in Proc. 4th Int. Congr

Photosynthesis (eds: D. O. Hall, J. Coombs, and T. W. Goodwin), The Biochemical Society, London, 409 (1977).

31. G. T. Brewington, "Studies of Photosynthetic Membranes Using Chlorophyll Fluorescence Lifetimes", PhD Thesis, Univ. California, Berkeley (LBL-9795) (1979).

32. G. S. Beddard, G. R. Fleming, G. Porter, G. F. W. Searle, and J. A. Synowiec, Biochim. Biophys. Acta 545, 165 (1979).

33. G. F. W. Searle, C. J. Tredwell, J. Barber, and G. Porter, Biochim. Biophys. Acta 545, 496 (1979).

34. J. Breton and N. E. Geacintov, Biochim. Biophys. Acta 594, 1 (1980).

35. A. J. Campillo, V. H. Kollman, and S. L. Shapiro, Science 193, 227 (1976).

36. A. Müller, R. Lumry, and M. S. Walker, Photochem. Photobiol. 9, 113 (1969).

37. J.-M. Briantais, H. Merkelo, and Govindjee, Photosynthetica 6, 133 (1972).

38. I. Moya, Govindjee, C. Vernotte, and J.-M. Briantais, FEBS Lett. 75, 13 (1977).

39. I. Moya, Biochim. Biophys. Acta 368, 214 (1974).

40. W. L. Butler, Ann. Rev. Plant Physiol. 29, 345 (1978).

41. H. Kramer and P. Mathis, Biochim. Biophys. Acta 593, 319 (1980).

42. V. Z. Paschenko, S. P. Protosov, A. B. Rubin, K. N. Timofeev, L. M. Zamazova, and L. B. Rubin, Biochim. Biophys. Acta 408, 143 (1975).

43. W. L. Butler and R. J. Strasser, Proc. Natl. Acad. Sci. USA 74, 3382 (1977).

44. V. A. Shuvalov, V. V. Klimov, E. Dolan, W. W. Parson, and B. Ke,

FEBS Lett. 118, 279 (1980).

45. P. Reisberg, J. A. Nairn, W. A. Haehnel, and K. Sauer, in preparation.

CHAPTER V

A WORKING MODEL FOR INTERPRETATION OF FLUORESCENCE DECAY KINETICS IN SPINACH CHLOROPLASTS

V-1. INTRODUCTION

In the discussion of Chapter IV and in Refs. [1] and [2], a working model was proposed which is consistent with our room-temperature fluorescence lifetime experiments. The complete kinetic scheme for this model is diagrammed in Fig. V-1. Chl a/b* and Chl a_2^* represent excited state chlorophyll in the chlorophyll a/b light-harvesting antenna (Chl a/b LH) and the chlorophyll a antenna of photosystem II (Chl a_2), respectively. These are the chlorophyll antenna components of photosystem II in Butler's tripartite model [3]. The kinetic paths connecting the Chl a/b* and Chl a_2^* to each other and to the the reaction center of photosystem II are identical to those of the tripartite model [3] except that, for simplicity, we have assumed that the fluorescence rate, k_F, and the radiationless decay rate, k_D, from Chl a/b* and Chl a_2^* are identical. The remaining states in Fig. V-1 are the possible states of the photosystem II reaction center; here, P_{680}, probably a chlorophyll a monomer, is the primary electron donor in photosystem II [4]; Ph, probably a pheophytin a molecule, is the primary electron acceptor in photosystem II [5-11]; and Q, probably a quinone molecule, is the secondary electron acceptor in photosystem II [12,13]. The top row represents the kinetic paths in photosystem II units with open reaction centers (Q oxidized), and the bottom row represents the

Figure V-1: Working model for the interpretation of the room-temperature lifetime experiments in spinach chloroplasts. k_f is a fluorescence rate; k_D, k_d, and k_d' are radiationless decay rates; k_{T32}, k_{T23}, k_{T20}, and k_{T02} are energy transfer rates; k_c, k_r, and k_p are electron transfer rates, and f (= 1-g) is the fraction of closed photosystem II reaction centers.

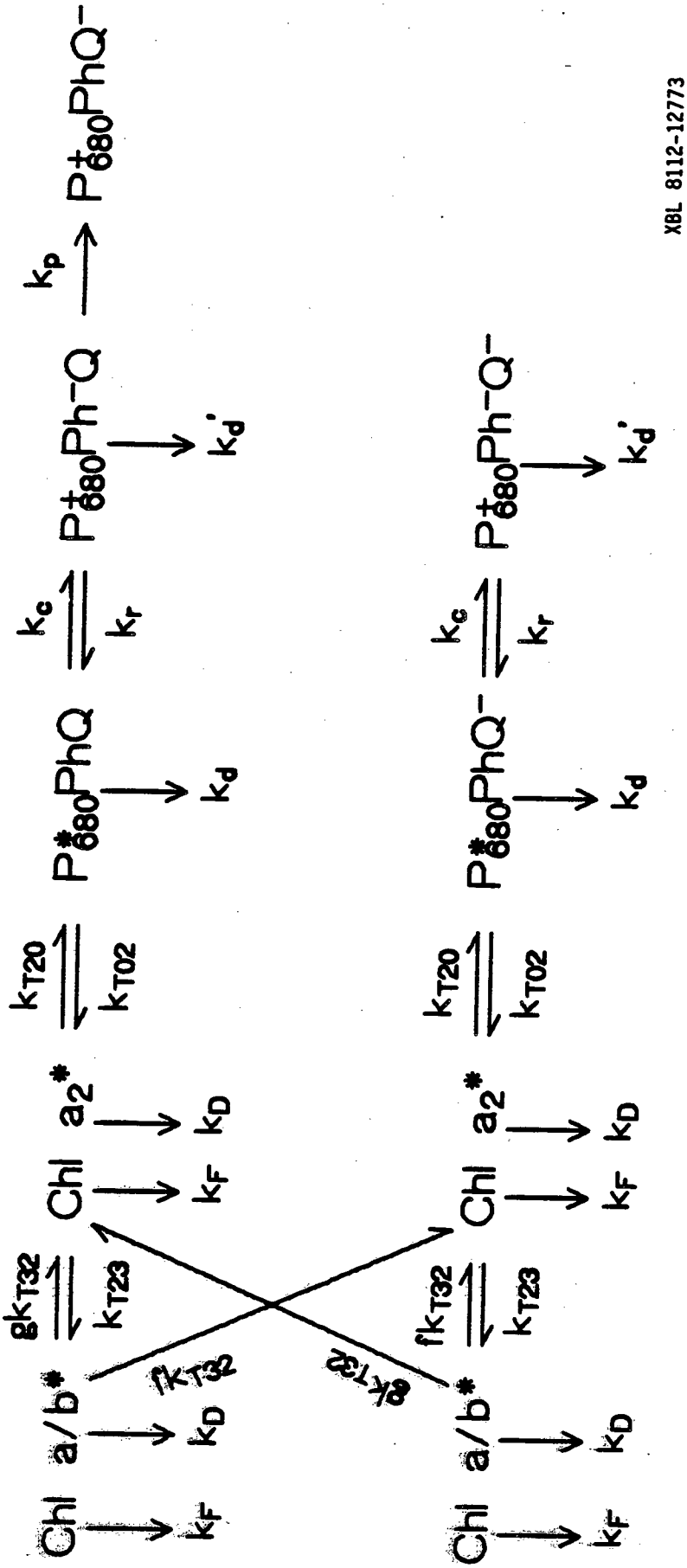
Chl a/b* → k_F, k_D
Chl a2* → k_F, k_D
P*680PhQ → k_d
P+680Ph−Q → k'_d
P+680PhQ− → k_d
P+680Ph−Q− → k'_d
k_T20 ⇌ k_T02
k_c ⇌ k_r
k_p →
gk_T32 ⇌ k_T23
fk_T32 ⇌ k_T23
fk_T32
gk_T32
XBL 8112-12773

kinetic paths in photosystem II units with closed reaction centers (Q reduced). The electron transfer processes which can occur in the photosystem II reaction center are derived from the model proposed by Klimov et al. [5-11].

In this chapter, I describe the use of the kinetic scheme in Fig V-1 to simulate the intensity dependence of the room-temperature fluorescence lifetime data from spinach chloroplasts isolated in the presence of 5 mM $MgCl_2$ (see Figs. IV-5 and IV-6). The simulation is begun by considering the F_{max} state, where all of Q is reduced. The simulation of the fluorescence properties of this state requires consideration of only the four states in the bottom row of Fig IV-1. The fluorescence intensity at time t is given by

$$F(t) = k_F([\text{Chl a/b}^*] + [\text{Chl a}_2^*]) \qquad (1)$$

where $[\text{Chl a/b}^*]$ and $[\text{Chl a}_2^*]$ are the concentrations of excited states in the Chl a/b LH antenna and the Chl a_2 antenna at time t, respectively. These time-dependent concentrations can be found by solving a system of linear differential equations which are derived from Fig. V-1 by mass action. For example, in the all-closed state, the time dependence of $[\text{Chl a}_2^*]$ follows

$$\frac{d[\text{Chl a}_2^*]}{dt} = -(k_F+k_D+k_{T23}+k_{T20})[\text{Chl a}_2^*] + k_{T32}[\text{Chl a/b}^*] \qquad (2)$$

$$+ k_{T02}[P_{680}^*PhQ^-]$$

For any set of rate constants and initial conditions, the system of linear differential equations can easily be solved numerically and F(t) found by use of Eq. (1). A three-exponential fit of the resulting F(t)

yields three components which can be compared to our fluorescence data. The rate constants and the initial conditions are varied until the three calculated components agree with our experimental F_{max} data which corresponds to the highest intensity data points in Figs. IV-5 and IV-6.

To simulate experiments at intermediate intensities, we consider all of the kinetic paths in Fig V-1, use the rate constants found from the F_{max} simulations, and vary f, the fraction of photosystem II units with Q reduced. These calculations give three fluorescence decay components as a function of the fraction of closed photosystem II reaction centers. To compare with our experimental data, the calculated decay components and the actual data are replotted as a function of the total fluorescence yield. The total fluorescence yield of the chloroplasts is normalized such that the fluorescence yield at the highest intensity is 100; the total fluorescence yield of the calculations is normalized such that the total fluorescence yield when f = 1 is 100.

In Figs. V-2 and V-3 are plotted the results of a complete simulation which reproduces all of our experimental data. The points in Figs. V-2 and V-3 are results from two different experiments one of which was presented in Figs. IV-5 to IV-7. The smooth lines are the results calculated from the set of rate constants and initial conditions listed in Table V-I. The rate constants under the F_{max} column are the ones used to reproduce the F_{max} data. The rate constants under the F_0 column are the additional ones used to reproduce the F_0 data. For points between F_0 and F_{max} ($f \neq 1$ and $f \neq 0$), k_{T32} and k_{T23} were varied in a smooth fashion between their values for the F_0 and F_{max} simulations. The reasons we adjusted k_{T32} and k_{T23} are discussed below in the section on

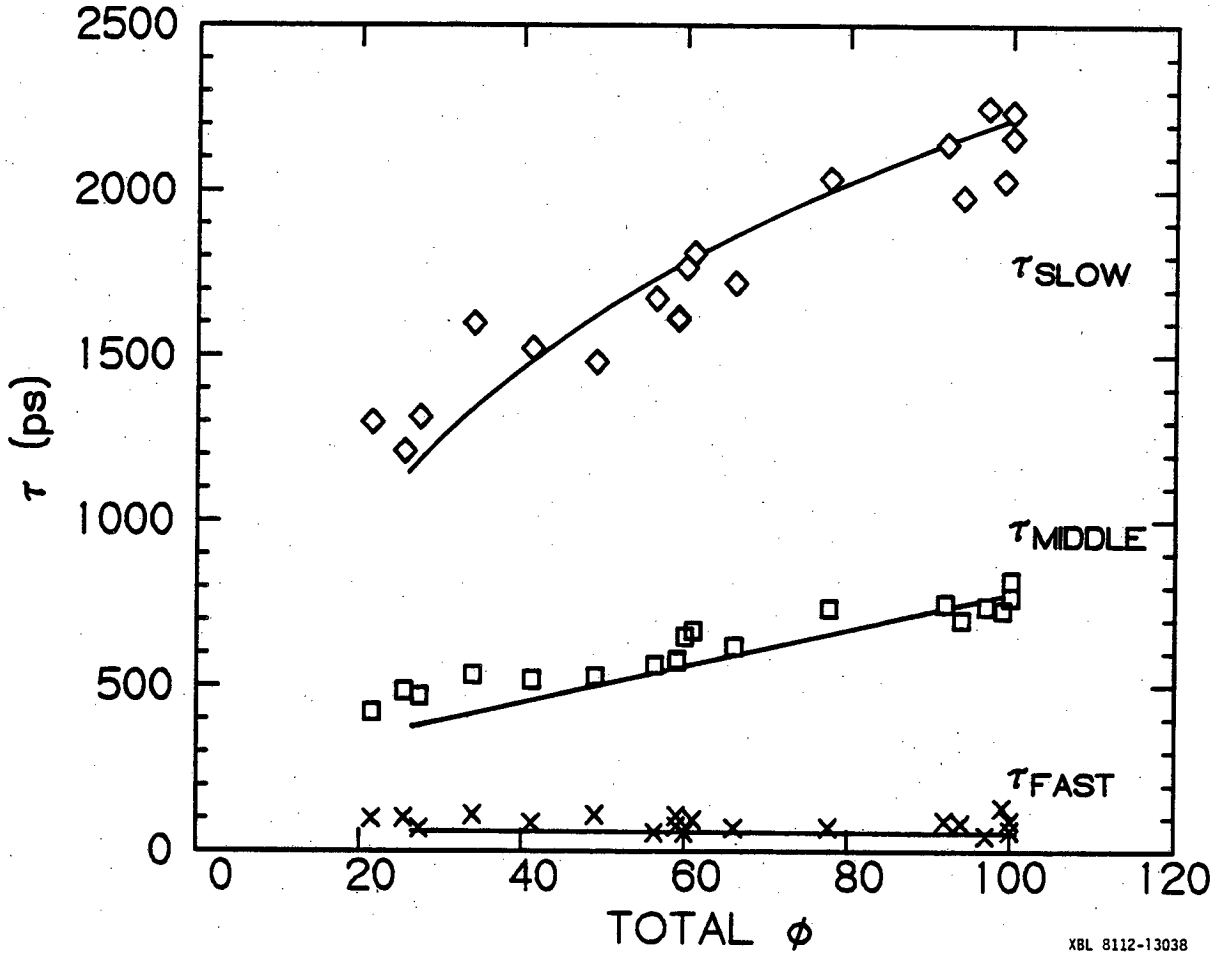

Figure V-2: Simulation of the intensity dependence of the fluorescence lifetimes from spinach chloroplasts at room temperature in the presence of Mg^{+2}. The points are experimental data, and the smooth curves are the results of our simulation. Rate constants and initial conditions for the simulation are in Table V-I.

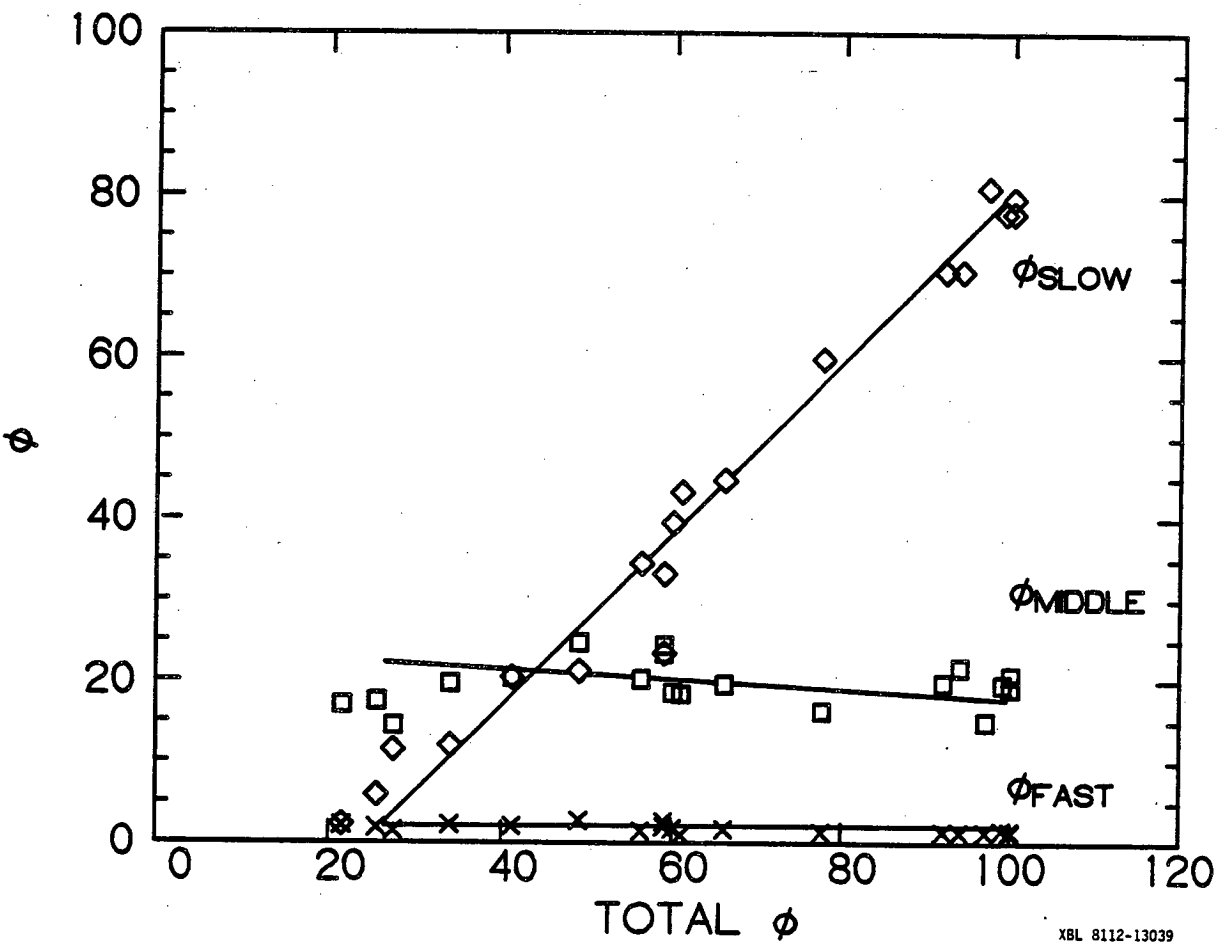

Figure V-2: Simulation of the intensity dependence of the fluorescence yields from spinach chloroplasts at room temperature in the presence of Mg^{+2}. The points are experimental data, and the smooth curves are the results of our simulation. Rate constants and initial conditions for the simulation are in Table V-I.

Table V-I: Set of rate constants and initial conditions that reproduces the fluorescence lifetimes and yields for the highest intensity points in Figs. IV-5 and IV-6. Rate constants are in units of $nsec^{-1}$. Initial conditions are probability densities at time = 0

F_{max}		F_0	
Rate constants		Rate constants	
k_{T32}(closed)	0.80	k_{T32}(open)	2.80
k_{T23}(closed)	0.50	k_{T23}(open)	1.75
k_{T20}	15.00	k_p	5.00
k_{T02}	13.00	k_r(open)	5.00
k_c	135.00		
k_r(closed)	85.00		
k_F	0.90		
k_D	0.24		
k_d	0.32		
k_d'	0.65		
Initial conditions			
Chl a/b*	0.50		
Chl a_2*	0.50		

the middle phase.

We see that our model is consistent with our data. The large number of parameters involved in the fits precludes a quantitative determination of each rate constant. The simulation procedure, however, gives insight into the origin of each component. The following sections discuss the origin of each component of the fluorescence decay and describe important features of the model which are required to fit the data. All of our calculations assume that the room-temperature fluorescence emanates from photosystem II; that is, from the Chl a/b LH antenna and the Chl a_2 antenna. The effect of ignoring photosystem I fluorescence is briefly discussed.

V-2. THE SLOW COMPONENT

Our interpretation of the slow component is that it is "delayed" fluorescence due to excitation that returns to the chlorophyll antenna after a charge separation and recombination reaction in the photosystem II reaction center. The yield of the charge recombination is high when photochemistry is blocked by reduction of Q. The assumption that P^*_{680} itself is non-fluorescent follows Butler's tripartite model [3]. The evidence for this assumption is that the emission spectrum of the slow component peaks at 680-685 nm like the chlorophyll antenna emission spectrum [1]. If P^*_{680} fluoresced, the expected emission would be red-shifted from 680 nm.

To understand the kinetics of the slow component, we examine a set of rate constants and initial conditions which reproduces the F_{max} data;

such a set is presented in Table V-I. This solution set has a very fast charge separation rate ($1/k_c$ = 7 ps) for electron transfer from P_{680} to Ph. This value is analogous to experimental numbers in bacterial reaction centers [14,15] and in photosystem I reaction centers [16]. Because k_c is large, when $P_{680}^{*}PhQ^{-}$ is formed either by excitation transfer from Chl a_2^{*} or by charge recombination from $P_{680}^{+}Ph^{-}Q^{-}$, the most probable next step is a charge separation. We expect that before energy transfer back to the chlorophyll antenna results in "delayed" fluorescence, the photosystem II reaction center will cycle between the states $P_{680}^{*}PhQ^{-}$ and $P_{680}^{+}Ph^{-}Q^{-}$ many times. Because the slow fluorescence lifetime component is relatively fast for "delayed" fluorescence, the charge recombination reaction which occurs many times before "delayed" fluorescence must be very fast. The solution set in Table V-I has a charge recombination rate that is comparable to the charge separation rate ($1/k_r$ = 12 ps). The states $P_{680}^{*}PhQ^{-}$ and $P_{680}^{+}Ph^{-}Q^{-}$ can accurately be considered to be in a state of quasi equilibrium. The lifetime of the slow component is approximately equal to the lifetime of the quasi equilibrium which is a weighted average of $1/k_d'$ (1500 ps) and $1/k_d$ (3300 ps) where k_d' and k_d are the radiationless decay rates of the reaction center states. The existence of a quasi equilibrium agrees with recent detailed quantum mechanical calculations on the charge separation in bacterial reaction centers by Wertheimer and Friesner [17,18].

The situation when Q is oxidized is similar except that the radiationless decay rate of $P_{680}^{+}Ph^{-}Q$ is dominated by k_p. We choose k_p to be similar to the rate of analogous electron transfer reactions in bacterial reaction centers [14,15] and in photosystem I reaction centers [19,20]. Because $1/k_p$ = 200 ps, the "delayed" fluorescence will have a

low yield and be fast - nearly as fast as the "prompt" fluorescence. We conclude that the slow fluorescence in the lowest intensity data in Figs. IV-5 and IV-6 is not "delayed" fluorescence from open photosystem II reaction centers. This slow component could be due to the presence of some closed photosystem II reaction centers. Alternatively, its origin could be some mechanism distinct from "delayed" fluorescence.

For simulations where a fraction f ($f \neq 1$ and $f \neq 0$) of the photosystem II reaction centers are closed, it is necessary to consider energy transfer between photosystem II units. If no energy transfer is possible, the lifetime of the slow component would remain constant and only its yield would decrease as f decreases. We observe, however, a decrease in the the slow phase lifetime. The lifetime decreases because excitation returning to the chlorophyll antenna from a closed reaction center may get quenched by transfer to an open reaction center. For a complete simulation, we must include energy transfer between photosystem II units.

The slow phase lifetime in chloroplasts isolated from peas grown in intermittent light is the same in F_0 as in F_{max}. These chloroplasts lack the Chl a/b LH proteins [21,22], which suggests that communication between photosystem II units is through the Chl a/b LH antenna. A refinement in our model, which is consistent with this result and with our data, is that the Chl a/b LH antenna is a lake antenna that is capable of transferring excitation to a large number of Chl a_2 antennae. Excitation in the Chl a/b LH antenna is transferred to a Chl a_2 antenna with rate constant k_{T32}. It will be transferred to the Chl a_2 antenna of a closed reaction center with probability f, and to the Chl a_2 antenna of an open reaction center with probability g = 1-f. We note that the

lifetime of the slow component decreases only two fold. If we introduce lake character to the Chl a_2 antennae, it is not possible to simulate such a small change.

V-3. THE MIDDLE COMPONENT

The two faster components of the fluorescence decay are "prompt" fluorescence which results from excitation lost prior to reaching a reaction center. The middle component reflects excitation that originates in the Chl a/b LH antenna. Its lifetime is approximately

$$\tau_{middle} = 1/(k_F + k_D + k_{T32}) \qquad (3)$$

where k_F, k_D, and k_{T32} are the rate constants for fluorescence, radiationless decay, and energy transfer from the Chl a/b LH antenna.

The lifetime of the middle phase decreases from 750 ps to 400 ps between F_0 and F_{max}. By equation (3), we see that it is possible to simulate this decrease only if the denominator is larger at F_0 than at F_{max}. We suggest that k_{T32}, which is the dominant rate in Eq. (3), is faster in the all-open state than in the all-closed state. This change may be related to energy distribution regulation mechanisms present in chloroplasts such as the state 1 to state 2 transition [23,24]. When a photosystem II reaction center is closed, the rate constant for energy transfer to that reaction center is decreased, and the probability of energy transfer to an open photosystem II reaction center or to photosystem I is increased. This situation favors efficient use of excited states. The change in the middle phase lifetime cannnot be

explained by changes in k_F or k_D, because large rates for these processes are inconsistent with the high yield of photochemistry present in the all-open state [25,26].

V-4. THE FAST COMPONENT

The fast component is "prompt" fluorescence which is due to excitation that originates in the Chl a_2 antenna and is lost prior to transfer to the reaction center. Its lifetime is approximately

$$\tau_{fast} = 1/(k_F + k_D + k_{T20} + k_{T23}) \quad (4)$$

where k_F, k_D, k_{T20}, and k_{T23} are rate constants for fluorescence, radiationless decay, and energy transfer from the Chl a_2 antenna. Eq. (4) is dominated by the rate constant k_{T20}. The yield of the fast component is very low because nearly all of the excitation that originates in the Chl a_2 antenna is rapidly transferred to the reaction center of photosystem II.

V-5. PHOTOSYSTEM I FLUORESCENCE

The Chl a/b LH antenna and the Chl a_2 antenna are two parts of Butler's tripartite model [3] - the third part is the chlorophyll a antenna associated with photosystem I (Chl a_1). The inclusion of Chl a_1 in our model should not substantially effect the interpretation of the three room-temperature fluorescence decay components. The room-temperature emission spectrum of the photosystem I antenna is similar to

the fluorescence emission spectrum of the photosystem II antenna [27]. Therefore, we might expect photosystem I fluorescence at 680 nm where we measured the fluorescence decay. In analogy with the interpretation of the fast phase, excitation originating in the Chl a_1 antenna would probably contribute a low yield of fast fluorescence. The lifetime of the photosystem I fast fluorescence would be approximately

$$\tau_{PSI} = 1/(k_F + k_D + k_{T1I}) \tag{5}$$

where k_F and k_D are as above, and k_{T1I} is the rate of energy transfer from Chl a_1 to the reaction center of photosystem I. Beddard et al. [28] have measured a fluorescence lifetime of 110 ps for photosystem I particles. This suggests that τ_{PSI} from Eq. (5) may be around 110 ps and that some of our fast phase may be due to excitation originating in Chl a_1.

If we include the excitation transfer between photosystem II and photosystem I, the interpretation of the middle phase would change only slightly. Instead of using Eq. (3), the lifetime of the middle phase would be approximately

$$\tau_{middle} = 1/(k_F + k_D + k_{T32} + k_{T31}) \tag{6}$$

where k_F, k_D, and k_{T32} are as above, and k_{T31} is the rate of energy transfer from the Chl a/b LH antenna to the Chl a_1 antenna.

Fluorescence emission spectra of subchloroplast particles indicates that there is no variable fluorescence originating from photosystem I [27,29]. Thus, we expect no contribution from photosystem I to the slow phase observed at room temperature. We note, however, that the lifetime of the slow component will be affected by changes in the rate of energy

transfer from photosystem II to photosystem I. In the tripartite model, transfer from photosystem II to photosystem I is irreversible, and increasing this rate is equivalent to increasing the rate of fluorescence quenching paths in the photosystem II antenna. Increasing the rate of fluorescence quenching paths in the photosystem II antenna tends to decrease the lifetime of the "delayed" fluorescence.

The quantitative inclusion of Chl a_1 into our analysis of the room-temperature fluorescence decay requires more experimental data. Detailed fluorescence lifetime experiments on photosystem I-enriched subchloroplast particles should resolve this problem.

V-6. SUMMARY

The results of this Chapter and Refs. [1] and [2] led to the working model for the origin of room-temperature fluorescence diagrammed in Fig. V-1. The basic structure of the model is derived from the tripartite model proposed by Butler [3]. The major addition is the explicit inclusion of the electron transfer processes involving pheophytin which occur in the reaction center of photosystem II [5-11]. A detailed kinetic analysis of this model shows that the total fluorescence which is emitted from both the Chl a/b LH antenna and the Chl a_2 antenna can be described by the sum of three exponentials. The origin of each phase is a complex interaction among the rate constants in Fig. V-1, but they can be described qualitatively as follows: 1) The fastest phase (about 100 ps) is kinetically controlled by the decay processes of the Chl a_2 antenna. These processes are dominated by the

transfer rate, k_{T20}, from the Chl a_2 antenna to the reaction center of photosystem II. 2) The middle phase (300-750 ps) is kinetically controlled by the decay processes of the Chl a/b LH antenna. These processes are dominated by transfer rates from the Chl a/b LH antenna to the Chl a_2 antenna and the Chl a_1 antenna ($k_{T32} + k_{T31}$). 3) The yield of the slow phase is controlled by the presence of Q^- and its lifetime is determined by two factors. The first factor is the kinetics of the charge recombination between P^+_{680} and Ph^- and the second factor is the rates of fluorescence quenching from the photosystem II antenna.

V-7. REFERENCES

1. W. Haehnel, J. A. Nairn, P. Reisberg, and K. Sauer, Biochim. Biophys. Acta, in press (1982).
2. P. Reisberg, J. A. Nairn, W. Haehnel, and K. Sauer, in preparation.
3. W. L. Butler, Ann. Rev. Plant Physiol. 29, 345 (1978).
4. G. Doring, H. H. Stiehl, H. T. Witt, Z. Naturforsch. Teil B 22, 639 (1967).
5. V. V. Klimov, A. V. Klevanik, V. A. Shuvalov, and A. A. Krasnovsky, FEBS Lett. 82, 183 (1977).
6. A. V. Klevanik, V. V. Klimov, V. A. Shuvalov, and A. A. Krasnovsky, Dokl. Akad. Nauk SSSR 236, 241 (1977).
7. V. V. Klimov, S. I. Allakhverdiev, and V. Z. Paschenko, Dokl. Akad. Nauk SSSR 236, 1204 (1978).
8. V. V. Klimov, S. I. Allakhverdiev, and A. A. Krasnovsky, Dokl. Akad. Nauk SSSR 249, 485 (1980).
9. V. V. Klimov, S. I. Allakhverdiev, S. Demeter, and A. A. Krasnovsky, Dokl. Akad. Nauk SSSR 249, 227 (1980).
10. V. V. Klimov, S. I. Allakhverdiev, S. I. Shutilova, and A. A. Krasnovsky, Sov. Plant Physiol. 27, 315 (1980).
11. V. V. Klimov, E. Dolan, and B. Ke, FEBS Lett. 112, 97 (1980).
12. L. N. M. Duysens and H. E. Sweers, in Microalgae and Photosynthetic Bacteria (eds. Japanese Society of Plant Physiologists), Univ. of Tokyo Press, Tokyo, 353 (1963).
13. J. Amesz and L. N. M. Duysens, in Topics in Photosynthesis, Primary Processes in Photosynthesis (ed. J. Barber), Vol. 2, Elsevier/North-Holland Press, Amsterdam, 149 (1977).

14. K. J. Kaufman, P. L. Dutton, T. L. Netzel, J. S. Leigh, and P. M. Rentzepis, Science 188, 1301 (1975).

15. M. G. Rockley, M. W. Windsor, R. J. Cogdell, W. W. Parson, Proc. Natl. Acad Sci USA 72, 2251 (1975).

16. J. M. Fenton, M. H. Pellin, Govindjee, and K. J. Kaufman, FEBS Lett. 100, 1 (1979).

17. R. Friesner and R. Wertheimer, Proc. Natl. Acad Sci. USA, submitted.

18. R. Wertheimer and R. Friesner, J. Chem. Phys., submitted.

19. V. A. Shuvalov, B. Ke, and E. Dolan, FEBS Lett. 100, 5 (1979).

20. V. A. Shuvalov, A. V. Klevanik, A. V. Sharkov, P. G. Kryukov, and B. Ke, FEBS Lett. 107, 313 (1979).

21. J. H. Argyroudi-Akoyunoglou and G. Akoyunoglou, Plant Physiol. 46, 247 (1970).

22. P. A. Armond, C. J. Arntzen, J.-M. Briantais, and C. Vernotte, Arch. Biochem. Biophys. 175, 54 (1976).

23. N. Murata, Biochim. Biophys. Acta 172, 242 (1969).

24. C. Bonaventura and J. Myers, Biochim. Biophys. Acta 189, 366 (1969).

25. M. Kamen, in Primary Processes in Photosynthesis, Academic Press, New York, 105 (1963).

26. B. Kok and G. Hoch, in Light and Life (eds. W. D. McElroy and B. Glass), Johns Hopkins, Baltimore, 397 (1971).

27. N. K. Boardman, S. W. Thorne, and J. M. Anderson, Proc. Natl. Acad. Sci. USA 56, 586 (1966).

28. G. S. Beddard, G. R. Fleming, G. Porter, G. F. W. Searle, and J. A. Synowiec, Biochim. Biophys. Acta 545, 165 (1979).

29. R. B. Park, K. E. Steinbeck, and P. V. Sane, Biochim. Biophys. Acta 253, 204 (1971).

CHAPTER VI

EFFECT OF MAGNESIUM ON THE ROOM-TEMPERATURE FLUORESCENCE DECAY KINETICS IN SPINACH CHLOROPLASTS

VI-1. INTRODUCTION

The addition of cations to broken chloroplasts induces changes in the primary processes of photosynthesis. These changes include: (1) a dramatic increase in the room-temperature fluorescence yield of DCMU poisoned chloroplasts [1-4], (2) an increase of the 685 nm fluorescence at low temperature relative to the 735 nm fluorescence [2-4], (3) an increase in the photosystem II quantum efficiency [2-4], and (4) a decrease in the photosystem I quantum efficiency [2-4]. Murata [2-4] postulated that cations decrease the rate of spillover from photosystem II to photosystem I and that cationic regulation of this rate may be the basis of the state 1 to state 2 transition observed in intact chloroplasts [5,6]. In his model, state 1 (the dark state) is analogous to the state of high cation concentration, with low photosystem II to photosystem I spillover; state 2 is analogous to the state of low cation concentration, with high photosystem II to photosystem I spillover. More recent work suggests that the cation effect on energy distribution between photosystem II and photosystem I is more complicated. Butler and Kitajima [7] concluded from fluorescence induction data at low temperature that, in addition to decreasing the rate of photosystem II to photosystem I spillover, Mg^{+2} increases the absorption cross section of photosystem II. The analysis of Henkin and

Sauer [8] indicates that the only effect of Mg^{+2} may be an increase in the absorption cross-section of photosystem II.

Joliot and Joliot [9] reported that the fluorescence induction curve for intact chloroplasts in whole cells of Chlorella pyrenoidosa displays a sigmoidal rise. They attributed the sigmoidicity to the ability of energy to transfer between photosystem II units. They proposed a theoretical relation between the probability of transfer between photosystem II units, ρ, and the shape of the fluorescence induction curve; the fluorescence induction curve from intact chloroplasts indicates that $\rho=0.55$ [9]. Experiments with broken chloroplasts shows that the fluorescence induction curve is sigmoidal in the presence of Mg^{+2}, but exponential in the absence of Mg^{+2}; the two curves correspond to $\rho=0.5$ to 0.6 in the presence of Mg^{+2} and ρ decreasing to a low value in the absence of Mg^{+2} [10-13]. The conclusion is that Mg^{+2} is required for energy transfer between photosystem II units to exist.

Several possibilities have been presented for explaining the mechanism of the cationic regulation of energy distribution. Izawa and Good [14] found that chloroplasts isolated in low salt medium have unstacked thylakoid membranes and that the addition of salts induces thylakoid stacking. This stacking is correlated with increased light scattering and with the fluorescence increases described above [15,16]. Murakami and Packer [15] and Murata [16] concluded that thylakoid stacking may be the mechanism behind the cation effect and the state 1 to state 2 transition. More recent experiments show that thylakoid stacking and fluorescence yield changes are separable phenomena; that is, one effect can be induced independently of the other [17,18].

Experiments with mutants indicate that a Mg^{+2} effect and a state 1 to state 2 transition is absent in photosynthetic organisms that lack the chlorophyll a/b light-harvesting protein [19]. The conclusion is that an interaction between Mg^{+2} and the chlorophyll a/b light-harvesting protein induces some change which can control the energy distribution between photosystem II and photosystem I [19-21].

In this chapter, I describe the measurement of the three components of the fluorescence decay described in Chapters IV and V (See also Refs. [22] and [23]) as a function of the concentration of Mg^{+2}. This experiment was done on the all-open state (F_0 level) and on the all-closed state (F_{max} level) in spinach chloroplasts at room temperature. To examine the extent of energy transfer between photosystem II units, it is necessary to look at the fluorescence decay when some of the photosystem II reaction centers are open and some are closed. For experiments in the partially closed state, we have measured the intensity dependence of the fluorescence decay kinetics for spinach chloroplasts in the absence of Mg^{+2}. We find that most of our data can be explained by assuming that Mg^{+2} has two effects. The addition of Mg^{+2} to thylakoids from broken spinach chloroplasts isolated in a Mg^{+2} free buffer, first decreases the rate of energy transfer or spillover from photosystem II to photosystem I; this first effect saturates at low concentrations of Mg^{+2} (< 0.75 mM). A second effect, saturating at about 2 mM Mg^{+2}, causes an increase in both the absorption cross section and the extent of energy transfer between photosystem II units.

VI-2. MATERIALS AND METHODS

Broken spinach chloroplasts were isolated by methods similar to those described in Chapter IV except that portions of the chloroplast pellet were resuspended in several different buffers. Each buffer contained 10 mM HEPES-NaOH (pH 7.5), 0.1 M sucrose, and 5 mM NaCl. Each buffer also either had no Mg^{+2}, or contained a concentration of $MgCl_2$ equal to the concentration desired for the fluorescence measurement. The chloroplasts were allowed to equilibrate in these buffers for at least 1 hour. The chlorophyll concentration was adjusted to 18 µg chlorophyll/ml by dilution with the appropriate resuspending buffer. For experiments at the F_0 level, we added 1.25 mM ferricyanide as electron acceptor, 1.25 mM ferrocyanide to control the redox potential, and 2.5 µg/ml gramicidin D as uncoupler. These levels of added anionic electron acceptors along with their coion, K^+, do not induce ionic effects in the room-temperature fluorescence properties of broken spinach chloroplasts. The chloroplast sample was rapidly stirred in a 1 cm x 1 cm cuvette, and each sample was replaced every 10 min if more data accumulation was needed. For experiments at the F_{max} level, we added 12.5 µM DCMU and 2 mM hydroxylamine hydrochloride. To close the reaction centers, the sample was illuminated with about 10 flashes of saturating intensity immediately before the lifetime measurement. The intensity dependence experiment was done like an F_0 experiment, except that only gramicidin D was added to the resuspending buffer. All measurments were carried out at room temperature (20-22°C), and the cuvette was painted black for reasons described in Chapter IV.

The single-photon timing apparatus and the methods of numerical

analysis are described in Chapter III.

VI-3.RESULTS

1. Mg^{+2} Dependence of F_0 Level Fluorescence

Table VI-I summarizes some of the results from Chapter IV (see also Ref. [22]) which have been renormalized to facilitate comparison of the yields between different experiments. The effects of adding Mg^{+2} to spinach chloroplasts at the F_0 level are: 1) a decrease in the lifetime of the slow phase with no change in its yield, 2) a slight increase in the lifetime of the middle phase accompanied by a doubling of the yield, and 3) a decrease in the yield of the fast phase. The change in the fast phase, however, may be within the uncertainty of our measurements because the fast phase is the most difficult phase to resolve. The dependence of the three lifetimes on Mg^{+2} concentration is plotted in Fig. VI-1. The slow phase increases somewhat at low levels of Mg^{+2} and then decreases to its final value, with the decrease being complete by $[Mg^{+2}]$ = 2 mM. We note that, like the fast phase, the slow phase is a small part of the total F_0 decay and is difficult to resolve. The precise details of the change in the slow phase lifetime will need confirmation, but we generally observe a decrease in the slow phase lifetime upon the addition of 5 mM Mg^{+2}. The lifetimes of the fast and middle phases show only minor changes.

In Fig. VI-2 are plotted the total yield and the yield of each component versus Mg^{+2} concentration. The total yield increases about 30% saturating at $[Mg^{+2}]$ = 0.75 mM; this increase is in good agreement with

Table VI-I: Lifetimes and relative yields of the fluorescence from spinach chloroplasts. These data show the effects of adding 5 mM Mg^{+2} at both the F_0 and F_{max} levels. All results are from chloroplasts isolated from a single set of spinach leaves. The yield figures are normalized such that $\Sigma\phi$ at F_{max} in the presence of Mg^{+2} equals 100.

	No Mg^{+2}			+5 mM Mg^{+2}		
Level	τ	ϕ	$\Sigma\phi$	τ	ϕ	$\Sigma\phi$
F_0	130	4.4		100	2.5	
	360	9.4	17	420	19.5	25
	1500	3.2		1200	3.0	
F_{max}	160	3.5		50	1.0	
	530	20.7	44	750	17.0	100
	1700	19.8		2000	82.0	

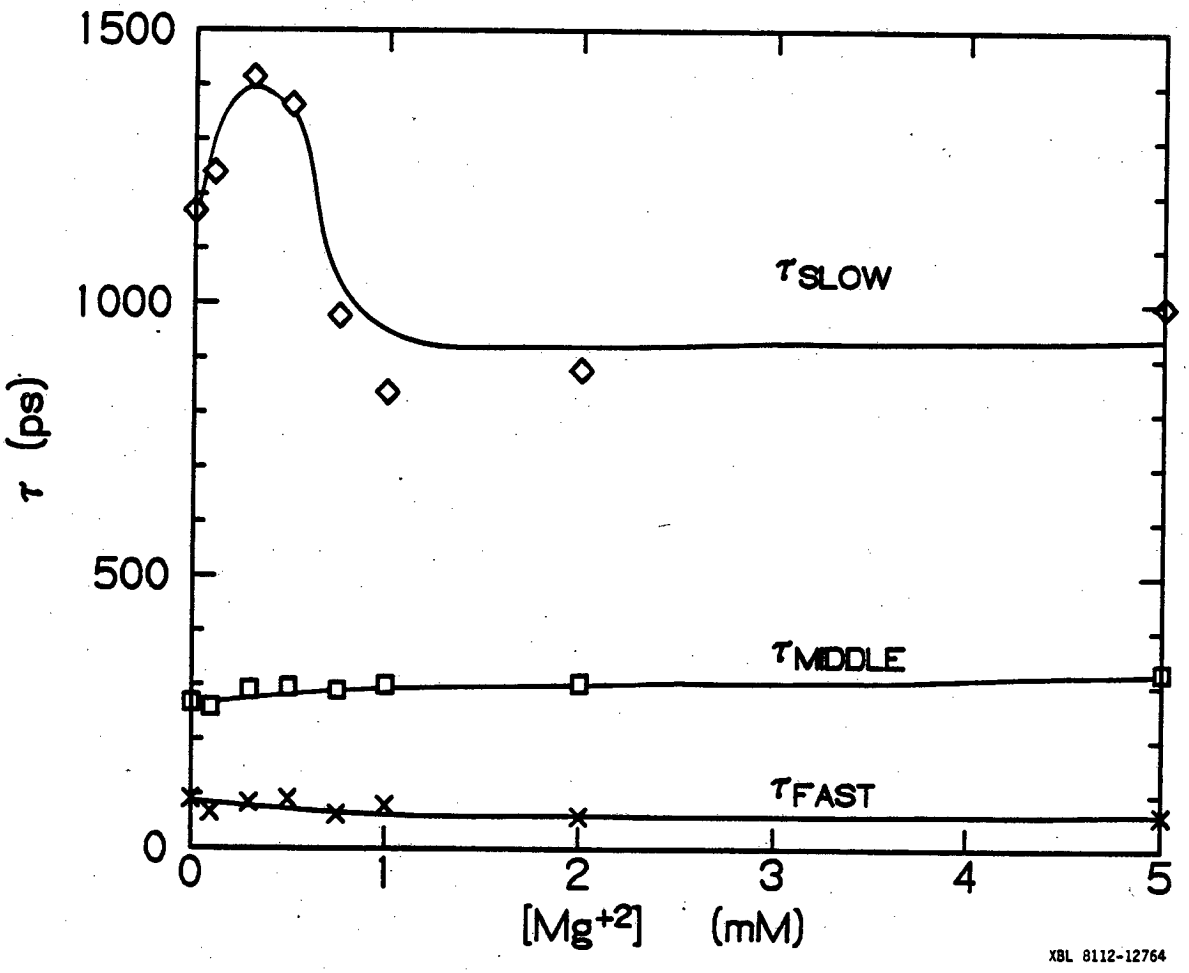

Figure VI-1: Lifetimes of the components of the fluorescence decay in spinach chloroplasts at the F_0 level as a function of the concentration of Mg^{+2}.

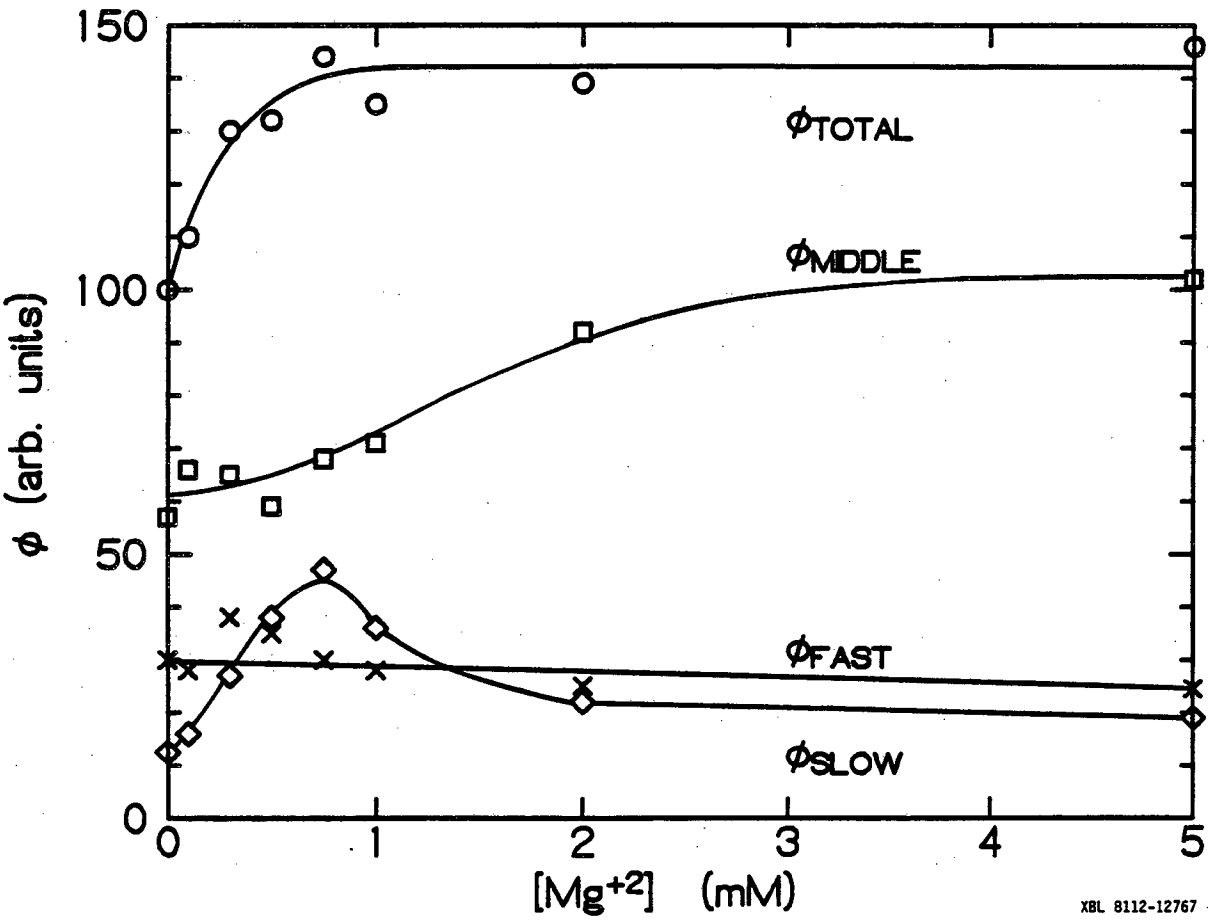

Figure VI-2: Total yield and yields of the components of the fluorescence decay in spinach chloroplasts at the F_0 level as a function of the concentration of Mg^{+2}. Yields are normalized such that $\Sigma\phi$ in the absence of Mg^{+2} equals 100.

the results of Henkin and Sauer [8]. The other changes are quite complex. The yield of the slow phase increases four fold peaking at $[Mg^{+2}]$ = 0.75 mM and then decreases to near its original value. The decrease is complete at about $[Mg^{+2}]$ = 2 mM. Despite difficulty in resolving the lifetime of the slow phase, the rise and fall of its yield was observed to be similar in each sample. It is therefore likely that the rise and fall of the lifetime of the slow phase mentioned above is real. The yield of the middle phase remains approximately constant up to 1 mM and then approximately doubles, with the doubling nearly complete by $[Mg^{+2}]$ = 2 mM.

2. Mg^{+2} Dependence of the F_{max} Level Fluorescence

The effects on the F_{max} level resulting from increasing the concentration of Mg^{+2} added to broken spinach chloroplasts are: 1) an increase in the lifetime of the slow phase accompanied by a four fold increase in its yield, 2) an increase in the lifetime of the middle phase accompanied by a slight decrease in its yield, and 3) changes in the fast phase which probably do not lie outside the uncertainty of our measurement. The fast phase in the F_{max} level is especially difficult to resolve because it is a very small component relative to the other two phases. The lifetimes of the three components versus Mg^{+2} concentration are plotted in Fig. VI-3. The lifetime of the slow phase increases from 1170 ps to 1600 ps, saturating at $[Mg^{+2}]$ = 0.75 mM or less. The range of the change, 1170 ps to 1600 ps, is different from the range in Table IV-I (1700 ps to 2000 ps); the discrepancy is probably due to sample variability. Despite the differences in ranges, the saturation of the effect at $[Mg^{+2}]$ = 0.75 mM is reproducible for the slow phase lifetime.

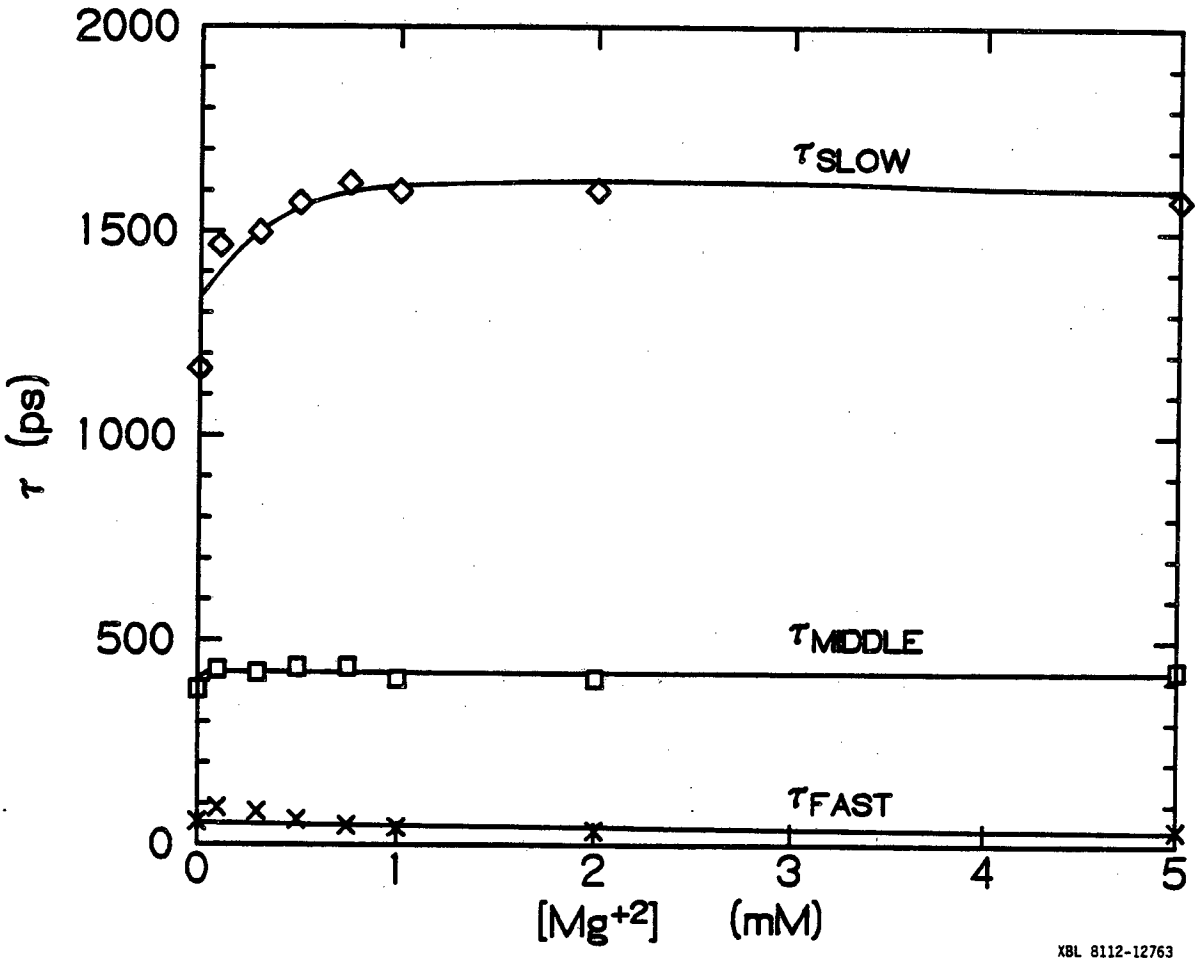

Figure VI-3: Lifetimes of the components of the fluorescence decay in spinach chloroplasts at the F_{max} level as a function of the concentration of Mg^{+2}.

The lifetime of the middle phase increases only slightly from 380 ps to 430 ps; the increase occurs at low Mg^{+2} concentration (< 0.75 mM). The smaller change here as compared to Table VI-I could also be due to sample variability. We have always seen an increase in this lifetime at the F_{max} level upon the addition of Mg^{+2}. The increase is sometimes small, and the increase presented in Table VI-I represents about the maximum effect.

The total yield and the yield of each component versus Mg^{+2} concentration are plotted in Fig. VI-4. The total yield doubles, saturating at $[Mg^{+2}]$ = 2 mM; this increase is in close agreement with the results of Henkin and Sauer [8]. All of the increase is accounted for by a four fold increase in the yield of the slow phase, and this increase also saturates at $[Mg^{+2}]$ = 2 mM. The only other effect is a slight decrease in the yield of the middle phase saturating at about $[Mg^{+2}]$ = 1 mM.

3. Intensity Dependence of the Fluorescence Decay Kinetics in the Absence of Mg^{+2}

The effect of intensity on the three kinetic components of spinach chloroplasts in the presence of Mg^{+2} is plotted in Figs. IV-5 to IV-7 (see Chapter IV). The results show a smooth transition from the F_0 values to the F_{max} values given in Table VI-I. Here, we have repeated the same experiment in the absence of Mg^{+2}. The results plotted in Figs. VI-5 and VI-6 show smooth transitions between results similar to the F_0 and F_{max} values given in Table VI-I. The lifetime of the slow phase is nearly constant at about 1350 ps. The slow phase yield increases 8.3 fold. The lifetime and yield of the middle phase increase somewhat, the

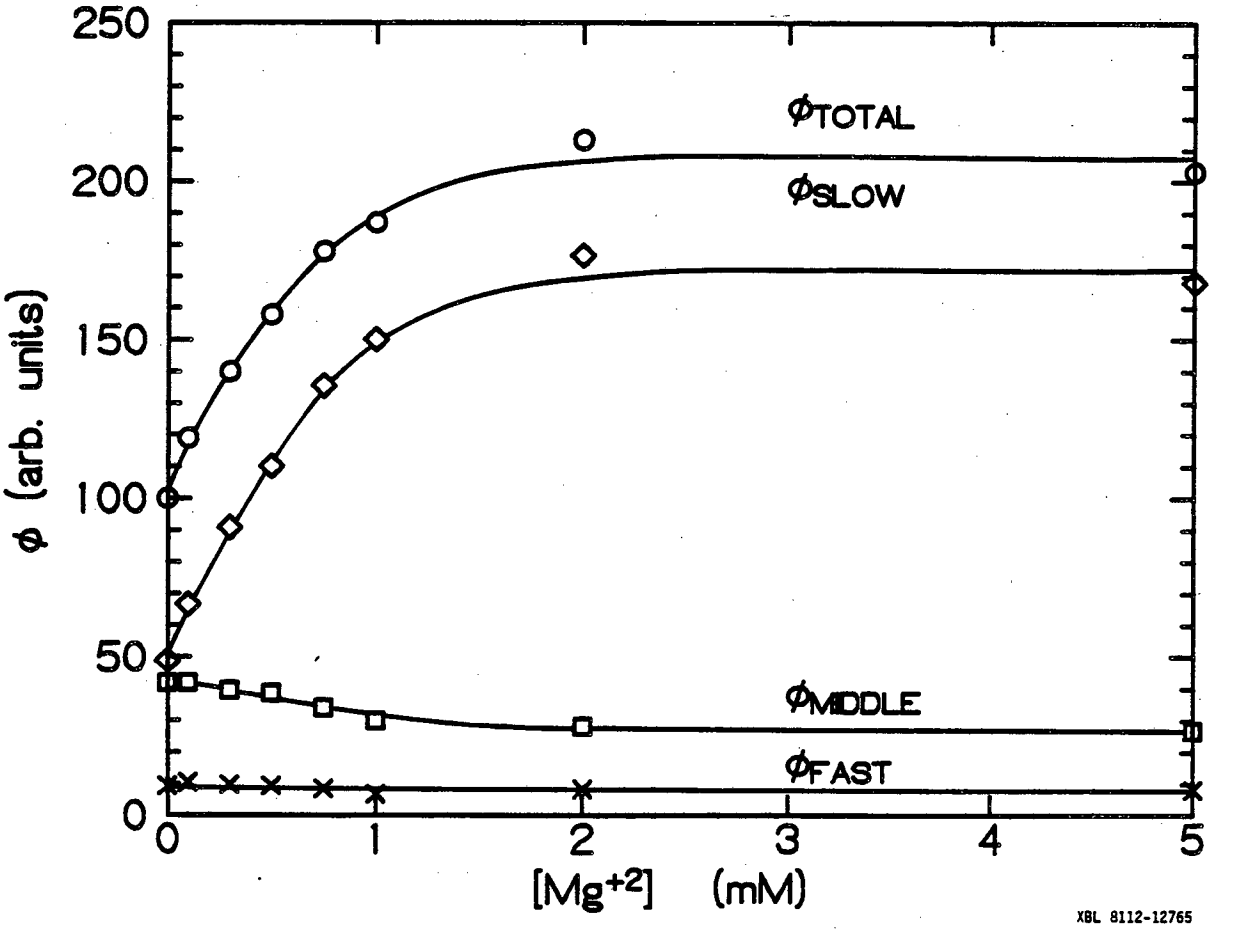

Figure VI-4: Total yield and yields of the components of the fluorescence decay in spinach chloroplasts at the F_{max} level as a function of the concentration of Mg^{+2}. Yields are normalized such that $\Sigma\phi$ in the absence of Mg^{+2} equals 100.

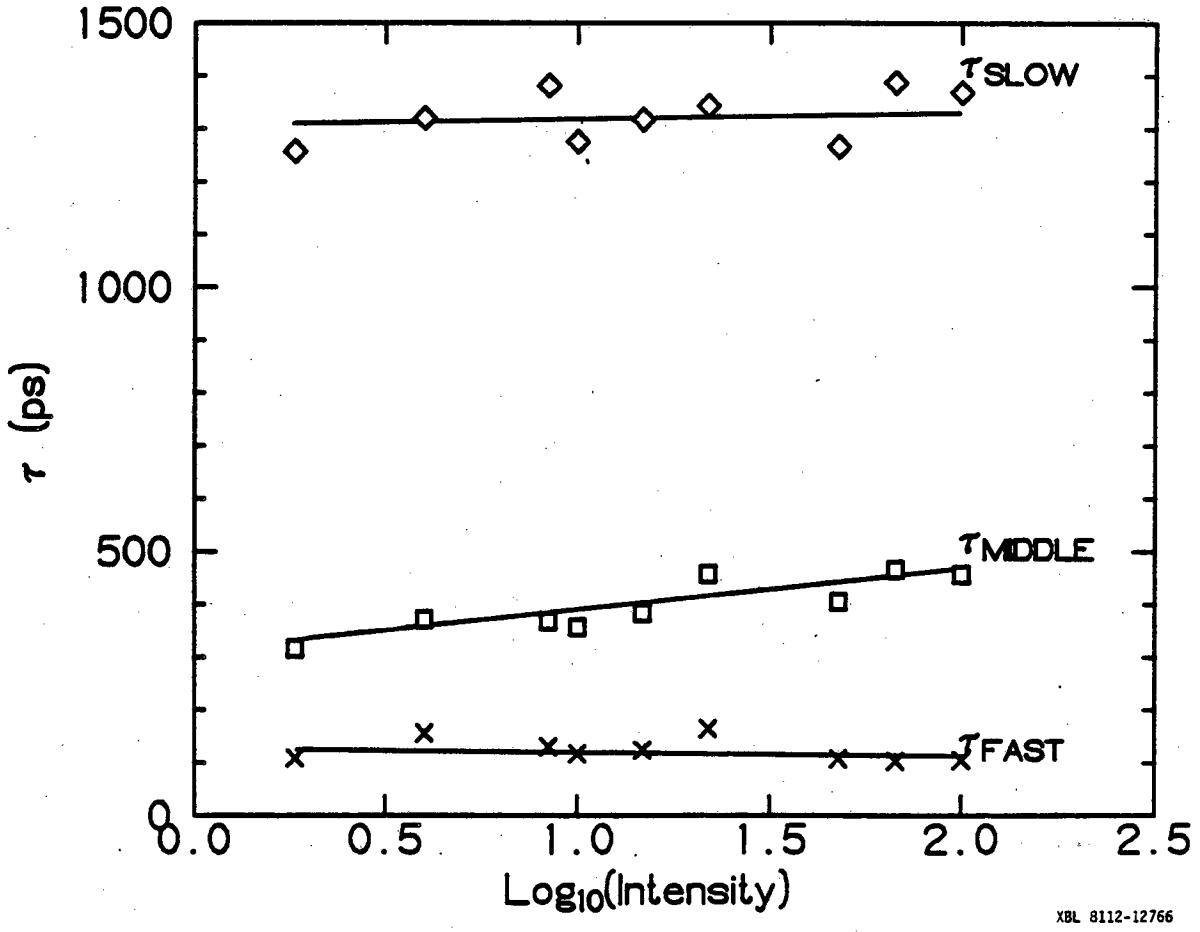

Figure VI-5: Lifetimes of the components of the fluorescence decay in spinach chloroplasts isolated in the absence of Mg^{+2} as a function of laser intensity

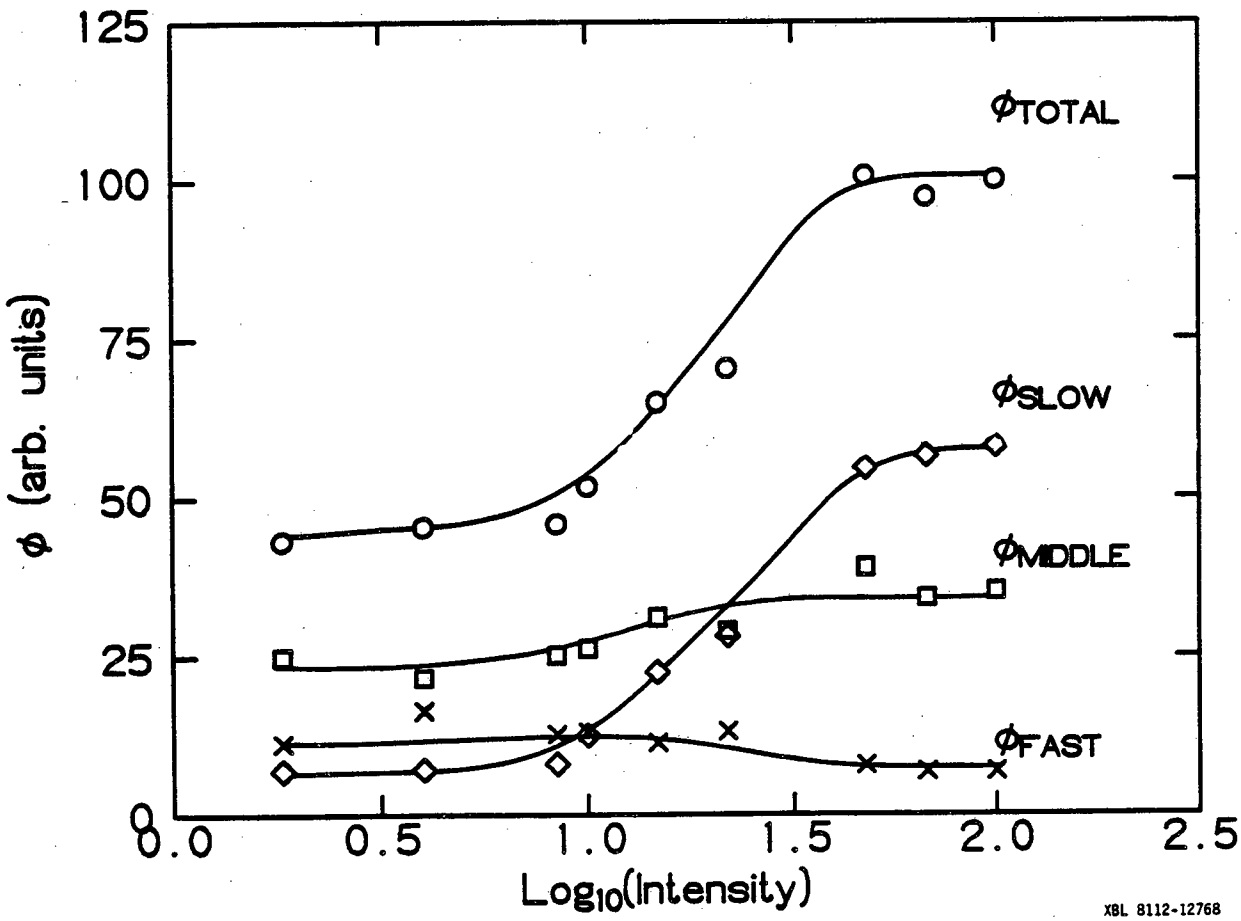

Figure VI-6: Total yield and yields of the components of the fluorescence decay in spinach chloroplasts isolated in the absence of Mg^{+2} as a function of laser intensity. Yields are normalized such that $\Sigma\phi$ at the highest laser intensity equals 100.

yield increasing about 60-70%. The lifetime of the fast phase remains constant and its yield decreases.

VI-4. DISCUSSION

1. Comparison with other Mg^{+2} Dependent Fluorescence Lifetime Measurements

Because we have resolved three fluorescence decay components where other studies have resolved only two components [24-26] or one component [27], it is difficult to compare our results quantitatively to literature results. A qualitative comparison, however, reveals that our data can be reconciled quite well with other Mg^{+2}-dependent fluorescence lifetime measurements [24-28]. Searle et al. [25] looked at the effect of adding Mg^{+2} to wild-type barley chloroplasts at both the F_0 and F_{max} levels. At F_0, they saw very small changes in the lifetimes of two components and a slight increase in the yield of their slow component (600 to 650 ps). Our result for F_0 agrees with this result, if we note that their slow phase is probably an average of our middle and slow phases. The effect of adding Mg^{+2} at the F_{max} level has been examined for chloroplasts from wild-type barley [25] and from peas [24,26]. All three studies [24-25] recorded increases in yields which predominate in the slow part of the fluorescence. The slow fluorescence lifetime was found either to increase [24,25] or remain constant [26]. Our results are in essential agreement with these results as well. These previously reported Mg^{+2} effects, however, are generally smaller because a two component analysis averages some of the middle phase into the slow

phase.

Moya et al. [27], using the technique of phase fluorimetry with a one component analysis, measured the fluorescence lifetime as a function of intensity both in the presence and absence of Mg^{+2}. A plot of their average lifetime versus total yield showed that in the absence of Mg^{+2} the average lifetime is proportional to the total yield and it increases from 0.4 ns in the all-open state to 1.0 ns in the all-closed state. A plot of an average lifetime calculated from our intensity dependent data in the absence of Mg^{+2} (see Figs. VI-5 and VI-6) by Eq. (1) in Chapter IV is identical to the results of Moya et al. [27] (plot not shown). The deceptively simple linear relationship between average lifetime and total yield has influenced the conclusions of several authors.

2. Interpretation of the Mg^{+2} Effect

The first discussions of the Mg^{+2} effect postulated that addition of Mg^{+2} decreases the rate of spillover from photosystem II to photosystem I [2-4]. In the model in Chapter V, this decrease would be a decrease in k_{T31}. Because, as discussed in Chapter V, the middle phase lifetime is approximately equal to $1/(k_{T32} + k_{T31})$, (See Eq. (6) in Chapter V) a decrease in k_{T31} should result in an increase in the middle phase lifetime. At both F_0 and F_{max} in Table VI-I and in Figs. IV-1 and IV-3, we see an increase in the middle phase lifetime. The changes are usually small and completed by $[Mg^{+2}]$ = 0.75 mM. We conclude that changes in the photosystem II to photosystem I spillover rate may be taking place but that they are completed at very low concentrations of Mg^{+2} and therefore, cannot account for all the observed fluorescence changes at higher concentrations.

The largest Mg^{+2} effects observed are changes in the slow phase at F_{max}. The increase in the slow phase lifetime (see Fig. IV-3) is complete by $[Mg^{+2}]$ = 0.75 mM. This increase could be due to a direct affect of Mg^{+2} on the kinetics of the charge recombination step in the photosystem II reaction center. Alternatively, the lifetime increase could be due to changes in the chlorophyll antenna. An increase in lifetime would be brought about by decreases in rate constants for quenching paths in the chlorophyll antenna. One such decrease could be a decrease in the photosystem II to photosystem I spillover rate. It is therefore possible, that the lifetime increases in the middle and slow phases, both of which are completed at low Mg^{+2} concentrations, are both due to changes in the photosystem II to photosystem I spillover rate.

Both mechanisms discussed above, by which Mg^{+2} induces an increase in the slow phase lifetime, should also cause an increase the slow phase yield. The yield of the slow phase continues to increase up to $[Mg^{+2}]$ = 2 mM, however, while the lifetime effects are completed at a lower concentration of Mg^{+2}. A mechanism to account for this continued yield change is a Mg^{+2} induced increase in the effective absorption cross-section of photosystem II. An increase in the photosystem II absorption cross-section would cause the yield of the slow phase to increase without increasing its lifetime. The conclusion that both spillover changes and absorption cross section changes occur upon the addition of Mg^{+2} is in agreement with the work of Butler and Kitajima [7].

The intensity dependence of the fluorescence kinetics can be used to examine the extent of energy transfer between photosystem II units. A striking difference between the results in Figs. VI-5 and VI-6, in the

absence of Mg^{+2}, and the results of a similar experiment in the presence of 5 mM Mg^{+2} presented in Figs. IV-5 to IV-7 (see also Table VI-I and Ref. [22]), is that in the absence of Mg^{+2}, the lifetime of the slow phase is almost constant. As discussed in Chapter V, changes in the slow phase lifetime in the presence of Mg^{+2} probably result from communication between photosystem II units through the Chl a/b LH antenna. The results shown in Figs. VI-5 and VI-6 suggest that Mg^{+2} is required for communication to exist and that, in the absence of Mg^{+2}, there is no communication between photosystem II units. This conclusion is consistent with the results of fluorescence induction experiments in the presence and absence of Mg^{+2} [10-13].

The Mg^{+2} dependence of the F_0 kinetics are more complex, but they can be rationalized using the above conclusions. At low concentrations of Mg^{+2}, the photosystem II antenna is in a puddle or disconnected state and Mg^{+2} is causing an increase in the rate of photosystem II to photosystem I spillover and/or a direct effect on the kinetics of the charge recombination. The low-level Mg^{+2} effects on the slow phase are expected to be an increase in its lifetime and yield (Note: the presence of a slow phase in F_0 is probably due to the presence of some closed photosystem II reaction centers even in the dark - see Chapters IV and V). At higher levels of Mg^{+2}, the photosystem II antenna begins to allow communication between photosystem II units. In this state, excitation returning to the chlorophyll antenna following a charge recombination can now be quenched by transfer to an open photosystem II reaction center. The result is a shortening of the lifetime and a decrease in the yield of the slow phase. Our model, therefore, predicts the rise and fall of the slow phase yield, which we reproducibly observe. The fact

that the yield decrease is completed by $[Mg^{+2}]$ = 2 mM gives us new information about the levels of Mg^{+2} required to bring about connections between photosystem II units. Our model, also predicts a rise and fall of the slow phase lifetime. Despite the difficulty in resolving the lifetime of the slow phase at the F_0 level, we believe the rise and fall shown in Fig. VI-1 is an accurate measure of its behavior.

The yield of the middle phase in the F_0 experiment increases with $[Mg^{+2}]$ until about $[Mg^{+2}]$ = 2 mM. This effect is consistent with an increase of the absorption cross section of photosystem II. However, we did not observe an increase in the yield of the middle phase in the F_{max} experiment.

Although it is difficult to be precise about changes in the fast phase, we consistently observed a decrease in its lifetime upon the addition of Mg^{+2}. As Mg^{+2} increases communication between photosystem II units, we postulate that it also strengthens the connection between the Chl a_2 antenna and the photosystem II reaction center. A Mg^{+2}-induced increase in the rate constant k_{T20} could account for the observered shortening of the fast phase lifetime.

3. Conclusion

The addition of Mg^{+2} to broken spinach chloroplasts isolated in the absence of Mg^{+2} has two effects which occur in different concentration ranges. As the Mg^{+2} concentration is increased from 0.0 to 0.75 mM, the rate constant for transfer between photosystem II and photosystem I decreases. It is possible that changes occuring in this concentration range also affect the kinetics of the charge recombination in the photosystem II reaction center. As the Mg^{+2} concentration is increased

up to 2.0 mM, changes in the Chl a/b LH antenna occur which both increase the absorption cross-section of photosystem II and bring about communication between photosystem II units. There is probably also an increase in the transfer rate between the Chl a_2 antenna the the photosystem II reaction center. Most of these correlations can be understood as a consequence of effects of Mg^{+2} on the organization of the Chl a/b LH antenna. This conclusion is in good agreement with the results of Lieberman et al. [19] who concluded that the Chl a/b LH antenna is required for Mg^{+2} effects.

VI-5. REFERENCES

1. P. Homann, Plant Physiol. 44, 932 (1976).
2. N. Murata, Biochim. Biophys. Acta 189, 171 (1969).
3. N. Murata, H. Tashiro, and A. Takayima, Biochim. Biophys. Acta 197, 250 (1970).
4. N. Murata, Biochim. Biophys. Acta 226, 422 (1971).
5. N. Murata, Biochim. Biophys. Acta 172, 242 (1969).
6. C. Bonaventura and J. Myers, Biochim. Biophys. Acta 189, 366 (1969).
7. W. L. Butler and M. Kitajima, Biochim. Biophys. Acta 396, 72 (1975).
8. B. M. Henkin and K. Sauer, Photochem. Photobiol. 24, 277 (1977).
9. A. Joliot and P. Joliot, C. R. Acad. Sci. Paris 258D, 4622 (1964).
10. P. Bennoun, Biochim. Biophys. Acta 368, 141 (1974).
11. J.-M. Briantais, C. Vernotte, and I. Moya, Biochim. Biophys. Acta 325, 530 (1973).
12. T. V. Marsho and B. Kok, Biochim. Biophys. Acta 223, 240 (1970)
13. P. Joliot, A. Joliot, and B. Kok, Biochim. Biophys. Acta 153, 635 (1968).
14. S. Izawa and N. E. Good, Plant Physiol. 41, 544 (1966).
15. S. Murakami and L. Packer, Arch. Biochem. Biophys. 146, 337 (1971).
16. N. Murata, Biochim. Biophys. Acta 245, 365 (1971).
17. A. Telfer, J. Nicolson, and J. Barber, FEBS Lett. 65, 77 (1974).
18. J. Barber, in Chlorophyll Organization and Energy Transfer in Photosynthesis, Ciba Found. Symp. 61, 283, Elsevier/North-Holland Press, Amsterdam (1979).

19. J. R. Lieberman, S. Bose, and C. J. Arntzen, Biochim. Biophys. Acta 502, 417 (1978).

20. P. A. Armond, C. J. Arntzen, J.-M. Briantais, and C. Vernotte, Arch. Biochem. Biophys. 175, 54 (1976).

21. D. J. Davis, P. A. Armond, E. L. Gross, and C. J. Arntzen, Arch. Biochem. Biophys. 175, 64 (1976).

22. W. Haehnel, J. A. Nairn, P. Reisberg, and K. Sauer, Biochim. Biophys. Acta, in press (1982).

23. P. Reisberg, J. A. Nairn, W. Haehnel, and K. Sauer, in preparation.

24. J. Barber, G. F. W. Searle, and C. J. Tredwell, Biochim. Biophys. Acta 501, 174 (1978).

25. G. F. W. Searle, C. J. Tredwell, J. Barber, and G. Porter, Biochim. Biophys. Acta 545, 496 (1979).

26. G. S. Beddard, G. R. Fleming, G. Porter, G. F. W. Searle, and J. A. Synowiec, Biochim. Biophys. Acta 545, 165 (1979).

27. I. Moya, Govindjee, C. Vernotte, and J.-M. Briantais, FEBS Lett. 75, 13 (1977).

28. K. Sauer and G. T. Brewington, in Proc. 4th Intl. Congr. Photosynthesis (eds. D. O. Hall, J. Coombs, and T. W. Goodwin), The Biochemical Society, London, 409 (1977).

CHAPTER VII

FLUORESCENCE DECAY KINETICS DURING THE P TO S FLUORESCENCE DECLINE IN SPINACH CHLOROPLASTS

VII-1. INTRODUCTION

The yield of chlorophyll a fluorescence in chloroplasts exhibits a slow quenching from an initial high-yield state (P state) to a steady state low-yield state (S state) [1-3]. There is general agreement that the slow quenching is caused by a structural change of the membrane in the chloroplasts [4]; it has recently been postulated that this structural change can be induced by two distinct mechanisms [5,6]. The first mechanism involves Mg^{+2} efflux from the thylakoids caused by H^{+} uptake into the thylakoids [7-12]. This mechanism is dominant at low light intensity and can be inhibited or reversed by uncouplers; it is termed ionophore-reversible or Mg^{+2}-dependent quenching [5,6]. The second mechanism does not involve Mg^{+2} ion movement and may reflect conformational changes of the coupling factor [13]. This mechanism is dominant at high light intensity and is not reversed by uncouplers; it is termed ionophore-resistant quenching [5].

In this chapter, I present the measurement of the three phases of the fluorescence decay described in Chapters IV through VI (see also Refs. [14-16]) during the P to S transition under conditions where ionophore-reversible quenching is dominant. Briantais et. al. [17] have proposed that while quenching under these conditions is associated with Mg^{+2} efflux, the quenching is not a reversal of the well known Mg^{+2}

effect [18]. In particular, the spillover from photosystem II to photosystem I, as measured by the ratio of the 735 nm peak to the 685 nm peak of the fluorescence spectrum at 77K [17], is the same in the P state as it is in the S state, while it is different in chloroplasts isolated in the presence or absence of Mg^{+2}. By comparing the lifetimes and yields in the P state and the S state to those in chloroplasts in the presence and absence of Mg^{+2} [14,16], we find, contrary to Briantais et al. [17], that the P to S transition appears to be a reversal of the Mg^{+2} effect.

VII-2. MATERIALS AND METHODS

Broken chloroplasts were isolated from freshly harvested spinach leaves by the methods described in Chapter IV. The P to S decline was measured for a chloroplast sample in 10mM HEPES-NaOH buffer (pH 7.5) containing 0.1 M sucrose, 5 mM $MgCl_2$, 5 mM NaCl, and 18 µg/ml of chlorophyll. The chloroplasts were excited at 620±5 nm using the laser dye Rhodamine 6G. Fluorescence was monitored at 680±5 nm. The intensity of light hitting the chloroplast supension was approximately 40 kerg/cm^2/sec, and this was sufficient to induce the P to S transition. Measurements where done on a small volume (0.3 ml) that was uniformly illuminated to prevent artifacts due to diffusion of chloroplasts into and out of the beam.

The single-photon timing apparatus and the methods of numerical analysis are described in Chapter III.

VII-3. RESULTS

Fig. VII-1 shows the photon flux (fluorescence intensity) versus time for a typical sample. The initial rise from F_0 to F_{max} or from the O state to the P state [19] is not resolved. The slow quenching from the P state to the S state is observed to occur with a half time of about 75 seconds. The total extent of the quenching is between 50% and 60%.

Addition of 1 μM gramacidin D prior to illumination inhibits the quenching; thus, our conditions favor the ionophore-reversible quenching mechanism [5,6]. The intensity of our excitation source (about 40 kerg/cm^2/sec) is four times higher than that used by Krause [6] to measure ionophore-reversible quenching, but his excitation was broad-band red light from 630 nm to 680 nm while our excitation is at 620±5 nm. Absorption by chloroplasts at 620 nm is lower than it is between 630nm and 680nm.

Accurate single-photon timing data require accumulating enough counts to achieve a good signal-to-noise ratio in the fluorescence decay data. We accomplished this by illuminating 7 fresh dark-adapted chloroplast samples and collecting photon timing data during the intervals marked in Fig. VII-1. Addition of data from the corresponding intervals of the 7 chloroplast samples gives a sufficiently high signal-to-noise ratio. Fig. VII-2 shows the raw data for the earliest time (10s) and the latest time (435s). The bottom of Fig. VII-2 shows plots of the deviations between the best three-exponential fits and the raw data.

Fig. VII-3 is a plot of the lifetimes of the three components during the P to S transition. The lifetime of each phase decreases by

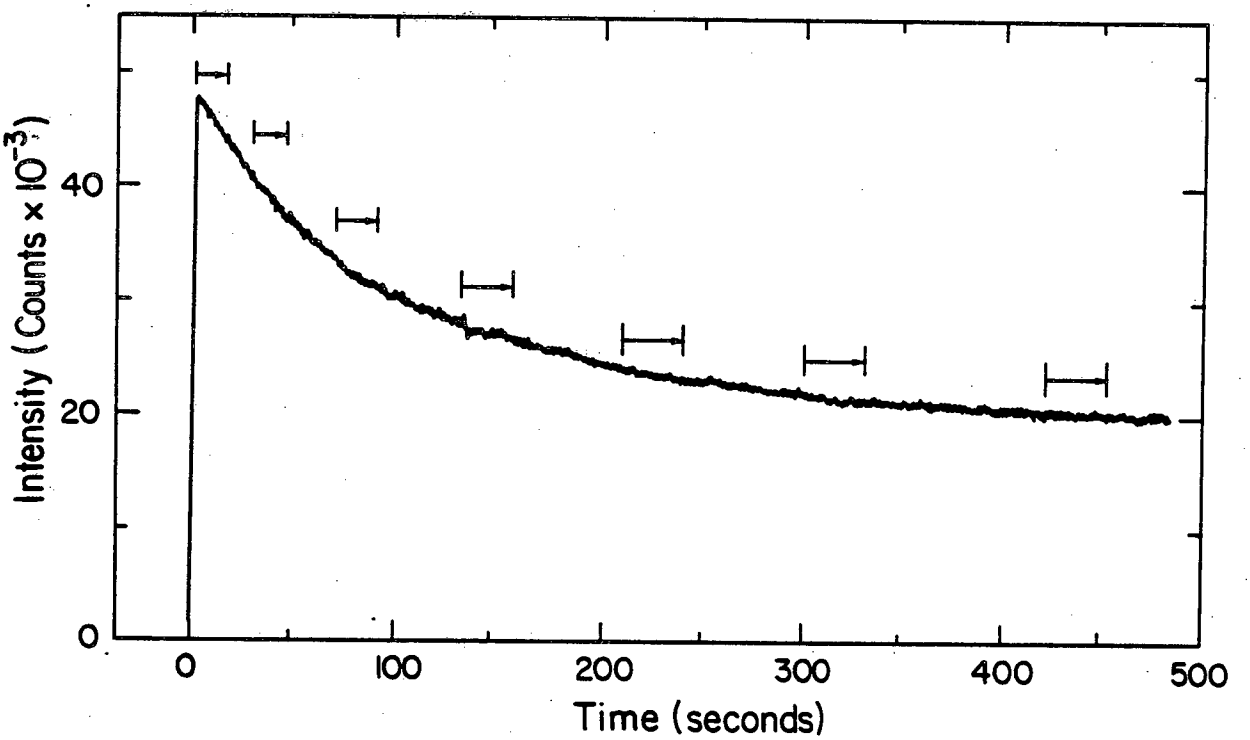

XBL 811-4441

Figure VII-1: Fluorescence photon flux rate for a typical sample of spinach chloroplasts undergoing a P to S transition. Data for lifetime measurements were collected during the intervals marked on the figure. At time = 0, the dark adapted sample is exposed to light.

Figure VII-2: Single-photon timing data for fluorescence decays at the earliest time ($F_{T=10s}(t)$) and at the latest time ($F_{T=435s}(t)$). E(t) is the response function for our single-photon timing system. The smooth lines through the two F(t)'s are the best three-exponential fits, and the two lower plots are the deviations between these fits and the raw data.

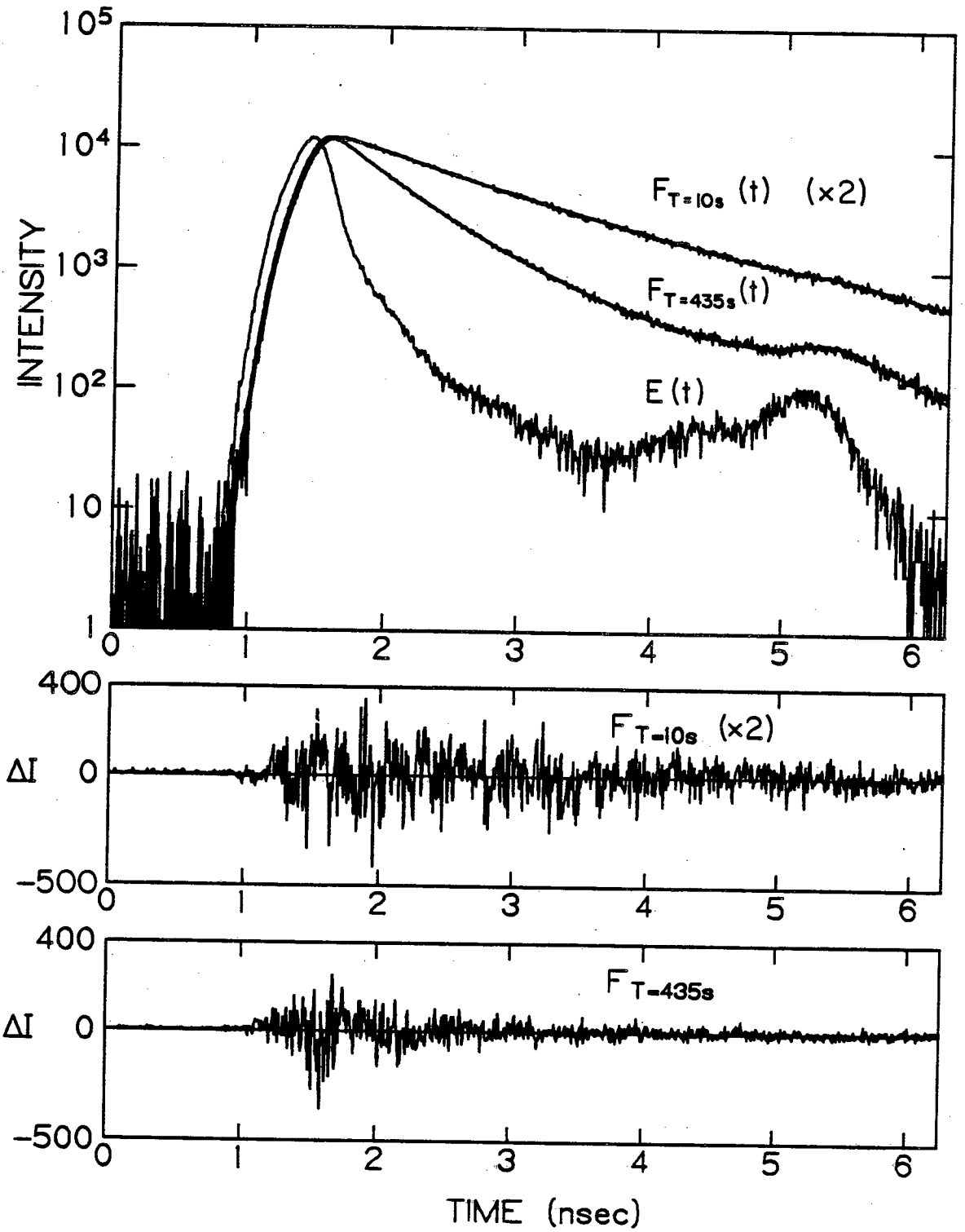
INTENSITY
10^5
10^4
10^3
10^2
10
1
$F_{T=10s}$ (t) (×2)
$F_{T=435s}$(t)
E(t)
0 1 2 3 4 5 6
400
ΔI 0
-500
$F_{T=10s}$ (×2)
$F_{T=435s}$
TIME (nsec)

XBL 811-4440

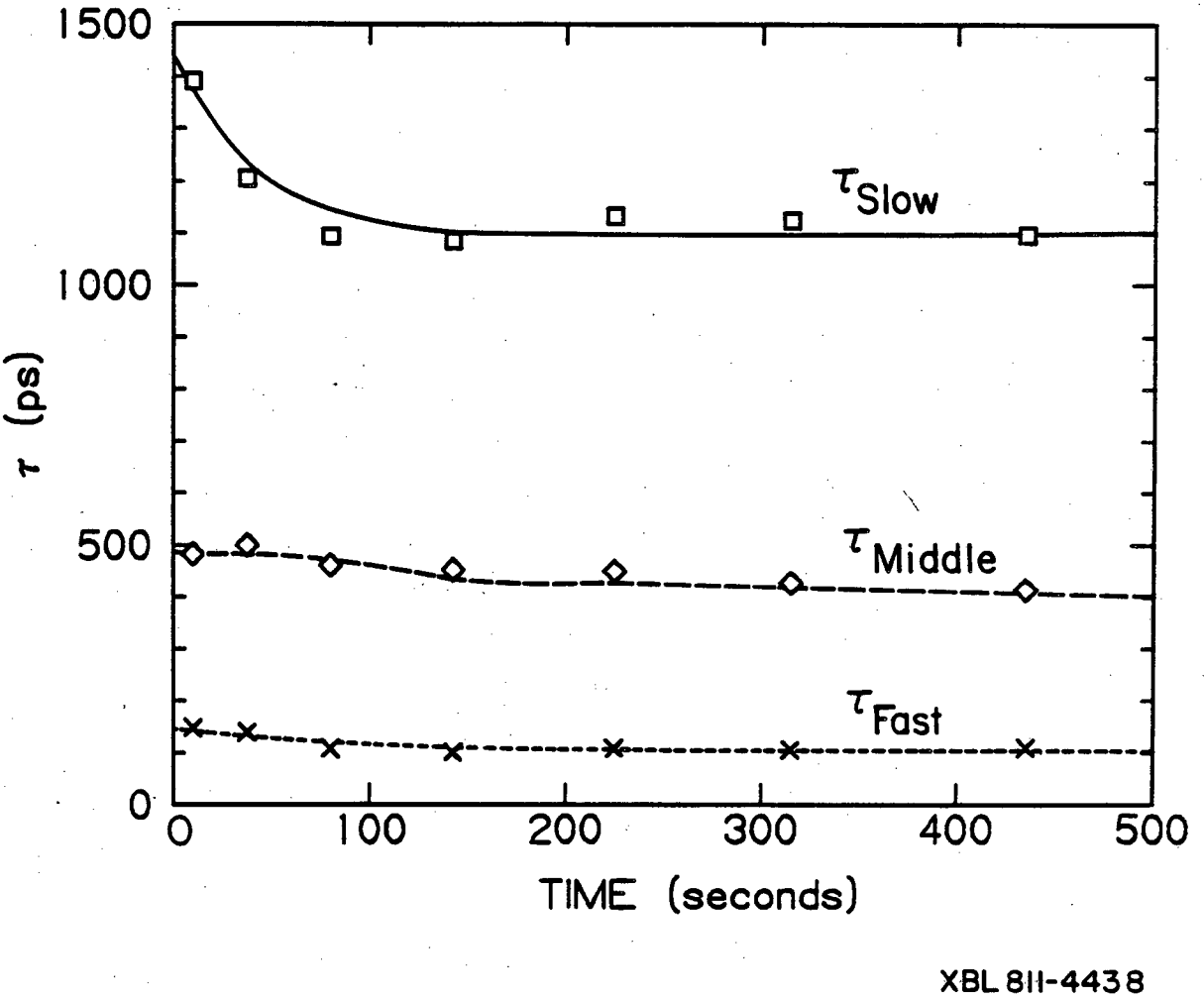

Figure VII-3: Lifetimes of the three phases during the P to S transition.

20%. Fig. VII-4 plots total yield and the yield of each component during the P to S transition. The total yield decreases about 60%, and all of this decrease is accounted for by a 6.2-fold decrease in the yield of the slow phase. This 6.2 fold decrease in yield is accompanied by much less dramatic changes in τ_{slow}. The yields of the two faster phases increase, but by a factor of less than two. It is difficult to be precise about the fastest phase, because it amounts to less than 5% of the fluorescence.

As mentioned in the Introduction, ionophore-reversible quenching involves Mg^{+2} efflux from the thylakoids. Even though Briantais et. al. [17] have concluded that some characteristics of the S state differ from those of chloroplasts devoid of Mg^{+2}, it is still tempting to equate the fluorescence decline results with the loss of the Mg^{+2}-stimulated fluorescence increase. To explore further this question, we compare lifetime data in the P and S state to the Mg^{+2} effect on fluorescence lifetimes reported in Chapter VI and Ref. [15]. Table VII-I summarizes the comparison. In both the P to S experiment and the $\pm Mg^{+2}$ experiment, the fast and middle phases behave similarly. The fast phase increases in yield with only small changes in the lifetime. (The fast lifetime is difficult to resolve accurately.) The middle phase increases in yield about 1.5 fold and decreases slightly in lifetime. The slow phase lifetime decreases by about the same extent in both cases, but its yield shows minor differences. In the P to S transition, the yield decreases 6.2 fold. In the S state the yield of the slow phase has decreased to about 1/2 of the yield of the middle phase. It may have decreased even more than this, because our first point is actually an average over the first 15 seconds; this averaging tends to lessen the observed decrease

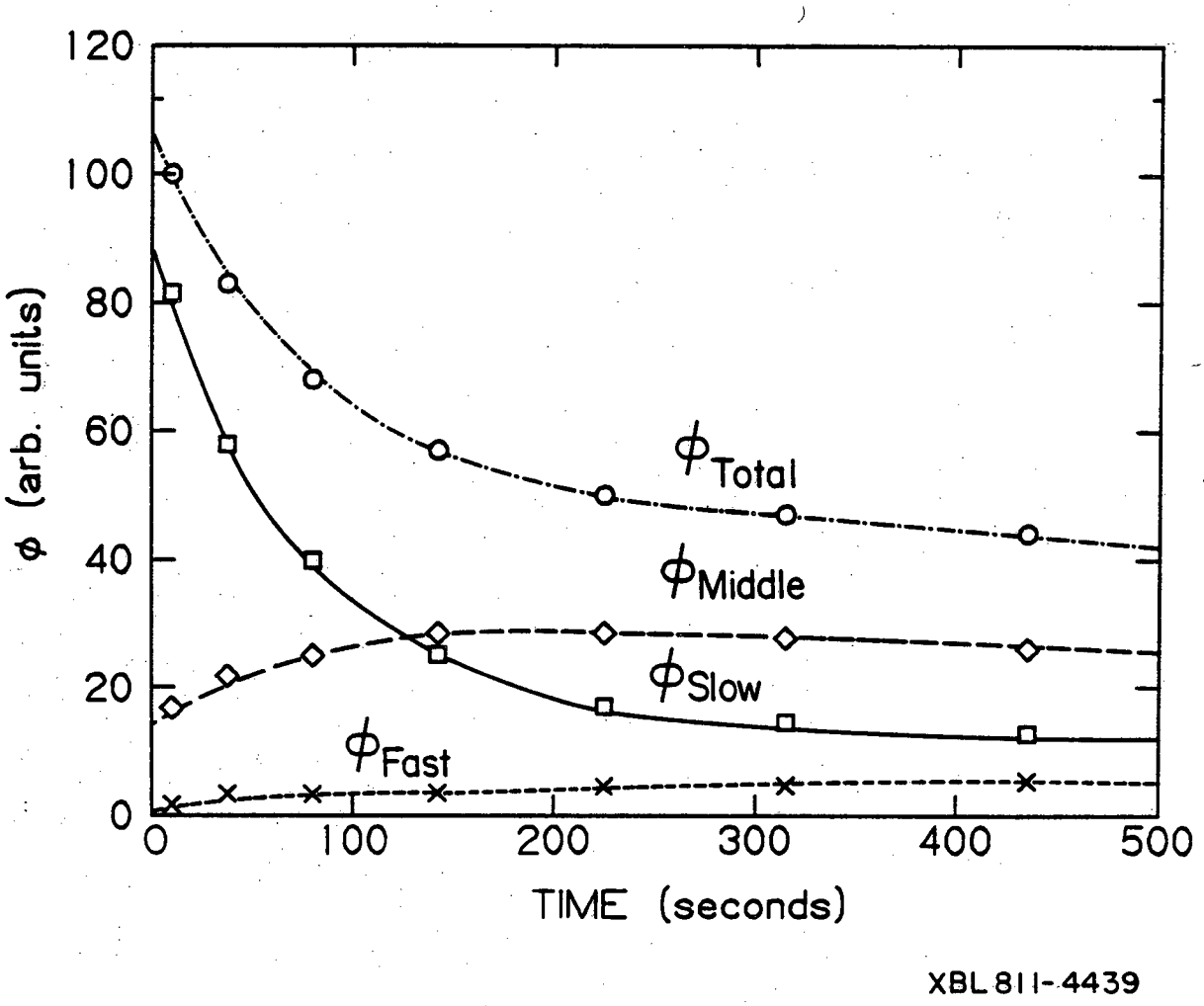

Figure VII-4: Yield of the three phases and total yield during the P to S transition.

Table VII-I: A comparison of the lifetime and yield changes upon going from the P state to the S state with the lifetime and yield changes in the presence and absence of Mg^{+2}. For the $\pm Mg^{+2}$ effect, 1 μM DCMU and 1 mM hydroxlamine hydrochloride were added to keep Q reduced. All lifetimes are in picoseconds.

	P TO S			$\pm Mg^{+2}$		
State	τ	Φ	Φ_{tot}	τ	Φ	Φ_{tot}
High Yield ($t=10s$ or $+Mg^{+2}$)	1390	81	100	1580	83	100
	480	17		430	13	
	150	2		40	4	
Low Yield ($t=435s$ or $-Mg^{+2}$)	1100	13	44	1160	24	49
	410	26		380	21	
	110	5		60	5	

in the slow phase yield. In the $\pm Mg^{+2}$ experiment, the yield of the slow phase decreases only 3.5 fold, and it is still the largest component even in the absence of Mg^{+2}.

VII-4. DISCUSSION

The changes in the lifetimes and yields of the three fluorescence decay components between the P and S state and between the presence and absence of Mg^{+2} are very similar. This similarity suggests that the effect of the P to S transtion on energy distribution in the thylakoid membrane is the same as the effect of removing Mg^{+2}. In particular, the small decreases in the lifetimes of the middle and slow components reflect an increase in the rate of spillover from photosystem II to photosystem I. The large decrease in the slow phase yield and the small decrease in middle phase yield parallels the Mg^{+2} effect on these yields plotted in Fig. VI-4. These yield changes reflect changes in the rate of photosystem II to photosystem I spillover and changes in the absorption cross section of photosystem II (see Discussion section of Chapter VI).

Our conclusions are contrary to the results of Briantais et al. [17]. They froze chloroplast samples in liquid nitrogen at various times during the P to S transition. Unlike the fluorescence emission spectra at 77K of chloroplast samples in the presence and absence of Mg^{+2}, their frozen samples showed no change in the ratio of the 735 nm to 685 nm peak heights. One proposal to account for the discrepancy between their results and ours is that the P to S transition does induce a removal of the Mg^{+2} effect, but the mechanism of removal does not survive low

temperatures. In contrast, Mg^{+2} removal by isolation of the chloroplasts in the absence of Mg^{+2} induces changes which are still present at low temperature. These changes alter the low temperature emission spectrum.

VII-5. REFERENCES

1. N. Murata K. and Sugahara, Biochim. Biophys. Acta 189, 182 (1969).
2. C. A. Wraight and A. R. Crofts, Eur J. Biochem. 17, 319 (1970).
3. G. H. Krause, Biochim. Biophys. Acta 292, 715 (1973).
4. J. Lavorel and A. L. Etienne, in Primary Processes of Photosynthesis (Barber, J., ed.), Elsevier/North-Holland Press, Amsterdam 203 (1977).
5. P. M. Sokolov and T. V. Marscho, Biochim. Biophys. Acta 459, 27 (1977).
6. G. H. Krause, Planta 138, 73 (1978).
7. G. H. Krause, Biochim. Biophys. Acta 333, 301 (1974).
8. J. Barber and A. Telfer, in Membrane Transport in Plants (eds. J. Dainty and U. Zimmerman), Springer-Verlag, Berlin, 231 (1974).
9. J. Barber, A. Telfer, and J. Nicolson, Biochim. Biophys. Acta 357, 161 (1974).
10. J. Barber, A. Telfer, J. Mills, and J. Nicolson, in Proceedings of the Third International Congress on Photosynthesis, Israel (ed. M. Avron), Elsevier/North-Holland Press, Amsterdam, 53 (1974).
11. J. Barber, J. Mills, and J. Nicolson, FEBS Lett. 49, 106 (1974).
12. J. Mills and J. Barber, Arch. Biochem. Biophys. 120, 306 (1975).
13. R. C. Jennings, F. M. Garlashi, and G. Forti, Biochim. Biophys. Acta 423, 264 (1976).
14. W. Haehnel, J. A. Nairn, P. Reisberg, and K. Sauer, Biochim. Biophys. Acta, in press (1982).
15. J. A. Nairn, W. Haehnel, P. Reisberg, and K. Sauer, in preparation.
16. P. Reisberg, J. A. Nairn, W. Haehnel, and K. Sauer, in preparation.

17. J.-M. Briantais, C. Vernotte, M. Picaud, and G. H. Krause, Biochim. Biophys. Acta 548, 128 (1979).

18. J. Lavorel and A.-L. Etienne, in Primary Processes in Photosynthesis (ed. J. Barber), Elsevier/North-Holland Press, Amsterdam, 203 (1977).

CHAPTER VIII

FLUORESCENCE DECAY KINETICS IN SPINACH CHLOROPLASTS AT LOW TEMPERATURE

VIII-1. INTRODUCTION

The fluorescence decay kinetics for spinach chloroplasts at room temperature has been found in Chapters IV through VII to be characterized by three exponential components [1-3]. The room-temperature fluorescence emission spectrum from spinach chloroplasts is broad and featureless with a peak at 680-685 nm and a tail extending to beyond 700 nm [4]. The spectra of the three fluorescence decay components are similar to each other [1]. Thus it is not possible to study the fluorescence decay from the different components of the photosynthetic unit independently by varying the detection wavelength. In contrast, at 77K the fluorescence emission spectrum, while still broad, is resolved into three peaks at 685 nm, 695 nm, and 735 nm [4,5]. From measurement of the fluorescence emission spectra of purified subchloroplast particles at 77K, it has been proposed that the origin of these three peaks are the Chl a/b LH antenna (685 nm), the Chl a_2 antenna (695 nm), and photosystem I (735 nm) [5].

Picosecond resolution of the fluorescence decay kinetics as a function of wavelength at 77K allows a selective study of the fluorescence properties of different parts of the photosynthetic unit. The fluorescence decay at short wavelengths ($\lambda \leq 680$ nm) is characterized by three exponential decay components which resemble those

at room temperature. At long wavelengths ($\lambda \geq 710$ nm), the fluorescence decay is described by one exponential rise component and two exponential decay components. The resolvable risetime is 50-100 ps, and the major decay component has a lifetime of about 3 ns. The other component, with a lifetime of 400-600 ps, is a small fraction of the total decay and appears to be associated with the tail of the short-wavelength fluorescence.

VIII-2. MATERIALS AND METHODS

Broken spinach chloroplasts were isolated by the methods described in Chapter IV. Measurements were done on chloroplast samples with a chlorophyll concentration of 18 µg/ml. The chloroplasts were suspended in 10mM HEPES-NaOH buffer (pH 7.5) containing 0.1M sucrose, 5mM $MgCl_2$, 5mM NaCl, 12.5µM DCMU, and 1.25mM hydroxlamine hydrochloride. DCMU and hydroxlamine hydrochloride were added to assure that all of the photosystem II reaction centers were closed by reduction of the secondary electron acceptor Q. The sample was illuminated while being cooled to low temperature (77K) by immersion in liquid nitrogen in an optical dewar.

The single-photon timing system and the methods of numerical analysis are described in Chapter III.

VIII-3. RESULTS

The fluorescence decay components from spinach chloroplasts at 77K

for detection wavelengths $\leq$ 680 nm are summarized in Table VIII-I. These components are similar to the three components observed in spinach chloroplasts at room temperature that are suspended in the same buffer; i.e., spinach chloroplasts in the presence of Mg^{+2}, DCMU, and hydroxlamine hydrochloride. Two apparent differences between the room- and low-temperature results are that the slow and middle phases are faster at 77K and that the relative yield of the slow phase is 40-50% less at 77K.

At wavelengths $\geq$ 710 nm, we observe a very different fluorescence decay, which is characterized by three different kinetic components. One component is a risetime of 50-100 ps and the other two are decays of 400-600 ps and 2200-3200 ps. The lifetimes of these three components are plotted as a function of emission wavelength in Fig. VIII-1.

At the longest wavelengths (λ > 740 nm), the 400-600 ps phase is less than 3% of the total fluorescence yield. The resolved rise and slow decay components that predominate have approximately equal amplitudes which are opposite in sign. This fact suggests that the rise and slow decay can be assigned to a single pigment bed of chlorophyll. The observable rise of 50-100 ps is the time required for energy transfer to this pigment bed, which then fluoresceses at long wavelengths and decays with a 3 ns lifetime. The yield of the fluorescence emitted from the long-wavelength pigment bed of chlorophyll, the yield of the 400-600 ps component, and the total yield as a function of emission wavelength are plotted in Fig. VIII-2. The yield of the fluorescence emitted from the long-wavelength pigment bed of chlorophyll follows the fluorescence spectrum beyond 710 nm, and in this wavelength region the yield of the 400-600 ps component decreases to a low level.

Table VIII-I: Amplitudes, lifetimes, and fluorescence yields of the three fluorescence decay components in spinach chloroplasts at 77K in the presence of 5 mM $MgCl_2$, 12.5 μM DCMU, and 1.25 mM hydroxlamine hydrochloride. Amplitudes and yields are in percent of the total.

λ(nm)	α	τ (ps)	φ
670	8	1590	40
	38	310	40
	54	110	20
680	13	1520	48
	49	320	39
	38	140	13

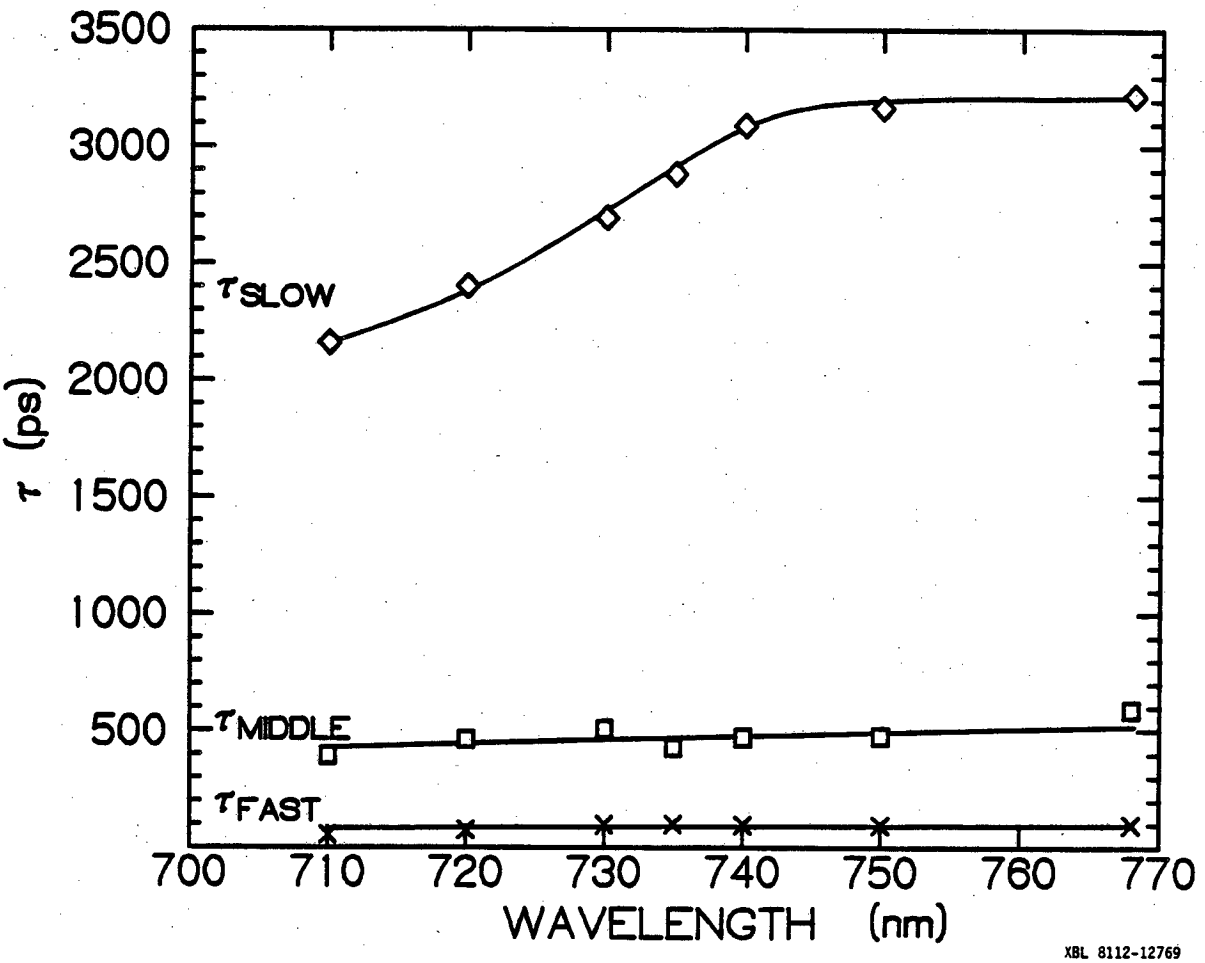

Figure VIII-1: Lifetimes of the three components in the long-wavelength fluorescence decay at 77K in spinach chloroplasts as a function of the wavelength of emission.

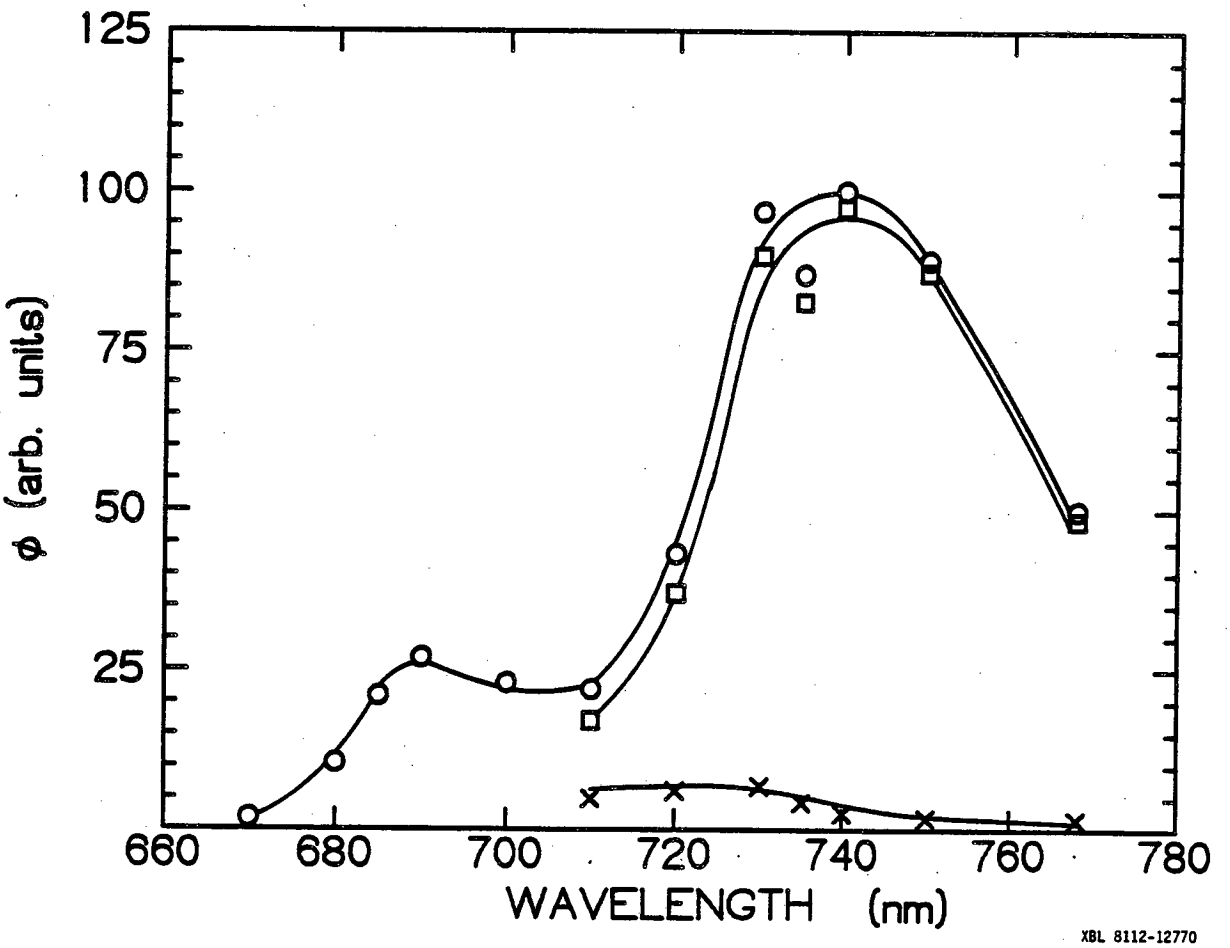

Figure VIII-2: Total fluorescence yield (o), yield of the fluorescence emitted from the long-wavelength pigment bed of chlorophyll (□), and yield of the 400-600ps component (×) in spinach chloroplasts at 77K as a function of the wavelength of emission.

At intermediate wavelengths it was not possible to fit the data adequately with either three or four kinetic components, presumably owing to overlap of the short-wavelength and the long-wavelength emissions. The resulting decay is multiphasic and complex.

VIII-4. DISCUSSION

We propose that there are five exponential kinetic components in the low-temperature emission of spinach chloroplasts in the presence of Mg^{+2}, DCMU, and hydroxlamine hydrochloride. Three of these components are observable at 670 nm and at 680 nm. These are a slow component with a lifetime of 1500-1600 ps, a middle component with a lifetime of about 300 ps, and a fast component with a lifetime of 100-150 ps. The weighted mean lifetime of the short-wavelength decay is 750-900 ps. This range is in agreement with short-wavelength measurements on pea chloroplasts by Wong *et al.* [6]. A two-component fit to our data is in agreement with the two-component analysis of 685 nm fluorescence from pea chloroplasts at 77K by Beddard *et al.* [7]. The fourth and fifth components that we observe predominate at long wavelengths and are best characterized beyond 750 nm, where they are > 97% of the total decay. The fourth kinetic component is a risetime of about 100 ps, and the fifth is a decay with about a 3200 ps lifetime. The long-wavelength decay is in reasonable agreement with literature values from pea chloroplasts [6,8,9] and from bean leaf [10] which range between 2100 ps and 3100 ps. A similar risetime of 135 ps at 735 nm in spinach chloroplasts illuminated at short wavelengths was reported by Campillo *et al.* [11],

but Butler et al. [10] reported that the long-wavelength fluorescence rise in pea chloroplasts illuminated at short wavelengths is less than the 50 ps resolution of their system. We find that a long-wavelength fluorescence risetime between 50 ps and 150 ps is reproducible.

At wavelengths between 685 nm and 700 nm each of the above five components is present to a large enough extent that the data cannot be fit with only three or four components. At wavelengths between 710 nm and 735 nm, the long-wavelength components are sufficiently dominant that three-exponential fits describe the data. The 400-600 ps component of the long-wavelength fits, which monotonically decreases in yield for wavelengths $\geq$ 730 nm, is probably the tail of the short-wavelength fluorescence. It is slower than the middle phase measured at short wavelengths because some of the short-wavelength slow phase is averaged into it. Analogously, the long-wavelength slow decay component lifetime decreases at wavelengths less than 740 nm because some of the short wavelength slow phase probably is averaged into it.

The fluorescence decay components at 670 nm and 680 nm are similar to the room-temperature decay components. We have studied the temperature dependence of these components and the absence of an abrupt transition in the temperature dependence suggests that the origin of these components is the same as the origin of the room-temperature components. Our analysis of the room-temperature fluorescence postulated that the slow component is "delayed" fluorescence which arises from excited chlorophyll antenna molecules populated after a charge recombination in the photosystem II reaction center [1,3]. This model accounts for the observed decrease in the relative yield of the slow phase at 77K; at low temperatures, the energetically uphill charge

recombination and energy transfer back to the chlorophyll antenna becomes less probable.

The fact that the amplitudes of the rise and of the slow decay of the long-wavelength fluorescence are equal but opposite in sign means that the chlorophyll pigment bed responsible for the long-wavelength emission receives most of its excitation through relatively slow (100 ps) energy transfer and not by direct absorption of the excitation pulse by the pigment molecules that subsequently emit. This pigment bed probably contains a small number of chlorophyll molecules, which is consistent with the assignment of the long-wavelength fluorescence to a chlorophyll trap, C705, located in photosystem I [9,10,12]. The risetime of about 100 ps reflects the time required for energy to transfer from the bulk chlorophyll antenna to C705. In future studies we hope to determine whether there is a "variable" component of PS I fluorescence that is distinct from that resulting from excitation transfer controlled by the state of the PS II reaction center.

REFERENCES

1. W. Haehnel, J. A. Nairn, P. Reisberg, and K. Sauer, Biochim. Biophys. Acta, in press (1982).
2. J. A. Nairn, W. Haehnel, P. Reisberg, and K. Sauer, in preparation.
3. P. Reisberg, J. A. Nairn, W. Haehnel, and K. Sauer, in preparation.
4. N. K. Boardman, S. W. Thorne, and J. M. Anderson, Proc. Natl. Acad. Sci. USA 56, 586 (1966).
5. K. Satoh and W. L. Butler, Plant Physiol. 61, 373 (1978).
6. D. Wong, H. Merkelo, and Govindjee, FEBS Lett. 104, 223 (1979).
7. G. S. Beddard, G. R. Fleming, G. Porter, G. F. W. Searle, and J. A. Synowiec, Biochim. Biophys. Acta 545, 165 (1979).
8. W. L. Butler, C. J. Tredwell, R. Malkin, and J. Barber, Biochim. Biophys. Acta 545, 309 (1979).
9. V. B. Tusov, B. N. Koratovskii, V. Z. Paschenko, and L. B. Rubin, Dokl. Akad. Nauk SSSR 252, 1500 (1980).
10. W. L. Butler and K. H. Norris, Biochim. Biophys. Acta 66, 72 (1963).
11. A. J. Campillo, S. L. Shapiro, N. E. Geacintov, and C. E. Swenberg, FEBS Lett. 83, 316 (1977).
12. K. Satoh and W. L. Butler, Biochim. Biophys. Acta 502, 103 (1978).

CHAPTER IX

CONCLUSION

IX-1. ORIENTATIONAL AVERAGING

Concrete methods for applying our density of states approach to orientational averaging problems are described in Chapter II. These methods involve detailed formulas for calculation of density of states functions that encompass a large range of problems. The complete formulas are presented in Tables II-I, II-II, and II-III. Density of states functions not included in these tables can be evaluated by the techniques outlined in Chapter II and presented in Refs. [1-3].

Our orientational averaging techniques were originally developed for analysis of spectroscopy on photosynthetic systems [4,5], but they should be applicable to many biological systems. I hope that scientists interested in spectroscopy of partially ordered systems have found that the details presented in this thesis and in Refs. [1-5] make our orientational averaging techniques understandable and usable.

IX-2. FLUORESCENCE DECAY KINETICS

The picosecond resolution of the fluorescence decay kinetics in chloroplasts presented in this thesis and in Ref. [6] represent the first high time resolution, high signal-to-noise ratio investigation of these kinetics. Our first new finding is that it takes three

exponentials to accurately describe the fluorescence decay. One slow phase is 1 to 2 ns, and two faster phases are 350 to 750 ps and 50 to 100 ps. The exact lifetimes and yields of each phase depend on the experimental conditions. The fastest phase has been missed in previous investigations because it is very fast and because it has a low yield.

A working model for the interpretation of the three decay components is presented in Chapter V. The model is an extension of Butler et al.'s tripartite model [7-9] to explicitly include electron transfer processes in the photosystem II reaction center [10-16]. Simulation procedures using the model illustrated in Fig. V-1 have given us an understanding of the origin of each fluorescence decay component [17]. The middle and fast phases are "prompt" fluorescence phases due to excitation in photosystem II that is lost prior to reaching the photosystem II reaction center. Their lifetimes are approximately equal to the time for energy transfer from the Chl a/b LH antenna and from the Chl a_2 antenna to the reaction center of photosystem II, respectively. The slow phase is "delayed" fluorescence that is due to excitation that returns to the chlorophyll antenna after undergoing a charge separation and recombination reaction in the photosystem II reaction center. The charge recombination reaction in the photosystem II reaction center occurs with a high yield when the reaction center is closed.

The working model provides a framework for interpretation and analysis of changes in fluorescence properties of chloroplasts that are related to sample conditions. There are numerous reports in the photosynthesis literature of how chloroplast preparation and treatment affect the total fluorescence yield (see reviews [7,18]). Many of these studies could be extended by resolving the fluorescence decay and

investigating how the chloroplast preparation and treatment affect the lifetime and yields of each component. Comparison of the measured total fluorescence yield with the published total fluorescence yield studies provides a built-in parameter that indicates we are studying the same phenomena. Our first attempts at such an experimental program are presented in Chapters VI and VII.

In Chapter VI is presented an examination of the effect of Mg^{+2} on the room-temperature fluorescence decay kinetics in spinach chloroplasts. The ability to measure the lifetime and yield of each phase led us to propose two effects that occur at different levels of added Mg^{+2} [19]. As Mg^{+2} is added to spinach chloroplasts isolated in the absence of Mg^{+2}, the connections between photosystem II and photosystem I are altered such that the rate of energy transfer from photosystem II to photosystem I is decreased. This effect saturates at $[Mg^{+2}]$ = 0.75 mM. At higher levels of added Mg^{+2} (up to 2 mM), the connections between photosystem II units are altered such that energy transfer between photosystem II units is possible and the absorption cross section of photosystem II is increased. Studies on the P to S fluorescence decline in spinach chloroplasts, presented in Chapter VII, suggest that the transition from the P state to the S state is analogous to the removal of the Mg^{+2} effect.

The photosynthesis literature also contains a large volume of work on low-temperature fluorescence intensity properties of chloroplasts [7]. Our first examination of the low-temperature fluorescence decay kinetics, which is presented in Chapter VIII, has uncovered five components [20]. Three components which predominate at short wavelengths appear to be analogous to the room-temperature components. A decrease in

the yield of the slow phase supports the interpretation that the slow phase originates from a charge recombination reaction that is energetically uphill. Two new components, which predominate at long wavelengths, appear to originate from a small pigment bed of chlorophyll analogous to the C705 chlorophyll trap in photosystem I proposed by Satoh and Butler [21]. One of these long-wavelength components is a resolvable risetime of 50 to 150 ps. The measured onset of fluorescence provides a direct observation of energy transfer from the bulk chlorophyll antenna to the pigment bed of chlorophyll responsible for the long-wavelength emission.

Possible future directions for fluorescence decay investigations are numerous. I will mention three projects which are already in progress:

(1). By varying the electrochemical potential of a chloroplast suspension, it is possible to reduce controlled amounts of Q [22-24]. The fluorescence yield change as a function of potential is quite complex and is suggestive of heterogeneity in the photosystem II reaction centers [22-24]. Resolution of the fluorescence decay kinetics as a function of potential may help to sort out some of the heterogeneity questions and suggest refinements for the model in Fig V-1.

(2). Fluorescence decay experiments with subchloroplast particles enriched in either photosystem I or photosystem II should enable a quantitative determination of the contribution of photosystem I to the room-temperature fluorescence. This result would enable more quantitative evaluation of spillover between photosystem II and photosystem I.

(3). Fluorescence from the pigment bed of chlorophyll responsible for the long-wavelength emission at low temperature can be probed independently of that from other components of the photosynthetic unit. Many possible experiments could elucidate the properties of this pigment bed. Examples include temperature dependence and excitation-wavelength dependence of the fluorescence risetime.

The aim of the fluorescence decay kinetics section of this thesis has been to initiate detailed picosecond resolution of the fluorescence decay in photosynthetic systems. We were able to uncover the complex nature of the fluorescence decay kinetics in spinach chloroplasts. The knowlege of three fluorescence decay components and the ability to measure these components provides more information than measuring only the total fluorescence yield. Thus, time-resolved fluorescence decay studies can greatly increase the effectiveness of fluorescence as a non-destructive probe into the photosynthetic unit. I believe that such studies can lead to a detailed understanding of the paths of energy transfer through the phoytosynthetic unit, kinetics of energy transfer between chlorophyll-proteins, and mechanisms behind energy regulation in chloroplasts. I hope the work presented in this thesis will prove to be the groundwork for such studies.

IX-3. REFERENCES

1. R. Friesner, J. A. Nairn, and K. Sauer, J. Chem. Phys. 71, 358, 5388 (1979).
2. R. Friesner, J. A. Nairn, and K. Sauer, J. Chem. Phys. 72, 221, (1980).
3. J. A. Nairn, R. Friesner, and K. Sauer, J. Chem. Phys. 74, 5398 (1981).
4. J. A. Nairn, R. Friesner, H. A. Frank, and K. Sauer, Biophys. J. 32, 733 (1980).
5. H. A. Frank, R. Friesner, J. A. Nairn, G. C. Dismukes, and K. Sauer, Biochim. Biophys. Acta 547, 484 (1979).
6. W. Haehnel, J. A. Nairn, P. Reisberg, and K. Sauer, Biochim. Biophys. Acta, in press.
7. W. L. Butler and M. Kitajima, Biochim. Biophys. Acta 376, 116 (1975).
8. W. L. Butler and R. J. Strasser, Proc. Natl. Acad. Sci. USA 74, 3382 (1977).
9. W. L. Butler, Ann. Rev. Plant Physiol. 29, 345 (1978).
10. V. V. Klimov, A. V. Klevanik, V. A. Shuvalov, and A. A. Krasnovsky, FEBS Lett. 82, 183 (1977).
11. A. V. Klevanik, V. V. Klimov, V. A. Shuvalov, and A. A. Krasnovsky, Dokl. Akad. Nauk SSSR 236, 241 (1977).
12. V. V. Klimov, S. I. Allakhverdiev, and V. Z. Paschenko, Dokl. Akad. Nauk SSSR 236, 1204 (1978).
13. V. V. Klimov, S. I. Allakhverdiev, and A. A. Krasnovsky, Dokl. Akad. Nauk SSSR 249, 485 (1980).

14. V. V. Klimov, S. I. Allakhverdiev, S. Demeter, and A. A. Krasnovsky, Dokl. Akad. Nauk SSSR 249, 227 (1980).

15. V. V. Klimov, S. I. Allakhverdiev, S. I. Shutilova, and A. A. Krasnovsky, Sov. Plant Physiol. 27, 315 (1980).

16. V. V. Klimov, E. Dolan, and B. Ke, FEBS Lett. 112, 97 (1980).

17. P. Reisberg, J. A. Nairn, and W. Haehnel, and K. Sauer, in preparation.

18. J. Barber, in The Intact Chloroplast (ed. J. Barber), Elsevier/North-Holland Press, Amsterdam, 89 (1976).

19. J. A. Nairn, W. A. Haehnel, P. Reisberg, and K. Sauer, in preparation.

20. J. A. Nairn, P. Reisberg, and K. Sauer, FEBS Lett., submitted.

21. K. Satoh and W. L. Butler, Biochim. Biophys. Acta 502, 103 (1978).

22. A. Melis, FEBS Lett. 95, 202 (1978).

23. P. Horton, Biochim. Biophys. Acta 635, 105 (1981).

24. A. P. G. M. Thielen and H. J. van Gorkom, FEBS Lett. 129, 205 (1981).

APPENDIX I

We follow the convention of Arfken [1], page 179, and define rotation matrices for rotations about the x, y and z axes by

$$R_x(\theta) = \begin{pmatrix} 1 & 0 & 0 \\ 0 & \cos\theta & \sin\theta \\ 0 & -\sin\theta & \cos\theta \end{pmatrix} \tag{1}$$

$$R_y(\phi) = \begin{pmatrix} \cos\phi & 0 & -\sin\phi \\ 0 & 1 & 0 \\ \sin\phi & 0 & \cos\phi \end{pmatrix} \tag{2}$$

$$R_z(\psi) = \begin{pmatrix} \cos\psi & \sin\psi & 0 \\ -\sin\psi & \cos\psi & 0 \\ 0 & 0 & 1 \end{pmatrix} \tag{3}$$

These rotation matrices have the following property: If $\underline{V}$ is some vector in the laboratory axis system (LAS), the coordinates of $\underline{V}$ in the LAS after $\underline{V}$ has been rotated counterclockwise through an angle α about the $\underline{i}$th LAS axis are

$$\underline{V}_r = R_i^{-1}(\alpha)\underline{V} = [R_i(\alpha)]^T\underline{V} \tag{4}$$

For density of states calculations, we need to know the coordinates of $\underline{V}$ in an axis system (the molecular axis system - MAS) that is related to the LAS by successive counterclockwise rotations of $\alpha_1, \ldots, \alpha_n$ about the $i_1, \ldots, i_n$ LAS axes. The unit vectors along the x, y, and z axes of the LAS are rotated by the n rotations into unit vectors along the x, y,

and z axes of the MAS. From Eq. (4), the coordinates of these rotated unit vectors in the LAS are

$$\hat{x}_r = R_n^{-1}(\alpha_n)\ldots R_1^{-1}(\alpha_n)\ \hat{x} \tag{5}$$

and analogously for $\hat{y}_r$ and $\hat{z}_r$. The coordinates of $\underline{V}$ in the MAS, denoted $\underline{V}'$, is thus given by

$$\begin{aligned}\underline{V}' &= (\underline{V}\cdot\hat{x}_r, \underline{V}\cdot\hat{y}_r, \underline{V}\cdot\hat{z}_r) \\ &= [R_n^{-1}(\alpha_n)\ldots R_1^{-1}(\alpha_1)]^T \underline{V} \\ &= \left[\prod_{i=1}^{n} R_i\ (\alpha_i)\right] \underline{V}\end{aligned} \tag{6}$$

1. G. Arfken, Mathematical Methods for Physicists (Academic, New York, 1970).

APPENDIX II

The three rotations that generate the ensemble of MAS's in a thin film are: 1) a free rotation of α_1 about the z axis, 2) a rotation of α_2 weighted by Eq. (9) in Chapter II about the x axis, and 3) a free rotation of α_3 about the y axis. In terms of α_1, α_2, and α_3, the field direction in the MAS, $\underline{V}'(\underline{\alpha})$, is

$$\underline{V}'(\underline{\alpha}) = R_z(\alpha_1)R_x(\alpha_2)R_y(\alpha_3)\begin{pmatrix}\cos\psi\\ \sin\psi\\ 0\end{pmatrix} \tag{1}$$

The z component of $\underline{V}'(\underline{\alpha})$ is

$$V_z'(\underline{\alpha}) = |\underline{V}|\cos\theta = |\underline{V}|(\cos\psi\cos\alpha_2\sin\alpha_3 - \sin\psi\sin\alpha_2) \tag{2}$$

Following Eq. (12) in Chapter II, we choose the change of variables

$$\alpha_1 = -\phi + f_1(v_1,\theta)$$

$$\alpha_2 = v_1 \tag{3}$$

$$\alpha_3 = \sin^{-1}\left(\frac{\cos\theta + \sin\psi\sin v_1}{\cos\psi\cos v_1}\right) \tag{4}$$

Evaluation of $\partial V_z'(\underline{\alpha})/\partial\alpha_3$ and substition into Eq. (11) in Chapter II results in

$$D(\theta,\underline{\Delta}) = \frac{\sin\theta}{N}\int dv_1 \cos v_1\, W_{DF}(v_1,\underline{\Delta})(\cos^2\psi\cos^2 v_1 - \cos^2\theta - 2\cos\theta\sin\psi\sin v_1 - \sin^2\psi\sin^2 v_1)^{-1/2} \tag{5}$$

where cos v_1 dv_1 = $\underline{dv}$ is the necessary volume element for a zxy rotation scheme. Expansion of the denominator and integration where the integrand is real yields Eq. (13) in Chapter II.

APPENDIX III

For an ensemble of MAS's generated by a zxyz rotation scheme, the field direction in the MAS, $\underline{V}'(\underline{\alpha})$, is given by

$$\underline{V}'(\underline{\alpha}) = R_z(\alpha_1)R_x(\alpha_2)R_y(\alpha_3)R_z(\alpha_4)\begin{pmatrix}\cos\psi\\ \sin\psi\\ 0\end{pmatrix} \tag{1}$$

The z component of the $\underline{V}'(\underline{\alpha})$ is

$$\begin{aligned} V_z'(\underline{\alpha}) = |\underline{V}|\cos\theta = |\underline{V}|[&\cos\psi(\cos\alpha_2\sin\alpha_3\cos\alpha_4+\sin\alpha_2\sin\alpha_4)\\ &+\sin\psi(\cos\alpha_2\sin\alpha_3\sin\alpha_4-\sin\alpha_2\cos\alpha_4)] \end{aligned} \tag{2}$$

Using a slight modification of Eq. (12) in Chapter II, we choose the change of variables

$$\begin{aligned} \alpha_1 &= -\phi + f_1(v_1,v_2,\theta)\\ \alpha_2 &= v_1\\ \alpha_3 &= \sin^{-1}\left(\frac{\cos\theta + \sin v_1 \sin(\psi-v_2)}{\cos v_1 \cos(\psi-v_2)}\right)\\ \alpha_4 &= v_2 \end{aligned} \tag{3}$$

Now

$$\frac{\partial V_z'(\underline{\alpha})}{\partial \alpha_3} = \cos v_1 \cos \alpha_3 \cos(\psi-v_2) \tag{4}$$

Using the α_3 result in Eq. (3) and substituting into Eq. (11) in Chapter II results in

$$D(\theta,\underline{\Delta}) = \frac{\sin\theta}{N} \int_{v_1} dv_1 \int_{v_2} dv_2 \cos v_1 W_1(v_2) W_2(v_1 \alpha_3)$$
$$\times [\cos^2 v_1 \cos^2(\psi - v_2) - \cos^2\theta - 2\cos\theta \sin v_1 \sin(\psi - v_2)$$
$$- \sin^2 v_1 \sin^2(\psi - v_2)]^{-1/2} \qquad (5)$$

where $\cos v_1 dv_1 dv_2 = \underline{dv}$ is the necessary volume element for a zxyz rotation scheme. Expansion of the denominator and integration where the integrand is real yields Eq. (22) in Chapter II.

APPENDIX IV

Application of the n dimensional change of variable theorem to Eq. (4), in Chapter II yields

$$\langle I \rangle = \frac{1}{N} \int_0^{\pi} d\theta \int_0^{2\pi} d\phi \int_0^{2\pi} d\omega \; I[\underline{V}_1'(\theta,\phi,\omega), \underline{V}_2'(\theta,\phi,\omega)]$$

$$\int_{v_1} dv_1 \cdots \int_{v_{n-3}} dv_{n-3} W(\theta,\phi,\omega,v_1,\ldots,v_{n-3}) J(\theta,\phi,\omega,v_1,\ldots,v_{n-3}) \quad (1)$$

where $J(\theta,\phi,\omega,v_1,\ldots,v_{n-3})$ is the Jacobian of the coordinate transformation. By inspection, we set

$$P(\theta,\phi,\omega,\underline{\Delta}) = \frac{1}{N} \int_{v_1} dv_1 \cdots \int_{v_{n-3}} dv_{n-3} W(\theta,\phi,\omega,v_1,\ldots,v_{n-3}) \quad (2)$$
$$\times J(\theta,\phi,\omega,v_1,\ldots,v_{n-3})$$

Following the approach of Chapter II (see also reference 5 of Chapter II), we pick the laboratory z axis to be the axis of the first rotation, $R_1(\alpha_1)$, and use the following transformation

$$\begin{aligned}
\alpha_1 &= f_1(\phi,v_1,\ldots,v_{n-3},\theta,\omega) \\
\alpha_2 &= v_1 \\
&\vdots \\
\alpha_{n-2} &= v_{n-3} \\
\alpha_{n-1} &= f_2(v_1,\ldots,v_{n-3},\theta,\omega) \\
\alpha_n &= f_3(v_1,\ldots,v_{n-3},\theta,\omega)
\end{aligned} \quad (3)$$

where α_{n-1} and α_n are defined by solving the two equations

$$\cos\theta = V'_{1z}(\alpha_2,\ldots,\alpha_n) \tag{4}$$

$$-\sin\theta\cos\omega = V'_{2z}(\alpha_2,\ldots,\alpha_n) \tag{5}$$

for α_n and α_{n-1} and setting $\alpha_2,\ldots,\alpha_{n-2}$ equal to $v_1,\ldots,v_{n-3}$.

As shown in reference 5 in Chapter II, under the above transformation,

$$\alpha_1 = -\phi + f_4(v_1,\ldots v_{n-3},\theta,\omega) \tag{6}$$

$$\frac{\partial\alpha_1}{\partial\phi} = -1 \tag{7}$$

and

$$\frac{\partial\alpha_i}{\partial\phi} = 0 \qquad i \neq 1 \tag{8}$$

From Eq. (6-8), the Jacobian simplifies to

$$|J| = \left|\frac{\partial\alpha_{n-1}}{\partial\theta}\frac{\partial\alpha_n}{\partial\omega} - \frac{\partial\alpha_{n-1}}{\partial\omega}\frac{\partial\alpha_n}{\partial\theta}\right| \tag{9}$$

By differentiating both sides of Eqs. (4) and (5) with respect to both θ and ω, we get four equations in the four unknowns $\partial\alpha_{n-1}/\partial\theta$, $\partial\alpha_n/\partial\omega$, $\partial\alpha_{n-1}/\partial\omega$, and $\partial\alpha_n/\partial\theta$. Solving these equations for the Jacobian yields

$$|J| = \frac{\sin^2\theta\sin\omega}{\left|\frac{\partial V_{1z}}{\partial\alpha_{n-1}}\frac{\partial V_{2z}}{\partial\alpha_n} - \frac{\partial V_{1z}}{\partial\alpha_n}\frac{\partial V_{2z}}{\partial\alpha_{n-1}}\right|} \tag{10}$$

with $\alpha_2,\ldots,\alpha_n$ replaced by their transformed variables $v_1,\ldots,v_{n-3}$, $f_2(v_1,\ldots,v_{n-3},\theta,\omega)$, and $f_3(v\text{-}1,\ldots,v_{n-3},\theta,\omega)$. Substitution into Eq. (2) yields Eq. (50) in Chapter II.

This report was done with support from the Department of Energy. Any conclusions or opinions expressed in this report represent solely those of the author(s) and not necessarily those of The Regents of the University of California, the Lawrence Berkeley Laboratory or the Department of Energy.

Reference to a company or product name does not imply approval or recommendation of the product by the University of California or the U.S. Department of Energy to the exclusion of others that may be suitable.

TECHNICAL INFORMATION DEPARTMENT
LAWRENCE BERKELEY LABORATORY
UNIVERSITY OF CALIFORNIA
BERKELEY, CALIFORNIA 94720

TECHNICAL INFORMATION DEPARTMENT
LAWRENCE BERKELEY LABORATORY
UNIVERSITY OF CALIFORNIA
BERKELEY, CALIFORNIA 94720